EXPLOITING FIBRIN KNOB:HOLE INTERACTIONS FOR THE CONTROL OF FIBRIN POLYMERIZATION

A Dissertation
Presented to
The Academic Faculty

by

Allyson Shook Ching Soon

In Partial Fulfillment
of the Requirements for the Degree
Doctor of Philosophy in the
School of Biomedical Engineering

Georgia Institute of Technology
December 2011

EXPLOITING FIBRIN KNOB:HOLE INTERACTIONS FOR THE CONTROL OF FIBRIN POLYMERIZATION

Approved by:

Dr. Thomas H. Barker, Advisor
School of Biomedical Engineering
Georgia Institute of Technology

Dr. Elliot L. Chaikof
Department of Surgery
Harvard University

Dr. Johnna S. Temenoff
School of Biomedical Engineering
Georgia Institute of Technology

Dr. Joel Collier
Department of Surgery
University of Chicago

Dr. L. Andrew Lyon
School of Chemistry and Biochemistry
Georgia Institute of Technology

Date Approved: October 06, 2011

To all who believe in the value of scientific research.

ACKNOWLEDGEMENTS

I wish to thank my advisor, who was most kind to take on an international student coming in without funding, all my lab mates and little undergraduate helpers, and also all the wonderful people I met during my 5-year stay in Atlanta. Most of all, I wish to thank my parents for being patient and supportive throughout this period, and my sisters for providing assorted technical and non-technical assistance.

TABLE OF CONTENTS

LIST OF TABLES

LIST OF FIGURES

SUMMARY

The minimization of blood loss represents a significant clinical need in the arena of surgery, trauma, and emergency response medicine. Fibrinogen is our body's native polymer system activated in response to tissue and vasculature injury, and forms the foundation of the most widely employed surgical sealant and hemostatic agent. Non-covalent knob:hole interactions are central to the assembly of fibrin that leads to network and clot formation. This project exploits these affinity interactions as a strategy to direct fibrin polymerization dynamics and network structure.

Short peptides modeled after fibrin knob sequences have been shown to alter fibrin matrix structure by competing with native fibrin knobs for binding to the available holes on fibrinogen and fibrin. The fusion of such knob peptides to a non-native component should facilitate binding of the fused component to fibrinogen/fibrin, and may permit the concomitant modification of the fibrin matrix. We examined this hypothesis in a three-step approach involving (a) analyzing the ability of tetrapeptide knob sequences to confer fibrin(ogen) affinity on a non-fibrin protein, (b) investigating the effect of knob display architecture on fibrin(ogen) structure, and (c) designing a temperature-responsive knob-displaying construct to modulate fibrin(ogen) affinity at different temperature regimes, thus altering fibrin(ogen) structure.

We demonstrate that fibrin network structure may be modulated using multivalent knob-displaying structures. Further optimization of the temperature-responsive knob-display system proposed should facilitate the development of a temperature-triggered polymerizing fibrin mixture for surgical applications.

CHAPTER 1

INTRODUCTION

Uncontrolled hemorrhage has consistently been the leading cause of death due to military trauma [1] and ranks second, after central nervous system injuries, in civilian trauma deaths [2]. Severe blood loss also poses a major challenge in cardiovascular and orthopedic surgical procedures, often necessitating the use of limited resources such as human blood products, or expensive hemostatic agents such as recombinant activated clotting factor VII (rFVIIa; NovoSeven®) [3, 4]. With the tightening of hospital budgets, topical hemostats, on top of cauterization and ligature techniques, are now increasingly important tools in surgical practice [5, 6]. Fibrin sealants are particularly prominent as the only material approved by the Food and Drug Administration (FDA) for multiple indications as hemostat, adhesive, and sealant [7].

Fibrin forms the foundation of our body's native hemostatic system and is activated as the final step of the coagulation cascade in response to tissue and vasculature injury. In the surgical setting, fibrin sealants are administered as two-component systems comprising the precursor fibrinogen, and the activating enzyme, thrombin [8, 9]. Due to the high concentrations of fibrinogen (80-120 mg/mL) and thrombin (300-600 NIH-U/mL) used to ensure rapid clotting, there is a high chance of clogging the delivery system at the point of deployment. This limits the utility of this inherently biocompatible material in procedures where surgical timing and precision is paramount. In response, we seek to develop a fibrin mixture that only forms a cohesive matrix upon warming at the site of application. By shifting the clotting trigger from enzyme to temperature, we expect to improve the handling of fibrin sealants, particularly for minimally invasive surgeries where the product has to be delivered via long narrow catheters to the point of application.

To facilitate the develop of this temperature-triggered in situ polymerizing fibrin mixture, this work examines the utility of affinity interactions, specifically fibrin knob:hole interactions, in the manipulation of fibrin matrix properties. Fibrin network formation from fibrinogen is mediated by both thrombin and clotting factor XIII (FXIII), the latter of which is commonly co-purified with plasma-derived fibrinogen. In particular, the non-covalent knob:hole affinity interactions effected by thrombin cleavage are directly responsible for the rapid assembly of fibrin monomers into protofibrils and fibrils, which feeds into activated FXIII (FXIIIa) crosslinking activity by the juxtaposition of its substrate sites. Knob:hole interactions therefore play a crucial role in directing fibrin network structure and consequently, matrix properties. We hypothesize that the perturbation of these interactions through the addition of knob-displaying non-fibrin entities will modulate the mechanical properties of the resulting fibrin matrix.

The addition of synthetic peptide knob mimics (glycine-proline-arginine-proline; GPRP) has been shown to arrest fibrin assembly at high dosages [10]. Similarly, we expect the addition of knob-displaying conjugates to alter the native 1:1 knob-to-hole ratio in polymerizing fibrin mixtures, hence impact matrix structure and stability. Since knob:hole interactions are central to fibril assembly, we anticipate that knob display configuration will also have an effect on fibrin(ogen) assembly dynamics and resulting network structure. In addition, non-covalent affinity interactions are inherently sensitive to the surrounding conditions and in combination with a stimuli-responsive element, should facilitate the design of temperature-responsive conjugates that differentially perturb fibrin matrix structure at different temperature regimes.

This thesis examines our starting hypothesis in three stages. First, we demonstrate that the presentation of a short tetrapeptide knob sequence is sufficient to confer fibrinogen and fibrin affinity on a non-fibrin protein. Here, we introduced GPRP on the N-terminus of the model protein, fibronectin type III domains 9-10 (FNIII9-10) through

recombinant protein engineering. The expressed protein, GPRP-FNIII9-10, was shown to bind stably and specifically to fibrinogen and fibrin (detailed in Chapter 3).

Second, we demonstrate that knob-display configuration affects fibrinogen and fibrin structure. Here, we conjugated GPRP to the terminal ends of 2-arm and 4-arm polyethylene glycol (PEG) structures via sulfhydryl-maleimide chemistry. These multi-arm conjugates, $GPRP_2$-PEG and $GPRP_4$-PEG, formed networks with fibrinogen and altered fibrin assembly dynamics (detailed in Chapter 4). The structure of the resulting network was shown to be dependent on the conjugate size.

Finally, we developed a thermo-responsive knob-displaying mixed micelle system that alters fibrin structure in a temperature-dependent manner. Here, we expressed GPRP on the N-terminus of diblock temperature-responsive elastin-like polypeptides (ELP) using recombinant protein engineering. The expressed proteins, GPRP-ELP_B-ELP_A and GPSP-ELP_C-ELP_A, formed mixed micelles exhibiting variable avidities for fibrinogen at different temperature regimes (detailed in Chapter 5).

In summary, this work demonstrates our ability to alter the distribution of physical (non-covalent) and chemical (covalent) crosslinks within fibrin networks through the addition of knob-displaying constructs, thereby altering clot structure. This strategy provides an orthogonal means of manipulating fibrin network structure and mechanical properties, driving matrix formation from being a purely enzyme-triggered process towards one that is stimulus-responsive.

CHAPTER 2

LITERATURE REVIEW

Many strategies in tissue engineering and regenerative medicine focus on the use of provisional matrices to harness the healing resources of the body for tissue repair. By providing a three-dimensional scaffold with the appropriate spatial and temporal cues, the invading or encapsulated cells can populate and remodel the matrix to match the surrounding milieu, creating a seamless transition between host and replacement tissue [11-13].

The fibrin networks that form spontaneously at injury sites *in vivo* are the foundation of our body's native provisional matrix. Following external application of fibrin sealants during surgeries, the matrices formed are similarly resolved within days to weeks and appear to promote angiogenesis and local tissue growth and repair [9]. To preserve these favorable properties, we seek to modify the fibrin matrices using components that have also been shown to have favorable biocompatible and/or biodegradable properties.

This chapter reviews the mechanisms behind fibrin matrix formation, particularly the role of knob:hole interactions in fibrin assembly and FXIIIa crosslinks in network stabilization. Methods of altering fibrin network structure in the interest of applying these scaffolds in tissue engineering and regenerative medicine applications are also covered. A review of PEG and ELP-based materials as potential scaffolds is also included.

2.1. Fibrinogen and Fibrin

Fibrinogen circulates at ~3 mg/mL in the blood as a 340 kDa glycoprotein comprising a symmetrical pair of three protein chains - Aα, Bβ and γ (Figure 1A). Fibrin(ogen) features numerous binding sites for pro-coagulant proteins (thrombin, factor XIII), pro-fibrinolytic proteins (plasminogen, tissue plasminogen activator), anti-fibrinolytic proteins (plasminogen activator inhibitor), growth factors (fibroblast growth factor-2, vascular endothelial growth factor, platelet derived growth factor), extra-cellular matrix components (fibronectin, heparin), and cell receptors (integrins, cadherins) [14, 15]. A number of these components are co-purified with plasma-derived fibrinogen in commercial fibrin sealants and support the formation and remodeling of the fibrin matrix, thereby aiding the smooth transition of the provisional scaffold into the local tissue structure as the wound heals. Fibrin therefore has many favorable biological properties as a scaffold material for use in tissue engineering and surgical applications [16, 17].

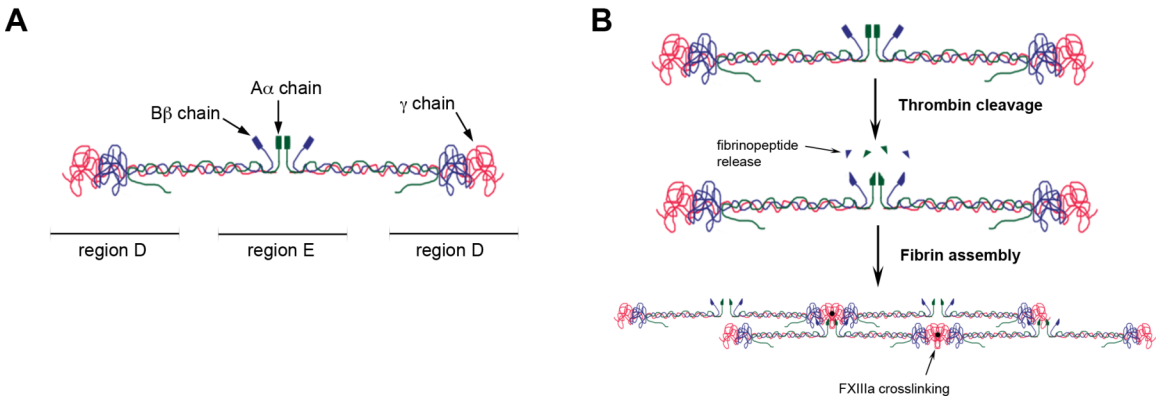

Figure 1. Fibrinogen and fibrin polymerization schematic. (A) Illustration of the basic fibrinogen structure depicting the Aα chain in green, Bβ chain in blue, γ chain in red. The length of the αC tail is variable depending on the species and isoform. (B) Steps involved in fibrin polymerization. Note: FXIIIa-catalyzed γ-γ crosslinking is shown in a longitudinal configuration for visual clarity.

2.1.1. Fibrin Network Formation

Fibrin network formation, or fibrin polymerization, from its precursor fibrinogen is initiated upon activation of the clotting enzymes, prothrombin and FXIII. *In vivo*, prothrombin is proteolytically cleaved and activated by activated clotting factor X in the first common step of the intrinsic (or contact factor) and extrinsic (or tissue factor) activation pathways of the coagulation cascade.

The activated serine protease, thrombin, catalyzes the removal of fibrinopeptides (FpA, FpB) from the N-terminal regions of the Aα and Bβ chains of fibrinogen, exposing short peptide sequences known as knob 'A' and knob 'B' that bind to hole 'a' and hole 'b' in the C-termini of neighboring fibrin(ogen) molecules (Figure 1B). The cleaved fibrin monomers without FpA and FpB are denoted $(\alpha\beta\gamma)_2$, in contrast with precursor fibrinogen, $(A\alpha B\beta\gamma)_2$.

The central location of the knobs in region E, contrasting with the distal location of the holes in region D, results in the formation of half-staggered two-stranded protofibrils that associate to form the fibrin network. Thrombin also activates the transglutaminase, clotting factor XIII (FXIII). Activated FXIII (FXIIIa) initiates the formation of γ-glutamyl-ε-lysyl amide bonds between substrate sites on the γ and α chains of adjacent fibrin(ogen) molecules.

The timescale for the chemical crosslinking of fibrin is typically orders of magnitude (minutes to hours) larger than the assembly of monomers initiated by the release of fibrinopeptides (seconds to minutes). Fibrin network structure is therefore largely dictated by the release kinetics of the fibrinopeptides and concomitant exposure of

knobs, whose knob:hole binding kinetics is in turn dependent on factors such as enzyme, substrate and ion concentration.

2.1.2. Knob:Hole Interactions

Four types of knob:hole interactions may be postulated, namely, A:a, A:b, B:a, B:b. Early studies employing classical binding assays between fibrinogen and synthetic peptide sequences mimicking knob 'A' (glycine-proline-arginine-proline; GPRP) and knob 'B' (glycine-histidine-arginine-proline; GHRP) suggested that these sequences had separate and distinct binding sites, although some cross-reactivity was observed [10]. X-ray crystallographic structures of fibrinogen fragment D together with knob 'A' and 'B' mimics confirmed the notion that knob 'A' bound to hole 'a' located in the C-termini of the γ chains while knob 'B' bound to the homologous hole 'b' of the β chains [18].

Laser tweezer (or gradient optical trap) experiments using fibrinogen and knob A-displaying or knob A- and B-displaying fibrin fragments found that A:a interactions were the dominant interactions, with measured individual binding strengths of 125-130 pN and a low zero-force off-rate of 10^{-4} s^{-1} [19]. Abolishing the A:a interactions through the use of variant forms of fibrinogen, B:b binding strength was found to be ~15-20 pN [20]. Complementary experiments using surface plasmon resonance (SPR) found that the equilibrium binding constants between fibrinogen and knobs 'A' or both knobs 'A' and 'B' were statistically similar (5.8 ± 1.1 μM vs 3.7 ± 0.7 μM, $p = 0.14$), suggesting that A:a interactions are much stronger than B:b even though both participate in fibrinogen binding [21].

In general, thrombin-mediated FpA release, forming type I fibrin or $(\alpha B\beta\gamma)_2$ comprising A:a interactions, occurs at a faster rate than FpB release, forming type II

fibrin or $(\alpha\beta\gamma)_2$ comprising both A:a and B:b interactions [22-24]. In addition, certain snake-derived thrombin-like serine proteases preferentially cleave either FpA (e.g. batroxobin, ancrod) or FpB (e.g. venzyme). Notably, batroxobin-catalyzed fibrin clots are largely similar to thrombin-catalyzed clots, while venzyme-catalyzed clots are only stable below physiological temperatures [25, 26], suggesting that B:b interactions alone are not sufficient for the stable assembly of fibrin monomers. From a clinical perspective, the majority of human fibrinogen variants identified (i.e. due to dysfibrinogenemia, hypofibrinogenemia, or afibrinogenemia) can be traced back to amino acid substitutions near the knob 'A' and hole 'a', again suggesting that A:a interactions are key to stable fibrin assembly [27].

In conclusion, extensive research recognizes knob A mimics, in particular GPRP, as the strongest fibrin(ogen) binding tetrapeptude sequence. GPRP-conjugated affinity columns have been used for the purification of fibrinogen and the hole-containing fragment D [28]. GPRP-related peptides have also been postulated as potential anticoagulants, given their ability to disrupt fibrin assembly [10, 29, 30]. Similarly, this work focuses on the use of GPRP-conjugated constructs for the perturbation of fibrin polymerization dynamics.

2.1.3. Fibrin Crosslinks

FXIII, also known as the fibrin stabilizing factor, crosslinks the α and γ chains of fibrin(ogen), producing a mechanically stronger, more rigid and more elastic clot with increased resistance to fibrinolysis (reviewed in [31, 32]). FXIII circulates in the plasma at a concentration of 14-28 μg/mL, mainly in association with fibrinogen due to its large binding constant ($K_D \sim 10^{-8}$ M) for the molecule [33]. As such, FXIII is co-purified with

plasma-derived fibrinogen in most commercial fibrin sealants, contributing to fibrin crosslinking and clot strength following application [34].

FXIII is activated by proteolytic cleavage of thrombin, releasing the activation peptide and exposing the active-site cysteine. Typically, γ-γ dimers are formed within seconds of thrombin-activated polymerization, while higher order α-α and α-γ hybrid oligomers are formed more slowly as the clot matures [35, 36]. Crosslinking of non-fibrin proteins such as α_2 plasmin inhibitor and fibronectin to lysine residues on the α chain, while physiologically important, also occurs at a slower rate compared to γ-γ dimerization [37].

The higher crosslinking rate of fibrin as compared to fibrinogen is well established and commonly attributed to the favorable alignment of the substrate sites in the assembled fibrin fibril [38, 39]. Addition of a large excess of GPRP to polymerizing fibrin mixtures (thus disrupting fibrin assembly as demonstrated by [10]) slowed γ-γ dimerization by over 30-fold, but had no significant effect on fibrinogen mixtures [40].

Conversely, γ-γ crosslinking of fibrinogen or fragment D may be enhanced by the presence of thrombin-activated fragment E (containing knobs 'A') that forms a tether between the C-terminal γ modules (containing holes 'a') of fragment D [41]. The addition of GPRP reduced the crosslinking rate to basal levels, suggesting that fragment E acts as an organizing template to spatially orient fibrin(ogen) region D for favorable reaction with FXIIIa [41]. Similarly, a two-headed GPRP linker mimicking the tethering function of fragment E promoted γ-γ dimerization [42]. Large excess of the linker, where we would expect nonproductive binding (i.e. the two-headed GPRP linker essentially functions like monovalent GPRP), again reduced crosslinking to basal levels. Notably,

the ratio of linker to fragment D to achieve maximum % crosslinking was close to 1:1 [42], as we would expect from a 1:1 knob:hole interaction.

In short, FXIIIa crosslinking activity, particularly γ-γ dimerization, is strongly associated with fibrin assembly mediated by knob:hole interaction. By extension, we expect that alterations in fibrin network structure arising from fibrin assembly should have an impact on the crosslinking kinetics, thereby altering clot rheology.

2.1.4. Fibrin Network Structure and Clot Stiffness

Differences in clot stiffness can have significant physiological implications, in that highly rigid clots may be prone to thrombosis, while fragile clots may lead to premature lysis and re-opening of the wound [43]. From our understanding of fibrin clot formation, we expect clot rheology to be dependent on both the assembled network structure arising from non-covalent knob:hole interactions, as well as covalent crosslinks introduced by FXIIIa.

Fibrin network structure is typically modified by varying clotting conditions such as fibrinogen and thrombin concentration, buffer ionic strength (typically sodium chloride, NaCl [44]), calcium ion concentration (typically calcium chloride, $CaCl_2$), pH, and the use of alternative thrombin-like clotting enzymes (e.g. ancrod, batroxobin) [25, 45, 46]. Translucent clots formed at high thrombin or high NaCl concentration are commonly interpreted to be thin, highly-branched networks. Opaque clots are formed at low NaCl or high calcium concentration, conditions that apparently favor lateral aggregation of the fibrin protofibrils, giving rise to thicker bundles that scatter more light [46].

The relationship between fibrin polymerization kinetics and the resulting network structure was first formally established by Weisel and Nagaswami using a kinetic model [46]. In general, large fiber diameters and lengths were associated with minimal branching and the converse was also true. Following up, the group showed that greater branching led to increased clot rigidity but that the reduced fiber diameters also softened the network [47]. Thus, clot rigidity was maximal at an intermediate thrombin concentration of 0.25 NIHU/mL and at 0.15 mM $CaCl_2$. Interestingly, the authors also found that γ monomer depletion (due to γ chain crosslinking) was completed within 2 hours at 0.2 mM $CaCl_2$ while a progressive depletion of α monomers (due to α chain crosslinking) occurred from 0.2 to 20 mM $CaCl_2$ [47].

While it is clear that FXIIIa-catalyzed crosslinking increases clot stiffness, it is less clear how each type of crosslink (γ-γ dimers, γ_n multimers, α_n polymers, α_m-γ_n hybrids) contributes to clot rigidity. In the absence of crosslinks, fibrin clots have been shown to experience slight creep and irrecoverable deformation [48]. Diffusion of GPRP (thus disrupting fibril assembly) into such clots decreased the shear modulus and eventually liquefied the clot [49]. On the other hand, ligated clots displayed almost perfect elastic behavior in creep and creep recovery tests [50, 51]. Notably, the structural integrity of these clots appeared to be maintained even in the presence of GPRP [49], demonstrating the importance of the covalent crosslinks in maintaining clot stability independently of fibrin assembly mediated by knob:hole interactions.

FXIIIa-mediated crosslinking does not affect clot architecture and is not visible under electron microscopy [47]. Even though γ-γ dimerization occurs much faster than α chain crosslinking, it is thought that α_n polymers are the major contributors to clot

rigidity [52, 53]. However, caution must be taken in interpreting these early results due to the popular use of calcium and EDTA (ethylenediaminetetraacetate) to modulate the crosslinking activity of this calcium-sensitive enzyme [52]. As discussed above, calcium ion concentration also affects fibrin network structure and clot rigidity. Consequently, many recent papers use fibrinogen variants with mutated or deleted FXIIIa crosslinking sites to study the effect of crosslinking independently of clot structure.

Using a patient-derived antibody that inhibit α chain but not γ chain crosslinking, Ryan et al. found that the elastic modulus of the clot was reduced by twofold despite nearly complete γ-γ crosslinking [54]. Using recombinant fibrinogen without the C-terminal α chain FXIIIa crosslinking sites (α251 fibrinogen), Collet et al. showed that the clots produced were also less stiff and had a higher loss modulus than control clots [55]. However, they also found that ligated α251 fibrin clots were stiffer than their unligated counterparts, suggesting that γ chain crosslinking also contributes to the mechanical stability of clots [55]. Creating a fibrinogen variant with mutated γ chain crosslinking sites, Standeven et al. affirmed the contribution of γ-γ dimerization to clot stiffness [56]. In particular, γ-γ crosslinking may be a prerequisite for the production of higher-order crosslinked species (γ_n, α_n, α_m-γ_n) that maximally enhance network stiffness as the clot matures [54, 56].

In summary, clot stiffness is a function of both fibrin network structure as well as α and γ chain crosslinks, and that both factors are interrelated and interdependent under most experimental conditions used in literature.

2.1.5. Fibrinolysis

In vivo, the events that trigger coagulation also initiate the process of fibrinolysis via the activation of plasminogen to form the active serine protease, plasmin. The fibrinolytic process itself is modulated via a complex web of biochemical processes involving plasminogen activators (tPA, uPA), plasminogen activator inhibitors (PAI-1, PAI-2) and fibrinolysis inhibitors (thrombin-activated fibrinolysis inhibitor or TAFI), amongst others [57].

By varying ionic strength and thrombin concentration, Carr and Alving found that fibrinolytic rate increased with fibrin fiber diameter [58]. Here, exogenous tPa was added at the point of thrombin addition, or one hour post-clotting as an overlay. Clot dissolution was quantified using both turbidimetry and release of ^{125}I-labeled fibrinogen. In contrast, Kolev et al. found that fibrinolytic rate decreased with fibrin fiber diameter [59]. Here, the authors were interested in modeling the surface degradation rates of clots overlaid with plasmin (and several other proteases) of varying concentrations. While fibrin degradation was again monitored with release of ^{125}I-labeled fibrinogen, it should also be noted that the range of NaCl used in this work was of a different regime from Carr and Alving, which could explain the discrepancy.

A more recent paper from Weisel's group investigated the morphological features of fibrin formation and dissolution using gold-labeled fibrinogen under a confocal microscope [60]. This paper confirmed earlier suggestions that fibrinolysis occurred via lateral transection, leading to the progressive disaggregation of the whole fiber structure. However, while thinner fibers were digested more quickly, thicker fibers were more likely to undergo agglomeration, a process that has been shown to accelerate fibrinolysis [60]. In addition, it was discovered recently that the addition of knob B synthetic peptide

mimics increased clot turbidity but delayed fibrinolysis [61]. In particular, the authors pointed out that turbid clots generated using calcium ions were different from the turbid clots formed in the presence of these peptides, in that the latter delays the activation of plasminogen by tPA. Hence, the relationship between fiber diameter, or clot turbidity, and fibrinolytic rate is hardly straightforward.

A similar controversy exists with respect to evaluating the contribution of α and γ chain crosslinking towards fibrinolytic rates. Due to the complex regulatory mechanisms behind plasmin activation, it may well be true that we are unlikely to find any directly measurable relationship between fibrinolytic rate and the degree of crosslinking [56, 62].

2.2. Polyethylene glycol

Synthetic polymers are valued for their ease of synthesis and fabrication, leading to their present wide use in sutures and various implant and orthopedic devices. In particular, PEG has been used in a wide variety of biomedical applications, as non-fouling surface coatings [63, 64], as conjugates [65, 66], and as hydrogels or drug delivery scaffolds [67].

2.2.1. PEGylation

PEGylation, or the conjugation of PEG to molecules of interest, is an enabling technology that is routinely used to improve the pharmacokinetics of therapeutic drugs and small proteins (reviewed in [68-70]). PEGylation reduces the immunogenicity of molecules by reducing their accessibility to antibodies and proteolytic enzymes through steric hindrance imparted by the mobile polymer chains. The hydrophilic PEG chains also impart solubility and increase the hydrodynamic radius of the parent molecule, thus reducing kidney clearance and increasing the blood circulation time of small proteins or

peptides. In general, PEG less than 20 kDa in size is cleared by the kidney, while hepatobiliary clearance dominates above 50 kDa [68].

Conjugation via the sulfhydryl group of cysteine is one of the most specific methods of in vitro protein modification due to the lower abundance of cysteine residues as compared to amine-containing lysine residues [69]. Use of this strategy in PEGylation has been gaining popularity as genetic engineering and recombinant protein production allows for the introduction of deliberately placed cysteine residues for site-directed conjugation [71-74]. This is particularly useful when amino groups are involved in protein function since amine-mediated conjugation chemistries might inadvertently target the active site of the protein, resulting in an inactive conjugate. Notably, sulfhydryl-maleimide reactions can be carried out efficiently under mild conditions so as to preserve protein/peptide function [75].

The huge success of commercial PEGylated products (Adagen®, PEG-Intron® , Pegasys®, Neulasta®, etc.) has led to the ready availability of low polydispersity (M_w/M_n < 1.05) functionalized PEGs with a variety of functional groups and sizes (typically 2 kDa up to 40 kDa) for various applications in biomedical research.

2.2.2. PEG as Ligand Linkers

Successful commercialization of PEGylated constructs, typically molecules with one or more PEG chains attached, has also spurred the development of the reverse scenario, namely “multivalent conjugates” involving PEG structures with one or more active molecules attached. In its simplest form, this refers to the use of PEG as a flexible linker between two ligands, which should especially facilitate the binding of the ligand to targets with multiple binding sites [76]. Upon the binding of one of the ligands, the

diffusion of its tethered cognate will be constrained within a hemisphere of radius equal to the root-mean-square length of the linker, increasing its binding probability, hence enhancing the apparent affinity of the conjugate. Thus, the optimal linker length should be close to the distance between the ligand binding sites of the target [76].

In a comprehensive study on the effect of different PEG architectures on ligand binding, Baird et al. studied the effect of monovalent, bivalent, bismonovalent, bisbivalent and dendrimer PEG configurations on 2,4-dinitrophenyl (DNP) binding to anti-DNP immunoglobulin E (IgE) receptors on RBL mast cells [77]. Here, the authors found that there was an optimal linker length for achieving stable nonstimulatory intramolecular receptor crosslinking and that bisbivalent ligands were more effective inhibitors due to the presence of two DNP groups at each end of the conjugate. In a subsequent study modeling the interaction of these conjugates with anti-DNP IgE in solution, they again found the presence of an optimal linker length for achieving the maximum effective affinity and minimum IC_{50} [78].

In short, PEGylation provides a convenient and reproducible means of generating conjugates with different peptide display configurations on an inert backbone structure.

2.2.3. PEG Hydrogels

As a hydrophilic but biologically inert material, PEG may be functionalized and crosslinked to form hydrogels as replacement scaffolds for metabolically active soft tissues. The macroscopic properties (e.g. compressive modulus, mesh size) of these hydrogels may be tuned to the desired parameters by varying crosslinking density, which is in turn dependent on monomer and crosslinker structure and the specific polymerization conditions [79, 80].

PEG-based hydrogels are often used as blank-slate three-dimensional templates onto which biological functionalities may be added. Cell adhesion peptides (e.g. arginine-glycine-aspartate-serine or RGDS) for promoting cell attachment [81] and the incorporation proteolytic sensitive peptides sequences [82] are common modifications of synthetic PEG hydrogels.

2.2.4. PEG-Fibrin Hydrogels

Blends of natural and synthetic components are often used in the design of hydrogels for use in tissue engineering and regenerative medicine in order to fulfill both the mechanical and biological requirements of their intended application [83]. Thus, several attempts have also been made to blend the favorable mechanical properties of PEG with the rich biological properties of fibrinogen/fibrin.

Fibrinogen is stabilized by 17 interchain and 12 intrachain disulfide bonds [84]. By denaturing fibrinogen and reducing the disulfide bonds, then crosslinking the free sulfhydryls using PEG-diacrylate, Seliktar's group has created a variety of PEG-fibrin hybrid gels with varying structural characteristics (reviewed in [85]). By varying the relative proportions of fibrinogen and PEG, as well as the size of the PEG-diacrylate crosslinker used, they were able to achieve a range of elastic modulus from 0.01 to several kPa [86]. These gels exhibited a range of degradation rates, resulting in different cellular invasion kinetics [87].

In a different approach, Suggs' group used functionalized amine-reactive PEG (via benzotriazole carbonate or succinimidyl esters) to PEGylate fibrinogen [88, 89]. Since free lysine residues were used in the PEGylation reaction, fibrinogen did not have to be denatured or reduced, and can subsequently be crosslinked through the addition of

thrombin if the PEGylation ratio is less than 10 [89, 90]. Indeed, a structural investigation of Seliktar's sulfhydryl-targeted PEG-fibrinogen conjugates suggested that while the protein secondary structure was preserved, the unfolded polypeptides may not fold back into its native conformation and instead assemble to form elongated aggregates [91].

2.3. Elastin-Like Polypeptides

Elastin-like polypeptides or elastin-mimetic proteins are chemically or recombinantly synthesized biopolymers modeled after repeating sequences in the mammalian elastin protein [92]. The ability to produce high yields of ELPs with specific sequences using standard recombinant protein engineering methods has greatly facilitated the development of ELP nanostructures and materials with carefully tuned microscopic and macroscopic properties for diverse biomedical and biotechnogical applications [93, 94].

2.3.1. Inverse Phase Transitioning Behavior

ELPs reported in literature commonly comprise repeats of the pentapeptide sequence, VPGXG, where X may be any amino acid. Above a transition temperature, T_t, ELPs reversibly self-assemble by hydrophobic association, forming micron-sized aggregates that then coalesce to form a dense coacervate [95]. Based on the Urry model, the P^2G^3 dipeptide is responsible for the formation of type II β-turns that are key points in the folding/dehydration and unfolding/hydration process, while the guest residue in position 4 can be varied to create ELPs with different T_t [96, 97]. Multicanonical simulations of pentapeptides with substitutions in position 4 support the idea that the hydrophobicity of the guest residue affected conformational transition temperature but not secondary structure [98].

The simplest ELPs are designed using aliphatic amino acids (glycine, alanine, valine, isoleucine, leucine) as guest residues since these uncharged non-polar residues primarily respond to temperature for the thermodynamically driven collapse of the hydrated protein chain [99]. Their transition temperatures fall within the experimentally accessible range from approximately 5°C for poly(VPGLG) to 55°C for poly(VPGGG) [96]. In addition, the T_t of these ELPs were shown to vary linearly with the mole fraction of the guest residue within a copolymer, allowing further turning of the T_t if desired. Using recombinant protein design and production. Chilkoti's group has conducted extensive studies on the effects of ELP chain length, composition and concentration on the thermal transitioning behavior of ELPs containing glycine/alanine/valine as guest residues [100, 101].

The inverse phase transitioning behavior of ELPs has prompted many comparisons with the synthetic polymer equivalent, poly(N-isopropylacrylamide) or PNIPAM, which has a phase transitioning temperature at approximately 32°C. In particular, the cloud points of ELPs exhibit an unusually strong concentration dependence [100]. Comparisons with PNIPAM suggest that this may be due to chain stiffness arising from the β-turns within the protein chain below its T_t, thus preventing intramolecular association and coiling [102, 103]. This is congruent with the observation that the concentration dependence of the cloud point decreases with increasing ELP chain length and that a critical transition temperature is reached at sufficiently high protein concentrations [100].

2.3.2. ELPs as Protein Capture Tags

The thermally-induced hydrophobic collapse and aggregation of ELPs can be utilized as a convenient means of purifying ELPs and ELP-tagged proteins in a process known as inverse transition cycling (ITC) [104-106]. In particular, the addition of salt (of up to 3 M NaCl) allows the T_t to be modulated over a 50°C range, allowing ITC to be carried out isothermally at ambient conditions if desired [103, 105]. ELP-tagged proteins are produced with extremely high yields (> 100 mg per liter of culture) and can be stably stored frozen in buffer at high concentrations of 100-150 mg/mL without the need for protein stabilizers like glycerol [106]. In the case of poorly expressed proteins, free ELPs may be added as a co-aggregant to capture and purify the ELP-tagged protein [107].

The use of ELPs as capture tags was demonstrated by Chilkoti's group using immobilized ELPs on a nanopatterned surface. High salt was used to trigger the capture of ELP-tagged proteins on an ELP-conjugated surface, which could then be regenerated using a low salt buffer [108]. In a similar vein, Sun et al. developed a one-pot glyco-affinity precipitation protocol by conjugating carbohydrate ligands to ELPs via the glutamic acid residue using carbodiimide chemistry [109]. The glyco-ELP conjugates interacted with lectins in solution and co-precipitated with these proteins above T_t.

2.3.3. ELP hydrogels

The high biocompatibility of ELPs together with their ease of purification permits the use of large quantities of the material in tissue engineering and regenerative medicine. As proof of feasibility, Urry et al. demonstrated the successful *in vivo* application of several ELP variants in soft tissue augmentation and generation with the eventual goal of developing an injectable periurethral support material for correcting stress urinary incontinence [110].

While the shear modulus of an ELP solution below T_t is almost three orders of magnitude smaller than that of the coacervate above T_t, this can be changed by crosslinking the protein chains [111]. Crosslinked ELP hydrogels have been created using γ irradiation [112], glutaraldehyde or tris-succinimidyl aminotriacetate or tris(hydroxymethyl)phosphino-propionic acid targeting lysine residues [113-115], and tissue transglutaminase targeting lysine and glutamine resides [116]. Such crosslinked hydrogels are known to contract and expel water above their phase transition temperature [112, 114, 115].

Alternatively, physical "crosslinks" can be introduced via selective block collapse of triblock ELPs. These B-A-B triblock ELPs (where $T_{t,B} < T_{t,A}$) exist as monomers below the transition temperature but when heated above the phase transition ($T_{t,B}$), the flanking hydrophobic B blocks undergo desolvation and associate into micellar aggregates that act as virtual crosslinks between the central hydrophilic block [117]. Notably, careful control of the liquid phase transitions during hydrogel formation gave rise to scaffolds with varying meso- and nano-scale structures, resulting in differences in elastic moduli of over three orders of magnitude [118].

2.3.4. Self-Assembling ELP Systems

The ability to precisely control the composition and chain length of ELPs through genetic engineering has led to the use of ELP block copolymers for the development of various self-assembling systems [119]. In the simplest permutation, the steroid drug dexamethosone was passively encapsulated within microparticles of an elastin-like polymer, resulting in drug release over a period of up to 35 days [120].

In a more complex design, Chilkoti's group showed that ELP diblocks formed stable micellar structures of less than 100 nm in diameter following the thermally-induced collapse of the block with the lower T_t [121]. Presentation of the integrin-binding RGDS ligand on the hydrophilic block resulted in the temperature-triggered enhanced binding of the multivalent protein micelle to K562 cells expressing the $\alpha_v\beta_3$ integrin [122]. Diblock proteins with a crosslinkable ELP core (incorporating lysines) have also been created, facilitating study of the stabilized micellar structures under ambient conditions [123].

2.3.5. Short ELPs as Molecular Actuators

An intriguing area of ELP research capitalizes on chain conformation transition to effect a mechanical contraction. The potential for the use of ELPs as free energy transducers or molecular motors was first demonstrated by Urry et al. around the mid-1980s [124]. Given growing interests in the potential use of ELPs as molecular actuators, the mechanism behind the conformational transition of model ELP polypeptides has been studied by several different groups over the past decade [102, 125-128].

After demonstrating that short ELPs exhibit the same temperature-induced structural transitions as the longer polymers studied by other groups [128], Reiersen et al. substituted the inter-helix turn of protein A with an ELP linker. At high temperatures, the linker formed a type I β-turn, aligning the two helices of protein A and increasing binding affinity to IgG by 21-fold [129]. Similarly, Megeed et al. substituted the flexible linker between the V_H and V_L domains of the single-chain antibody anti-fluoresceine scFv 4D5Flu with an ELP linker [130]. Raising the temperature triggered contraction of the

linker and separation of V_H and V_L, disrupting the fluorescein binding site and resulting in faster ligand release [130].

In the reverse scenario, ligand binding has also been known to affect ELP transition characteristics. When the globular protein α-amylase was added to a solution containing its ELP-conjugated cognate ligand, the transition temperature of the mixture increased by 5.5°C, consistent with the increase of surface hydrophilicity of the ELP conjugate complex [101]. Similarly, binding of calcium to ELP-conjugated calmodulin lowered the surface charge of the protein, thus triggering aggregation of the conjugate under isothermal conditions [131].

CHAPTER 3

KNOB:HOLE INTERACTIONS CONFER FIBRIN AFFINITY

For this chapter, we examine the fibrin(ogen) binding dynamics of a model knob-displaying non-fibrin protein. Knob:hole interactions have been extensively studied over the past three decades using synthetic knob peptide mimics or knob-displaying fibrin fragments (refer to section 2.1.2 for details). Comparatively fewer papers deal with the study of knob:hole interactions in the context of non-fibrin proteins, much less the interaction of such knob-protein conjugates within a fibrin matrix. Nonetheless, the potential exists to exploit these stable and specific interactions as targeting modules for fibrin(ogen).

In one early attempt, Kuyas and Doolittle synthesized alkylamine derivatives of GPRP that were designed to bind to human serum albumin via their hydrophobic alkane groups [132]. While the GPRP-amidoalkanes were shown to be functional in the presence of albumin, it was not clear if the hydrophobic interaction between the alkane tail and albumin was strong enough to increase the residence time of the derivative peptide for the application of this system as an anticoagulant. Thus in a separate project, the A chain remnant peptide of two-chain urokinase-type plasminogen activator (tcuPA) was replaced by a GPRP-containing synthetic peptide in order to confer fibrin clot specificity, thereby reducing undesirable systemic activation of plasminogen [133]. The increased affinity of the GPRP-conjugated uPA for fibrin purportedly reduced the concentration of activator necessary to achieve the same fibrinolytic rate by five-fold. Similarly, Hua et al. expressed GPRP on the N-terminus of low molecular weight single-chain uPA and

analyzing relative fibrinolytic rates, suggested that the fusion had a six-fold greater affinity for fibrin clots [134]. Unfortunately, none of these papers directly characterized the affinity between the GPRP-fused protein and fibrinogen or fibrin.

Here, we hypothesized that non-fibrin proteins presenting knob sequences can be produced recombinantly and will bind stably and specifically to fibrinogen and fibrin via knob:hole interactions. We speculate that the stable knob:hole interaction should permit the retention of the knob-protein fusion within fibrin matrices. The model protein, FNIII9-10, was used to develop and optimize the expression system for the production of recombinant knob-displaying proteins.

The results obtained from this project were published in 2010 in Biomaterials 31(7): 1944-54 [135].

3.1. Experimental Design

We developed a platform system to rapidly clone and express recombinant proteins displaying different tetrapeptide sequences (GPRP, GPRV, GHRP) on their N-termini, thus mimicking the knob display configuration on activated fibrin molecules. The pGEX4T-1 vector from GE Healthcare encodes an N-terminal glutathione S-transferase (GST) tag followed by a thrombin cleavage site and a multiple cloning site (MCS). The cleavage site was mutated to code for the desired tetrapeptide sequences that would be exposed following thrombin cleavage. The coding frame of FNIII9-10 was then inserted into the multiple cloning site. This model protein is amenable to recombinant protein production [136, 137], has a known structure [138], is recognized by specific antibodies available commercially [136, 137], and does not contain any fibrinogen/fibrin binding sites .

The affinity of the different knob-FNIII9-10 conjugates towards immobilized fragment D was initially evaluated using surface plasmon resonance (SPR) to determine their relative equilibrium dissociation constant (K_D). The specificity of the interaction between immobilized GPRP-FNIII9-10 and fibrinogen was then evaluated using enzyme-linked immunosorbent assay (ELISA). The retention of GPRP-FNIII9-10 within fibrin matrices was then evaluated using a release assay with fixed sampling intervals.

3.2. Materials and Methods

3.2.1. Modification of pGEX4T-1

The original thrombin cleavage site in the pGEX4T-1 vector (GE Healthcare, Piscataway, NJ) was modified from LVPR↓GSPE to LVPR↓GPRV, LVPR↓GPRP and LVPR↓GHRP using the QuikChange® II-E Site-Directed Mutagenesis Kit (Stratagene, La Jolla, CA). All plasmids were introduced to and maintained in the electro-competent XL-1 Blue E. coli strain provided and cultured in LB + ampicillin plates at 37°C. Plasmids were extracted from cultures using the QIAquick Spin Miniprep Kit (QIAGEN, Valencia, CA) and verified via sequencing (Johns Hopkins Synthesis & Sequencing Facility, Baltimore, MD).

3.2.2. Amplification and Insertion of FNIII9-10 into Expression Vectors

The fibronectin type III domain 9-10 (FNIII9-10) was used as the model protein. The SalI site in the MCS was used to insert the FNIII9-10 open reading frame into the $pGEX4T_{GSPE}$, $pGEX4T_{GPRV}$, $pGEX4T_{GPRP}$ and $pGEX4T_{GHRP}$ vectors obtained above using standard molecular cloning techniques (enzymes purchased from NEB, Ipswich, MA). Briefly, the FNIII9-10 open reading frame was amplified in a high fidelity

polymerase chain reaction with Phusion High Fidelity DNA polymerase from the previously established pGEX4T-1-FNIII9-10 plasmid [136] using primers with flanking SalI sequences (underlined) and introducing Gly-Gly-Cys (bold) on the C-terminal if necessary: ACTGGTCGACTGGGTCTTGATTCCCCAACT and ACTGGTCGACTCA**GCAACCACC**TGTTCGGTAATTAATGGA. Vectors and insert were digested with SalI. The vectors were additionally dephosphorylated using heat-deactivate-able Antartic phosphatase to prevent self-ligation. The respective vectors and insert were ligated using T4 DNA Ligase and transformed into electro-competent XL-1 Blue cells. Selection for successfully ligated plasmids containing the insert was made on LB + ampicillin plates. The orientation of the FNIII9-10 insert was verified by in-colony PCR-screening using forward or reverse primers on the plasmid in combination with an internal primer within the insert. Colonies with the insert in the correct orientation were grown up for plasmid extraction. All plasmids were verified via sequencing.

3.2.3. Protein Production and Purification

Plasmids containing the FNIII9-10 insert were transformed into electro-competent BL21 E. coli and protein production of the GST-tagged proteins stimulated as recommended by the manufacturer. Following appropriate culture, cells were pelleted by centrifugation at 4°C and resuspended in ice-cold PBS supplemented with protease inhibitor (Roche, Indianapolis, IN), then lysed by adding 1 mg/mL of lysozyme followed by sonication. 1% Triton X and 10 U/mL of DNase was added and the lysate further incubated for 30 min with gentle agitation. The cell lysate was cleared of cellular debris by centrifugation followed by filtration through a 0.22 μm pore filter. Purification of the recombinant proteins was performed following the manufacturer's recommendation using

the ÄKTAFPLC with a GST Prep FF 16/10 column (GE Healthcare) for affinity purification of GST-tagged proteins. Washing and binding steps were done in filter-sterilized PBS and elution completed with glutathione (GSH) buffer (50 mM Tris-HCl, 10 mM reduced GSH, pH 8.0). The GSH buffer was then exchanged to PBS using an Amicon Ultra-15 centrifugal filter with MWCO 10,000 (Millipore, Billerica, MA). The GST-tagged protein was incubated overnight with bovine thrombin (MP Biomedicals, Solon, OH) dosed at 10 U per mg recombinant protein and the cleaved protein solution was reintroduced on the GST Prep FF 16/10 column to remove the GST tag, followed by the HiTrap Benzamidine FF column (GE Healthcare) to remove thrombin. Gxxx-FNIII9-10-(C) proteins were assessed for purity by SDS-PAGE and quantitated at Abs_{280nm} using the Nanodrop 1000 (Thermo Scientific, Wilmington, DE) using extinction coefficients calculated using an online peptide property calculator (found at http://www.basic.northwestern.edu/biotools/proteincalc.html), then aliquoted and stored at -80°C until use.

3.2.4. ELISA Binding Assays

A modified ELISA technique was used to establish the affinity of fibrinogen for the various Gxxx-FNIII9-10-C proteins covalently immobilized on maleimide-activated plates via their C-terminal cysteines. Sulfhydryl-containing proteins/peptides were added to pre-blocked maleimide-activated 96-well plates (Pierce, Thermo Scientific, Rockford, IL) at 10 μg/mL in conjugation buffer (CB) comprising 150 mM NaCl, 100 mM phosphate, 10 mM EDTA, pH 7.2, with attachment occurring via maleimide-sulfhydryl (thioether) linkages. TCEP (1 mM) was added to maintain sulfhydryl groups in the reduced form. Following, unreacted maleimide groups were quenched with 20 μg/mL

cysteine in CB. Human fibrinogen (25 μg/mL) was incubated with the substrates and unbound protein removed by washing. Bound fibrinogen was detected using HRP-conjugated goat anti-fibrinogen antibody (MP Biomedicals #55239) and 1-Step^{TM} Ultra TMB-ELISA (Pierce). The TMB reaction was quenched with 1 M H_2SO_4 before measuring the Abs_{450nm} using the SpectraMax M2 (Molecular Devices, Sunnyvale, CA). All intervening wash steps were conducted using washing buffer (WB) comprising 150 mM NaCl, 100 mM phosphate, 0.05% Tween-20, pH 7.2; all binding steps were conducted using binding buffer (BB) comprising PBS + 1% BSA. For basic affinity assays, the concentration of the fusion proteins was varied. For specificity assays, varying concentrations of Gxxx tetrapeptides (Genscript, Piscataway, NJ) were added to the fibrinogen solution during incubation with the covalently immobilized proteins.

3.2.5. Biotinylation of Gxxx-FNIII9-10 Proteins

Gxxx-FNIII9-10-C proteins were conjugated via the sulfhydryl group of the C-terminal cysteine to maleimide-functionalized biotin (maleimide-PEG_2-biotin; Pierce #21902) following the manufacturer's recommended protocol. Unreacted maleimide-PEG_2-biotin was removed using Slide-A-Lyzer dialysis cassettes with MWCO 3,500 (Pierce). The extent of biotinylation was determined using the Pierce Biotin Quantitation Kit (Pierce).

3.2.6. Fibrin Clotting Assays

Clotting was initiated in a 96-well plate format and the Abs_{350nm} used as a standard measure of turbidity. Briefly, increasing doses of the Gxxx-FNIII9-10-biotin proteins were preincubated with 4 mg/mL human fibrinogen (ERL #FIB3) in Tris+Ca buffer (140 mM NaCl, 5 mM $CaCl_2$, 20 mM Tris, pH 7.4). Following the 1 h

preincubation, clotting was initiated by adding 1 NIHU/mL of human thrombin (ERL) or batroxobin moojeni (Centerchem, Norwalk, CT), and 1 U/mL human FXIIIa (kindly donated by Baxter AG, Vienna Austria). Real time measurements of clot turbidity were taken every minute for 1 h. To determine the amount of unclotted protein, the clots were spun down and the supernatant or clot liquor was analyzed for total protein using the Quant-iT protein assay (Invitrogen, Carlsbad, CA).

3.2.7. Rheological Assays

The Bohlin CVO 120 high resolution rheometer (Malvern Instruments, Westborough, MA) with plate-plate geometry was used to assess the viscoelastic characteristics of fibrin clots at room temperature. Briefly, fibrinogen (preincubated with or without Gxxx-FNIII9-10-biotin as indicated) and enzyme mixtures with identical compositions as those used in the turbidity and clottability assays were mixed by pipetting and immediately added to the bottom plate. The upper plate (14 mm diameter) was immediately lowered to a gap size of 1 mm and the mixture was allowed to polymerize for 30 min in a humid chamber. Following, oscillating measurements were taken over a frequency range of 0.05 to 1.0 Hz at a constant strain of 0.5%.

3.2.8. Protein Release Assays

Analogous to the clotting assays, Gxxx-FNIII9-10-biotin was preincubated with fibrinogen in Tris+Ca buffer in 2 mL conical bottom tubes. Clotting was initiated by adding thrombin or batroxobin, and FXIIIa. After a one-hour incubation, the resulting clot was overlaid with 1 mL Tris+Ca buffer. The entire volume of buffer was removed and replaced with fresh buffer at 1, 4, 8, 12, 24, 48, 72, 96-h timepoints for analysis. Gxxx-FNIII9-10-biotin proteins in the recovered supernatant samples were quantitated

using a sandwich ELISA. Briefly, 96-well ELISA plates were coated with 5 μg/mL streptavidin, then washed and blocked with 1% BSA. The sample, mouse monoclonal anti-FNIII9-10 antibody (HFN7.1; Developmental Studies Hybridoma Bank, Iowa City, IA) and HRP-conjugated goat anti-mouse antibody (Pierce #1858413) were added sequentially to the plate with intervening wash steps. TMB was added to react with the HRP and the reaction quenched with 1 M H_2SO_4 before measuring the Abs_{450nm}.

3.2.9. Statistical Analysis

All experimental data are reported as mean ± SEM of at least 3 independent triplicate experiments. Results were analyzed using GraphPad PRISM 5.0. Statistical comparisons for all experimental sets were based on one-way ANOVA using the Tukey post-hoc test for pair-wise comparisons with significance defined by $p < 0.05$.

3.3. Knob-FNIII9-10 Preparation

We developed an expression vector system allowing the simple and rapid cloning of any gene-of-interest into a series of vectors that facilitates the production of any proteins-of-interest with any of three N-terminal fibrin knob sequence – GPRP, GPRV, GHRP.

3.3.1. Vector Development

The commercially available pGEX4T-1 expression vector is designed for the IPTG-induced expression of proteins with an N-terminal 26 kDa GST tag under control of the *tac* promoter. This tag can then be removed via thrombin cleavage, analogous to the process of fibrinogen activation wherein protein segments are proteolytically cleaved from the N-termini of the Aα and Bβ chains.

Using the unmodified pGEX4T-1 vector, the N-terminal sequence exposed upon thrombin cleavage of the expressed GST-tagged protein is GSPE, which does not bind to fibrin pockets. We modified this coding sequence on the expression vector to each of the desired tetrapeptide sequences using site-directed mutagenesis (Figure 2A). Site-directed mutagenesis was conducted using a commercially available kit that employs a PCR-based method of introducing base-pair substitutions, insertions or deletion on any plasmid vector *in vitro*.

The coding sequence for our model protein, the 20 kDa FNIII9-10 fragment, was then introduced into the MCS using standard molecular cloning techniques. Notably, the repeating modules of fibronectin, frequently described as having a beads-on-a-string structure, represent individually folded domains that should be amenable to tagging at the N- and C-termini. In some versions, the primers used for insertion of the FNIII9-10 open reading frame included the coding sequences for a C-terminal glycine-glycine-cysteine as an additional functional handle. Since FNIII9-10 does not contain any cysteine residues, this C-terminal cysteine provides a specific site for the sulfhydryl-targeted conjugation of the protein to maleimide-activated surfaces or components.

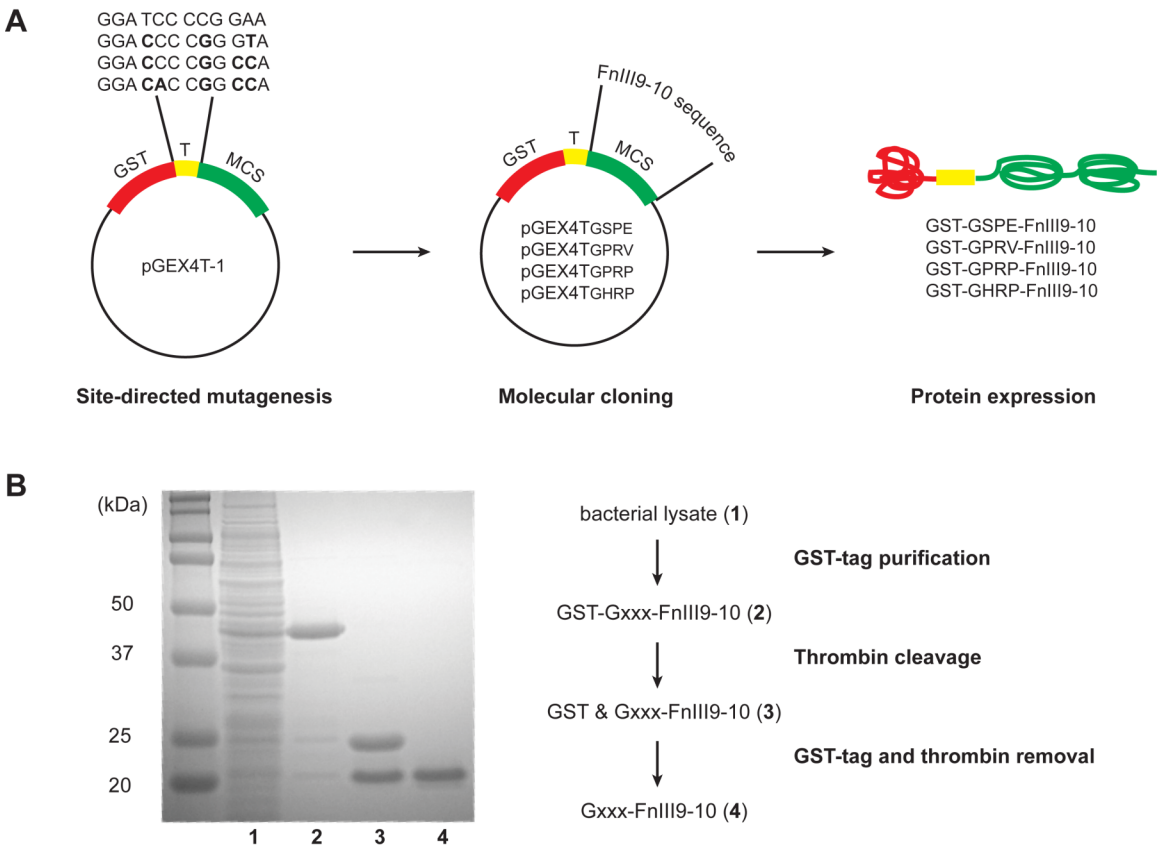

Figure 2. Gxxx-FNIII9-10 protein production and purification. (A) Molecular engineering of the pGEX4T-1 vector to express proteins with variable thrombin cleavage sites, LVPR↓Gxxx. Site-directed mutagenesis was used to modify the coding sequence for the thrombin cleavage site (T). Next, the open reading frame of the protein-of-interest, FNIII9-10, was inserted into the multiple cloning site (MCS). The expressed proteins comprise an N-terminal glutathione S-transferase (GST) tag, followed by the thrombin cleavage site and protein-of-interest. (B) Coomassie-stained SDS-PAGE gel demonstrating protein purity at the different stages of purification using affinity chromatography. GST-tagged Gxxx-FNIII9-10 (lane 2) was purified from contaminating proteins in the bacterial cell lysate (lane 1) via the GST affinity column. Thrombin-catalyzed cleavage releases the 26 kDa GST-tag from the 20 kDa Gxxx-FNIII9-10 protein (lane 3). Next, the thrombin and GST-tag were removed using benzamidine and GST affinity columns respectively, leaving the desired protein-of-interest (lane 4).

3.3.2. Protein Production and Purification

The GST-tagged proteins were expressed in the protease-deficient protein expression E. coli strain BL21 upon IPTG induction. Figure 2B shows a representative Coomassie-stained SDS-PAGE gel illustrating product purity at the different stages of protein purification using affinity purification via the ÄKTApurifier system. Notably, the

GST tag serves dual purposes as affinity tag and a measure of thrombin cleavage efficacy. Impaired thrombin cleavage efficiency due to modification of the thrombin-cleavage site was not encountered for these proteins.

Using this platform cloning and expression system we successfully expressed and purified the following knob-protein fusions: GSPE-FNIII9-10, GSPE-FNIII9-10-C, GPRP-FNIII9-10, GPRP-FNIII9-10-C, GPRV-FNIII9-10, GPRV-FNIII9-10-C, GHRP-FNIII9-10, GHRP-FNIII9-10-C.

3.4. Characterizing Fibrinogen/Fibrin Affinity

Initial SPR data collected by Stabenfeldt indicated that GPRP-FNIII9-10 was the strongest binder ($K_D = 3.0 \pm 0.1$ μM) to fibrinogen [135]. This finding was not surprising in light of the fact that the GPRP peptide binds to fibrinogen with the highest affinity (K_D ~20 μM) out of the three knob peptide sequences used in this work [139, 140]. Further investigations were therefore conducted using the high affinity GPRP-FNIII9-10 and the non-binding control GSPE-FNIII9-10.

The binding strength and specificity of the knob-protein fusions for fibrinogen was evaluated using ELISA. The knob-protein fusions were then added to fibrin matrices at sufficiently low molar ratios so as not to perturb fibrin polymerization dynamics and clot structure. The retention of the knob-protein fusions within fibrin matrices was evaluated using a standard protein release assay.

3.4.1. Evaluating GPRP-FNIII9-10 Affinity Using ELISA

Gxxx-FNIII9-10-C proteins were immobilized on maleimide-activated 96-well plates via maleimide-sulfhydryl chemistry, allowing the unidirectional presentation of their N-terminal knobs to fibrinogen-containing solutions in the wells. Using standard

ELISA techniques, the bound fibrinogen was detected using an anti-fibrinogen HRP-conjugate, with stronger signals corresponding to increased amounts of bound fibrinogen. Complementing the earlier SPR data, the ELISA results indicate that soluble fibrinogen bound to immobilized GPRP-FNIII9-10-C but not the control, GSPE-FNIII9-10-C (Figure 3A). This demonstrates the mechanism of action, that fibrinogen binds the knob-protein fusion via the knob sequences and not via interaction with the fibronectin domains in our model protein.

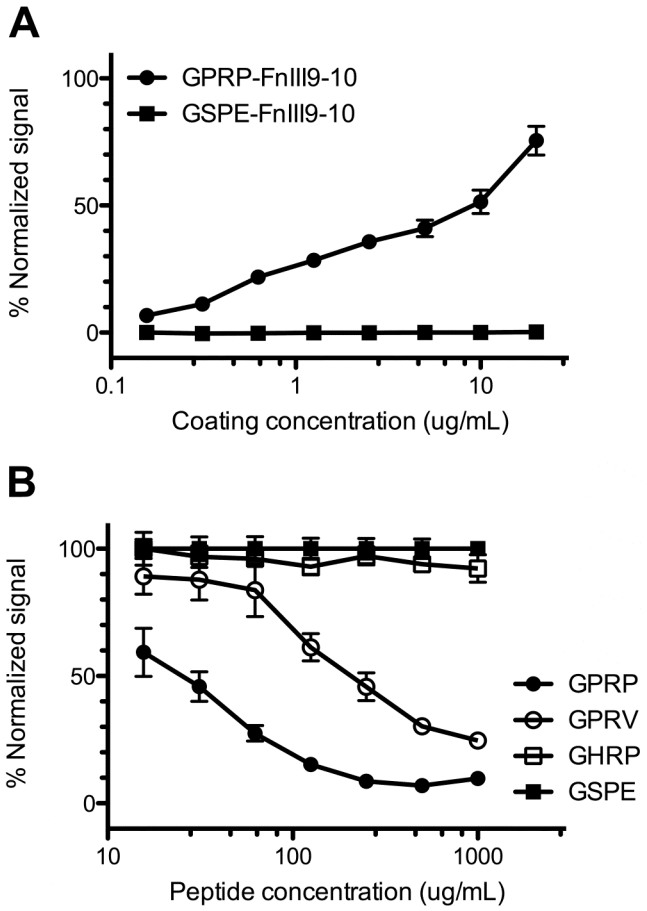

Figure 3. ELISA studies analyzing GPRP-FNIII9-10 affinity for fibrinogen. (A) Affinity assays demonstrating binding between immobilized GPRP-FnIII9-10-C, but not GSPE-FnIII9-10-C, and fibrinogen. ELISA plate readouts (Abs_{450nm}) were normalized against the maximum signal obtained using GPRPFPAC peptide (Genscript) at a coating concentration of 20 µg/mL. (B) Specificity assays

demonstrating that GPRP and GPRV peptides compete with immobilized GPRP-FNIII9-10 for fibrinogen. ELISA plate readouts were normalized against the signals obtained in the presence of the non-binding GSPE peptide to correct for osmolarity.

To further demonstrate specificity, synthetic fibrin knob peptides were added in large molar excess (10^2- to 10^4-fold) to the fibrinogen solution that was to be incubated with immobilized GPRP-FNIII9-10-C. As expected, free GPRP tetrapeptides competed with the immobilized GPRP-FNIII9-10-C for binding to fibrinogen, resulting in a dose-dependent inhibition of fibrinogen binding following a one-hour pre-incubation (Figure 3B). These results suggest that the GPRP sequence is the mediator of the interaction between the immobilized protein and fibrinogen.

The tetrapeptides GPRV and GHRP are also known to bind the same fibrinogen holes via knob:hole interactions, albeit with slightly different affinities and specificities [10]. Our results indicate that GPRV competed with GPRP-FNIII9-10 for binding to fibrinogen, but to a lesser extent as compared to GPRP, while GHRP was not a significant competitor to GPRP-FNIII9-10 under our experimental conditions. Notably, these results agreed with our SPR data suggesting that the affinity constant of GPRV-FNIII9-10 was at least an order of magnitude smaller than that of GPRP-FNIII9-10, while GHRP-FNIII9-10 had little affinity for immobilized fibrinogen fragment D [135]. These results therefore support the interpretation that the interaction between the GPRP-FNIII9-10 protein and fibrinogen is primarily mediated by the respective N-terminal tetrapeptide sequences through specific interactions with fibrinogen holes.

3.4.2. Fibrin Assembly in the Presence of GPRP-FNIII9-10

Since knob-protein fusions inherently exploit the knob:hole interactions involved in fibrin assembly, we first verified that the presence of the GSPE-FNIII9-10-biotin and GPRP-FNIII9-10-biotin conjugates did not significantly impede the clotting process or alter global matrix characteristics at the dosages used for the matrix release assays.

GPRP-FNIII9-10-C was conjugated to maleimide-functionalized biotin, generating GPRP-FNIII9-10-biotin conjugates that can be quantitated via sandwich ELISA. GPRP-FNIII9-10-biotin proteins were preincubated with fibrinogen before clotting was induced by the addition of FXIIIa and either thrombin (exposes both knobs 'A' and 'B') or batroxobin (exposes knobs 'A' only). The process of fibrin assembly can be inferred from the gross absorbance of the fibrinogen-containing mixture since the lateral aggregation of protofibrils during clotting results in a rapid rise in turbidity [46]. The turbidity curves obtained suggest that fibrin assembly in the presence of thrombin (Figure 4A) or batroxobin (Figure 4B) was not significantly impacted by the presence of GPRP-FNIII9-10-biotin, or the control GSPE-FNIII9-10-biotin, at the conjugate:fibrinogen molar ratio of 1:10. In comparison, the difference in turbidity profiles for thrombin- versus batroxobin-catalyzed clots is a clear reflection of mechanistic differences between the two enzymes.

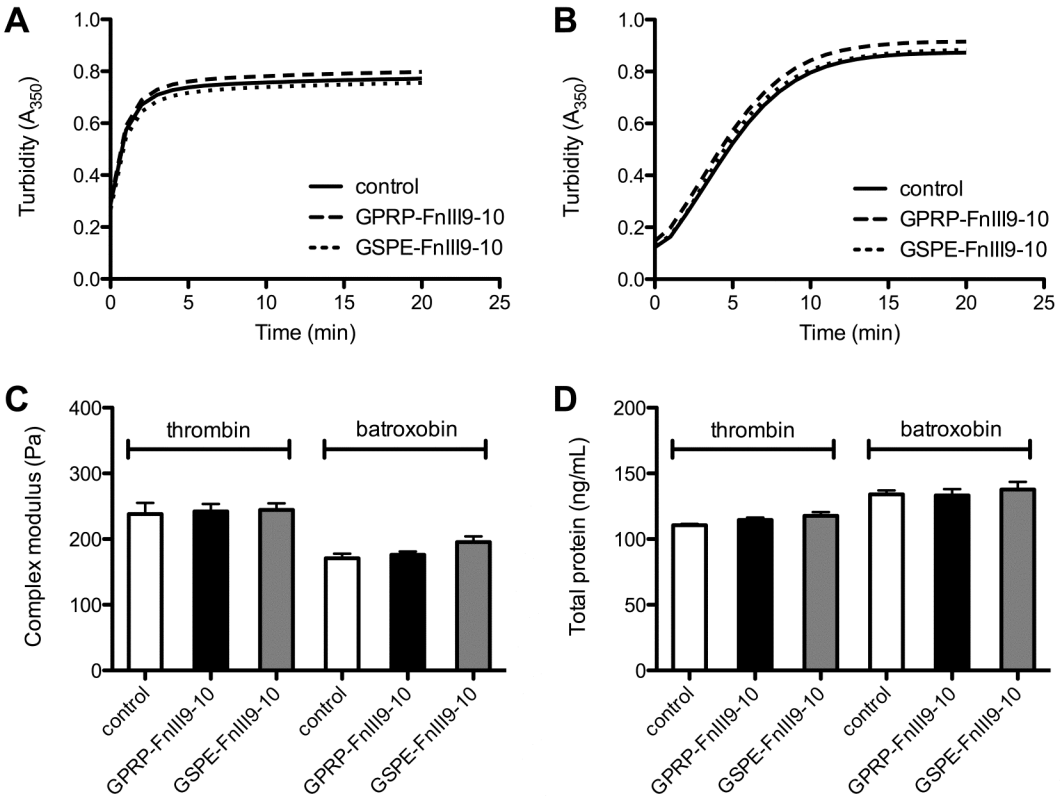

Figure 4. Fibrin assembly in the presence of GPRP-FNIII9-10 and GSPE-FNIII9-10. Clots were formed from 6 μM (= 2 mg/mL) fibrinogen solutions containing 0.6 μM GPRP-FNIII9-10-biotin or GSPE-FNIII9-10-biotin upon the addition of 1 U/mL FXIIIa and 1 NIHU/mL human α-thrombin or batroxobin moojeni. Control clots were formed in the absence of the conjugates. (A) Turbidity curves obtained in the presence of thrombin. (B) Turbidity curves obtained in the presence of batroxobin. (C) Complex moduli of the clots after 30 min clotting time. Measurements were taken at a frequency of 0.22 Hz and strain of 0.5%. (D) Quantitation of soluble protein in the clot liquor from clots after 1 h clotting time.

Rheological assaying of clots formed following a 30-minute clotting time suggests that the presence of either conjugate did not significantly affect the native viscoelastic properties of the clots (Figure 4C). Moreover, quantitation of the soluble proteins in the clot liquor (the remaining supernatant after spinning down the insoluble fibrin) also indicates that the presence of GPRP-FNIII9-10-biotin, or the control GSPE-FNIII9-10-biotin, did not significantly impact the clottability of the mixture (Figure 4D).

These results agree with past research showing that at least a 100-fold excess of the GPRP tetrapeptide was necessary to completely inhibit fibrin assembly [139] and suggest that the presence of knob-protein fusions will not significantly interfere with the formation of the fibrin matrix at the loading concentration used.

3.4.3. Retention in Fibrin Matrices Using Release Assays

We proceeded to examine the retention of GPRP-FNIII9-10-biotin conjugates within three-dimensional fibrin matrices by monitoring protein release from the clots into the surrounding buffer reservoir. In particular, we were interested in observing the release profiles from both normal thrombin-catalyzed clots and batroxobin-catalyzed clots. Batroxobin selectively exposes the knobs 'A' but not knobs 'B', theoretically leaving unoccupied fibrinogen holes that should be available for binding to GPRP-FNIII9-10-biotin, thus promoting its retention within the fibrin matrix.

As described in the previous section, the GPRP-FNIII9-10-biotin conjugates were preincubated with fibrinogen at a 1:10 molar ratio (conjugate:fibrinogen), before clotting was induced by the addition of FXIIIa and either thrombin or batroxobin. After a one-hour incubation period, the clot was overlaid with pre-warmed buffer and incubated at 37°C with agitation. Samples taken at regular intervals were evaluated for the presence of fibrin(ogen) and conjugate via sandwich ELISAs. In particular, the HFN7.1 conformation-specific antibody was used against the conjugates to demonstrate that the conformational integrity of the FNIII9-10 was preserved during the release assay. Moreover, GPRP-FNIII9-10-biotin is capable of binding to ELISA plates coated with fibrinogen and being detected by the same antibody (data not shown), indicating that the

conformational integrity of the FNIII9-10 domain is preserved even while bound to fibrin(ogen).

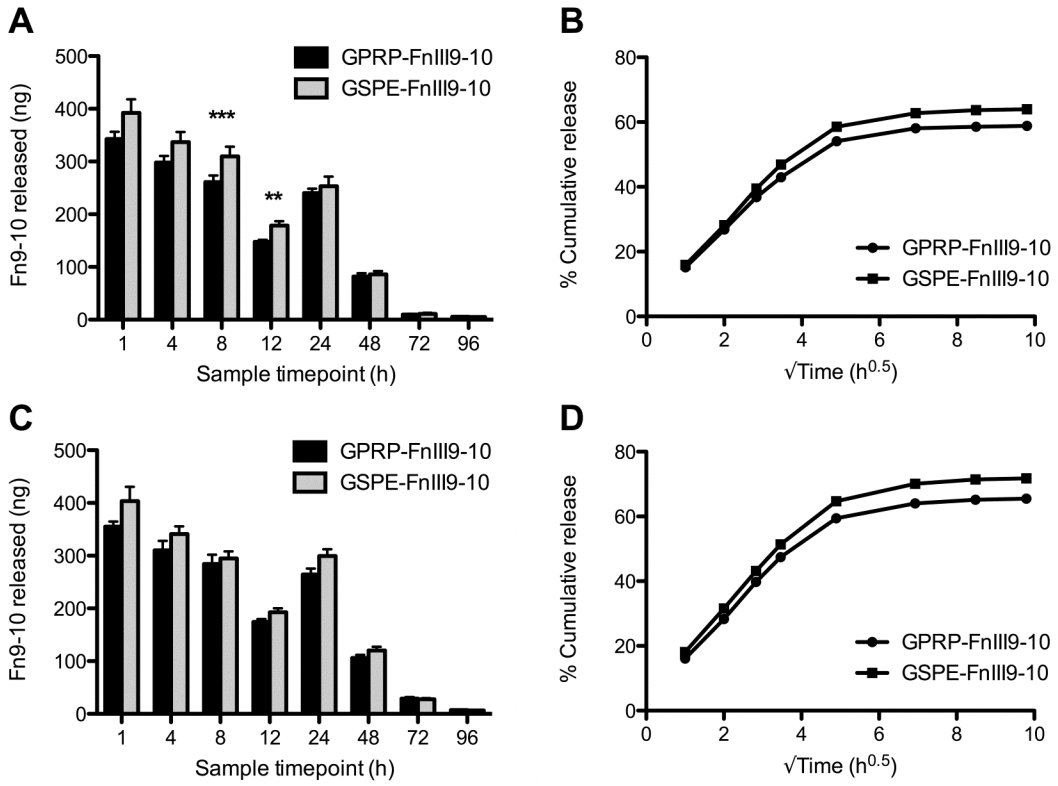

Figure 5. Release of GPRP-FNIII9-10 versus GSPE-FNIII9-10 from thrombin- or batroxobin-catalyzed fibrin clots. Clot compositions as described in Figure 4. 200 µL clots were overlaid with 1 mL Tris+Ca buffer and samples were taken at the designated timepoints over 4 days. (A, B) GPRP/GSPE-FNIII9-10-biotin measured in the samples taken from thrombin-catalyzed clots and the compiled release profiles. (C, D) Corresponding data from clots formed in the presence of batroxobin.

The amount of soluble fibrin(ogen) in all the samples remained below the detection limit (~10 ng/mL) of the fibrin(ogen) ELISA, indicating that the clots remained intact during the four-day incubation period (data not shown). From the FNIII9-10-biotin ELISA, we found that less GPRP-FNIII9-10-biotin was released within the first 24 hours as compared to GSPE-FNIII9-10-biotin for both the thrombin (Figure 5A,B) and

batroxobin (Figure 5C,D) clots, suggesting that the affinity between GPRP-FNIII9-10-biotin and fibrin(ogen) was able to retard the initial 'burst release' of protein from the fibrin matrix, resulting in an overall greater retention of the loaded protein within the clot. Nonetheless, statistical comparisons of the absolute quantity of protein released at each time point did not reveal significant differences between GPRP-FNIII9-10-biotin and GSPE-FNIII9-10-biotin release, particularly after the initial 24-hour burst release. Rather, more significant differences were found between the amounts of protein released from thrombin- versus batroxobin-catalyzed clots for both GPRP-FNIII9-10 (Figure 6A, B) and GSPE-FNIII9-10 (Figure 6C, D), suggesting that other factors may be involved in mediating protein retention past the 24-hour time point. In particular, fibrin clots formed under the catalysis of different enzymes and at different enzyme concentrations are structurally dissimilar, affecting gel porosity and protein diffusion characteristics [25, 45].

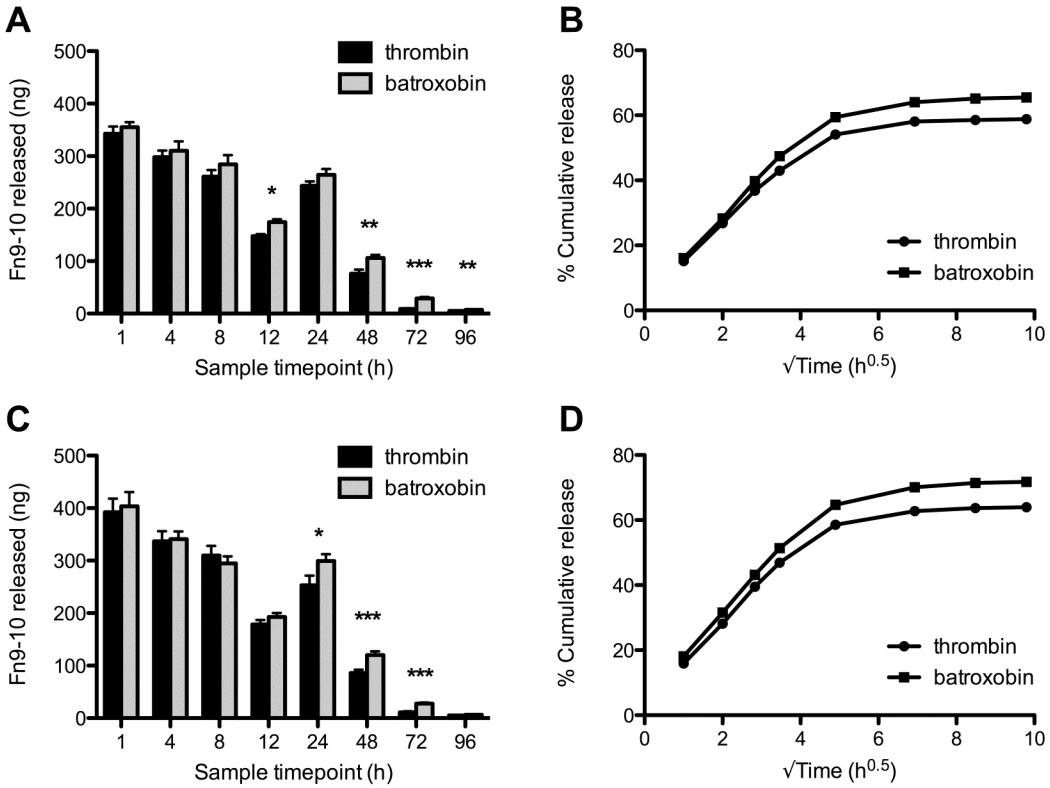

Figure 6. Release of GPRP-FNIII9-10 or GSPE-FNIII9-10 from thrombin- versus batroxobin-catalyzed fibrin clots. Clot compositions as described in Figure 4. 200 µL clots were overlaid with 1 mL Tris+Ca buffer and samples were taken at the designated timepoints over 4 days. (A, B) GPRP-FNIII9-10-biotin measured in samples taken from thrombin- or batroxobin-catalyzed clots and the compiled release profiles. (C, D) Corresponding data for GSPE-FNIII9-10-biotin release.

3.5. Discussion and Conclusions

We were able to successfully produce and purify recombinant fibrin-binding proteins with the generalized structure Gxxx-protein-(C), capitalizing on the N-terminal Gxxx sequence for protein retention within fibrin and the C-terminal cysteine as a functional handle. As proof-of-concept, we found that the high affinity GPRP sequence facilitates the specific binding of such fusion proteins to fibrinogen although it appeared that GPRP-FNIII9-10 was not retained to a significant extent within fibrin matrices past the 24-h timepoint.

It is possible that the fibrin-binding capacity of the GPRP-FNIII9-10-biotin conjugate was diminished when presented in a three-dimensional system of both fibrin holes and competing native fibrin knobs. Thus, Stabenfeldt developed a microfluidic perfusion system that allowed the real-time monitoring of protein incorporation, retention, and release within fibrin matrices to assist with our interpretation of the system's strengths and limitations [135]. Fibrin clots, pre-loaded with Alexa Fluor 633-labeled knob-protein fusion, were formed under similar conditions as used in the previous release assays and vigorously perfused to create a temporally-accelerated release system that could be monitored in real-time using confocal microscopy. Results from these studies showed that the high affinity binder GPRP-FNIII9-10-AF633, but not the control GSPE-FNIII9-10-AF633, was colocalized with the Alexa Fluor 555-labeled fibrin fibers. Following a rigorous 30-min perfusion (at 10 μL/min) of buffer, 12.8% of the fibrin matrix remained colocalized with GPRP-FN9-10-AF633, compared to 0.1% for the control, demonstrating a robust interaction between the fusion and fibrinogen.

We speculate that the retention characteristics of such knob-protein fusions may be further improved by increasing the overall affinity constant through the use of stronger fibrin-binding sequences or by introducing multivalency. In particular, we note that previous research using a heparin-based affinity system for the retention of proteins in fibrin matrices via non-covalent interactions with similar affinities (K_Ds in the μM range) suggest that a large (~thousand-fold) excess of binding sites is necessary to successfully retain such proteins within the fibrin matrix [141]. This poses a potential limitation for the use of single knob:hole interactions for the retention of proteins in fibrin matrices

since the number of available pockets is limited by fibrinogen concentration as well as the presence of competing knobs.

On the other hand, this work offers valuable insight into the significance behind the multimeric nature of the native fibrin(ogen) molecule, comprising up to four fibrin knobs (two knob ‘A’ and two knob ‘B’) per fully activated molecule. Specifically, suitably tagged recombinant proteins with pre-defined N-terminal sequences can be used as tools to bridge the current informational gap between studies utilizing short synthetic peptides and those focusing on multimeric fibrin fragments, particularly since the physiological relevance of each type of knob:hole interaction (A:a, A:b, B:a, B:b) to fibrin assembly remains controversial to this day.

CHAPTER 4

ALTERING FIBRIN NETWORK MORPHOLOGY

For this chapter, we are interested in evaluating the impact of fibrin knob-displaying flexible polymer linkers on polymerization dynamics, FXIIIa-catalyzed crosslinking, fibrin network structure and clot stiffness. Fibrin network structure is strongly dependent upon fibrinogen, thrombin and calcium concentrations [47]. In particular, the knob:hole interactions initiated by the removal of fibrinopeptides are instrumental in determining key network parameters such as fiber diameter and branching density, both of which may be inferred from clot turbidity measurements [46].

The addition of knob peptide mimics such as GPRP and GHRP perturbs clot turbidity and fibrin matrix formation in slightly different ways. GPRP-derived mimics inhibit fibril assembly through competitive binding, disrupting knob:hole interactions and increasing fibrinogen clotting time [139, 142]. On the other hand, GHRP-derived mimics enhance clot turbidity and delay plasmin-induced clot degradation presumably due to activation of αC domains enabling an alternative αC-αC based polymerization mechanism [61, 143].

Yet bivalent 900 Da $GPRP_2$-PEG conjugates were found to promote the end-to-end crosslinking of fibrinogen γ chains by FXIIIa [42], suggesting that the PEG linker tethered the adjacent holes ‘a’, contributing to the assembly of fibrinogen favoring FXIIIa activity. Thus, we propose the conjugation of sulfhydryl-terminated GPRPAAC peptides to the maleimide-terminated ends of different PEG structures, creating multivalent $GPRP_n$-PEG linkers capable of perturbing fibrin matrix structure through knob:hole

interactions. This unique non-covalent means of altering matrix structure should preserve the physiological complexity of the original protein while allowing the independent control of matrix mechanical properties by altering conjugate size and valency. We hypothesize that these distance-spanning $GPRP_n$-PEG conjugates will interact with soluble fibrinogen and fibrin monomer and impose structural changes to the fibrin polymer network structure generated in the presence of thrombin and/or FXIIIa.

The results obtained from this project were published in 2011 in Biomaterials 32(19): 4406-14 [144].

4.1. Experimental Design

Based on literature and our experience (see Chapter 3), the knob 'A' mimic, GPRP, has been shown to exhibit the most reproducible binding to fibrinogen pockets under different experimental conditions. This study continues to employ GPRP as the fibrin(ogen)-binding peptide and introduces GPSP as the non-binding control. The most commonly used PEG structures in current FDA-approved PEG conjugates are monofunctional linear PEG chains with sizes ranging from 5 kDa to 20 kDA, and branched PEG chains 40 kDa in size [69]. In keeping with this working range, the following maleimide-activated PEG varieties were used: 2, 3.5, 5, 7.5 kDa bifunctional MAL_2-PEG, and 2, 10, 20 kDa tetrafunctional MAL_4-PEG.

The effect of these multivalent knob-PEG conjugates on fibrin polymerization, network morphology, and fibrinolysis was examined in relation to the unconjugated knob peptide. The impact of these multivalent conjugates on FXIIIa crosslinking and clot stiffness was also evaluated.

4.2. Materials and Methods

4.2.1. Sulfhydryl-Maleimide Conjugation

Sulfhydryl-containing cysteine-terminated peptides (GPRPAAC and the control peptide GPSPAAC) were custom-ordered from Genscript (Piscataway, NJ) in pre-aliquoted and lyophilized form. Maleimide-activated components used were namely, 2, 3.5, 5, 7.5 kDa maleimide-PEG-maleimide, and 2, 10, 20 kDa 4-arm PEG maleimide (sourced from JenKem Technology, Allen, TX; 2 kDa 4-arm PEG from Creative PEGWorks, Winston Salem, NC).

The conjugation buffer comprised 100 mM phosphate buffer pH 7.2, 150 mM sodium chloride, 10 mM EDTA. Desired quantities of sulfhydryl-containing peptide and the maleimide-activated components were reacted in a 1.5:1 molar ratio and the reaction was monitored using Ellman's assay for free sulhydryls (Thermo Fisher Scientific, Waltham, MA). Reactions were generally complete within 2 h. Excess unconjugated peptide was removed from the conjugated product using Slide-A-Lyzer dialysis cassettes (Thermo Fisher Scientific) and deionized water as the exchange buffer. The product was aliquoted, then lyophilized and quantified.

The lyophilized conjugates were resuspended in water before use and analyzed for their PEG and amine components. PEG was quantified using the method of Sims and Snape and modified for a 96-well format [145]. Briefly, 80 μL of sample and 20 μL of 5% barium chloride solution (in 1 M HCl) were added sequentially to each well of a 96-well plate. 10 μL 0.1 N iodine solution was then added before taking the absorbance readings at 535 nm (Abs_{535nm}). 10 kDa PEG (Sigma, St Louis, MO) was used as the

calibration standard. Amines were quantified using the CBQCA assay kit (Invitrogen, Carlsbad, CA) with the respective peptides used to generate the standard curve.

4.2.2. Fibrin Polymerization and Degradation

Enzyme-catalyzed polymerization of mixtures of fibrinogen and $GPRP_n$-PEG, or control $GPSP_n$-PEG, conjugates was initiated in 96-well plates. Briefly, 10 μL of the conjugate and 40 μL of 2.5 mg/mL human fibrinogen (FIB-3; Enzyme Research Laboratories, South Bend, IN) were pre-incubated for 1 h. Following, 50 μL of 0.5 NIHU/mL human α-thrombin and 10 Loewy units/mL human FXIIIa (both from Enzyme Research Laboratories) were added to the fibrinogen mixture to initiate polymerization. The turbidity (Abs_{350nm}) of the mixtures was followed using a plate reader. To determine the amount of unclotted protein, the isolated clot liquor was analyzed for total soluble protein using the Quant-iT protein assay (Invitrogen). To obtain clot degradation profiles, 100 μL 0.01 mg/mL human plasmin (Enzyme Research Laboratories) was overlaid on the 100 μL clots in 96-well plates and agitated on the Eppendorf MixMate at 400 rpm. Turbidity readings and 5 μL sample aliquots were taken at 1, 3, 5, 7, 9-h timepoints for analysis of total soluble protein using the Quant-iT protein assay. All reactions were conducted in buffer comprising 25 mM Tris-HCl pH 7.5, 137 mM NaCl, 5 mM $CaCl_2$.

4.2.3. Crosslinking Assays

Coomassie-stained SDS-PAGE gels and Western blots were used to quantitatively and qualitatively assess the extent of FXIIIa-catalyzed crosslinking in fibrin clots. Briefly, mixtures of fibrinogen and $GPRP_n$-PEG, or control $GPSP_n$-PEG, conjugates were prepared as described in the turbidity assays. The mixtures were allowed to polymerize following enzyme addition for 1 h, followed by boiling for 5 min to quench further

reaction. An equal volume of 2X Laemmli buffer (Biorad, Hercules, CA) containing 5% beta-mercaptoethanol was added to the clots, which were further vortexed and boiled to ensure complete dissolution. Samples were electrophoresed on 10% SDS-PAGE gels. SimplyBlue (Invitrogen) was used for Coomassie-staining of the gels following the manufacturer's protocol. The stained gel was imaged using the Odyssey infrared imaging system (LI-COR, Lincoln, NE) in the 700 nm channel. The bands corresponding to the monomeric α, β, and γ chains on the Coomassie-stained gels were quantified using ImageJ, normalized against the non-crosslinkable β chain in each sample, then normalized against the uncrosslinked negative control samples run on each gel.

For Western blots, the proteins were transferred to Immobilon-FL PVDF membranes (Millipore, Billerica, MA) overnight. Following, the membranes were blocked with IR Blocking Buffer (Rockland, Gilbertsville, PA) and probed separately for the fibrinogen α chain (primary: sc-33917 from Santa Cruz Biotechnology, Santa Cruz, CA; secondary: IRDye 800CW donkey anti-goat IgG from LI-COR) and fibrinogen γ chain (primary: sc-133157 from Santa Cruz Biotechnology; secondary: IRDye 680LT donkey anti-mouse IgG from LI-COR). The membrane was stripped between blotting by incubating with 6 M guanidine hydrochloride at 65°C until the antibody fluorescent signal was eliminated.

4.2.4. Rheological Assays

The Bohlin CVO 120 high resolution rheometer (Malvern Instruments, Westborough, MA) with plate-plate geometry was used to assess the viscoelastic characteristics of fibrin clots at room temperature. Briefly, mixtures of fibrinogen and $GPRP_n$-PEG, or control $GPSP_n$-PEG, conjugates were prepared as described in the

turbidity assays. Following the addition of thrombin and FXIIIa, the solutions were mixed quickly by pipetting and immediately added to the bottom plate of the rheometer. The upper plate (14 mm diameter) was immediately lowered to a gap size of 1 mm and the mixture was allowed to polymerize for 1 h in a humid chamber. Following, oscillating measurements were taken over a frequency range of 0.05 to 1.0 Hz at a constant strain of 0.5%. Each condition was tested with at least 8 samples.

4.2.5. Confocal Imaging

Fluorescently-labeled fibrinogen was prepared by conjugation to the amine-reactive Alexa Fluor 555 succinimidyl ester (Invitrogen) following the manufacturer's recommendation. Clots containing 10% labeled fibrinogen were imaged using the Zeiss 510 laser scanning confocal microscope (Carl Zeiss, Thornwood, NY). Mixtures of fibrinogen and $GPRP_n$-PEG, or control $GPSP_n$-PEG, conjugates were prepared as described in the turbidity assays. Following the addition of thrombin and FXIIIa, the solutions were mixed quickly by pipetting and immediately added to a glass slide. The mixture was overlaid with a glass coverslip supported by a 0.3 mm spacer. The open ends of the chamber were sealed with nail polish and the mixture allowed to polymerize within the chamber for 1 h before imaging. A 20-section Z-stack (10 μm slices) of the 89×89 μm field under the 100× objective was captured for reconstruction of the 3D network structure. At least 3 clots were formed independently for each condition, with 4 random samplings taken per clot.

4.2.6. Statistical Analysis

All graphs and analyses were prepared in GraphPad PRISM 5.0. Results are presented as mean ± SD. Statistical comparisons for conjugate titration sets were based

on one-way ANOVA using the Tukey post-hoc test for pair-wise comparisons with significance defined by $p < 0.05$. Comparisons of conjugates and their paired controls (for crosslinking and rheological data) were made using the Student's t-test.

4.3. Knob-PEG Preparation

The initial phase of this work involved establishing a robust scheme for conjugate production and characterization. In particular, the preparation of PEGylated peptides posed special problems due to the small difference in molecular weight between the unreacted PEG (several thousand Da) and the conjugated PEG (with an additional 671 Da for GPRPAAC or 602 Da for GPSPAAC), leading to purification problems.

4.3.1. Conjugate Production

The sulfhydryl-maleimide reaction is a highly efficient reaction resulting in a stable thioether linkage when carried out at pH 6.5-7.5. The maleimide-activated PEG products we purchased generally carried specifications of >95% purity, <1.03 polydispersity, and >90% substitution. Similarly, the synthetic cysteine-containing peptides purchased were of >98% purity and stable in the reduced form (verified in-house using electrospray ionization mass spectrometry or ESI-MS).

The reaction conditions specified a slight molar excess of peptide over maleimide such that the reaction goes to completion. The unreacted peptide was then removed via extensive dialysis into water, bypassing the more complex purification of the peptide-PEG conjugate from unreacted PEG. The dialyzed product was then aliquoted, lyophilized and stored.

4.3.2. Conjugation Characterization

The lyophilized product was resuspended in water and analyzed for protein and PEG concentration. The presence of the conjugated PEG moiety interferes with most commercially available protein quantitation assays (e.g. Pierce's bicinchoninic assay, Invitrogen's Quant-iT^{TM} assay) but results from the detergent-tolerant CBQCA assay were the most consistent, showing a reproducible overestimation of peptide quantity in the presence of the peptide-PEG conjugate (Table 1). It is also duly noted that the CBQCA assay is sulfhydryl-sensitive and should only be used for the quantitation of conjugates following extensive dialysis to remove the excess unreacted peptide.

Table 1. Fraction of peptide detected by the CBQCA assay

Mixture composition	Fraction of peptide[a] (2 h post-mixing)	Fraction of peptide[a] (24 h post-mixing)
PEG + GPRP	0.988	0.999
PEG + GPRPAAC	0.604	0.843
MAL-PEG + GPRP	1.128	1.142
MAL-PEG + GPRPAAC	1.733	1.786

[a] Fraction of peptide detected normalized to peptide standards in the absence of any PEG moieties.

PEG was quantified using the method of Sims and Snape employing barium chloride and iodine solution [145]. An alternative method proposed by Ghosh employing the extraction of ammonium ferrothiocyanate into chloroform [90, 146] was attempted initially but led to inconsistent results, particularly when PEG was conjugated to the charged GPRPAAC peptide. Attempts to troubleshoot the protocol, including the addition of proteases to digest the conjugated peptide or buffer substitution to neutralize the peptide charges, failed to yield more reproducible data. In contrast, the results from the Sims and Snape method were consistent regardless of the peptide used (Table 2).

Table 2. Characterization of peptide-PEG conjugates

Conjugate	% PEG[a] yield	% Peptide[b] yield	Peptide : PEG
2 kDa $GPRP_2$-PEG	89	190	6.41
2 kDa $GPSP_2$-PEG	62	14	0.71
3.5 kDa $GPRP_2$-PEG	88	199	6.75
3.5 kDa $GPSP_2$-PEG	80	31	1.18
5 kDa $GPRP_2$-PEG	66	188	8.47
5 kDa $GPSP_2$-PEG	69	30	1.30
7.5 kDa $GPRP_2$-PEG	63	198	9.35
7.5 kDa $GPSP_2$-PEG	59	28	1.44
2 kDa $GPRP_4$-PEG	57	73	3.83
2 kDa $GPSP_4$-PEG	57	60	3.18
10 kDa $GPRP_4$-PEG	77	385	14.92
10 kDa $GPSP_4$-PEG	61	52	2.57
20 kDa $GPRP_4$-PEG	61	336	16.52
20 kDa $GPSP_4$-PEG	61	51	2.47

[a] PEG quantified by the method of Sims and Snape, calibrated against the respective maleimide-activated PEG reagent.
[b] Peptide quantified by the Invitrogen CBQCA amine assay, calibrated against GPRP or GPSP respectively.

Interestingly, the CBQCA assay appeared to overestimate the peptide content for the $GPRP_n$-PEG conjugates but not the $GPSP_n$-PEG conjugates. Indeed, if the results for the $GPSP_n$-PEG conjugates were true, it would imply that we were only able to achieve approximately 65% conjugation, instead of the 90% conjugation expected following complete reaction of the ~90% substituted maleimide-activated PEG. Due to uncertainty in the interpretation for the CBQCA quantitation, the results from the Sims and Snape PEG quantitation method were used for the quantitation of conjugates used in this work. In doing so, we have assumed that the PEG conjugates were 100% functionalized and that the conjugation to GPRPAAC or GPSPAAC was 100% complete.

4.4. Thrombin Clotting Time and Clot Turbidity

Fibrin clot structure can be inferred from turbidity profiles of clotting mixtures of fibrinogen and thrombin [46]. In general, thicker fibrin bundles are associated with turbid clots whereas thinner fibrin bundles result in clear or glassy clots. A clear mixture can also be indicative of the absence of fibril assembly and clot formation, such as in the

presence of large excess of knob 'A' mimics, notably GPRP. The use of real-time turbidity measurements of clotting mixtures in conjunction with end-point protein measurements allowed a rapid screen of clotting mixtures to identify mixture compositions that perturb, but not completely inhibit, the polymerization process.

4.4.1. Characterizing Fibrin Clot Formation

To establish the basic analytical parameters for fibrin clot formation, we assessed the clotting characteristics of fibrinogen in the presence of the control materials – peptides GPRP and GPSP, and non-functionalized PEG. As expected, the presence of the peptide GPRP reduced clot turbidity in a dose-dependent manner (Figure 7A), corroborating the early findings of Doolittle et al. [139]. In contrast, our control peptide, GPSP, did not significantly impact the turbidity profile of the clotting mixture at the corresponding dosages (Figure 7B). Interestingly, the presence of large amounts (100:1 molar ratio PEG-to-fibrinogen) of 10 kDa PEG amplified the turbidity of the clotting mixtures (Figure 7C). We note that early studies by Carr et al. found that dextran T70, poloxamer 188 and poloxamer 407 increased fibrin fiber size and clot turbidity [147-149] and that PEG may be acting in a similar fashion.

To further investigate this phenomenon, the initial (solid symbols) and final (open symbols) turbidity values of the different mixtures were plotted (Figure 7D), indicating that the presence of PEG increased the final absorbance but not the initial absorbance of the mixture, despite the 1 h preincubation step prior to the addition of clotting enzymes, thrombin and FXIIIa.

The clotting half-time, defined as the time required for the clot to reach half the final turbidity value, was calculated from the clotting curves (Figure 7E). The results

indicate that a 100:1 molar excess of GPRP not only reduced the overall turbidity but also increased the clotting half-time of the mixture. While PEG significantly increased mixture turbidity, it did not have a statistically significant impact on clotting half-time.

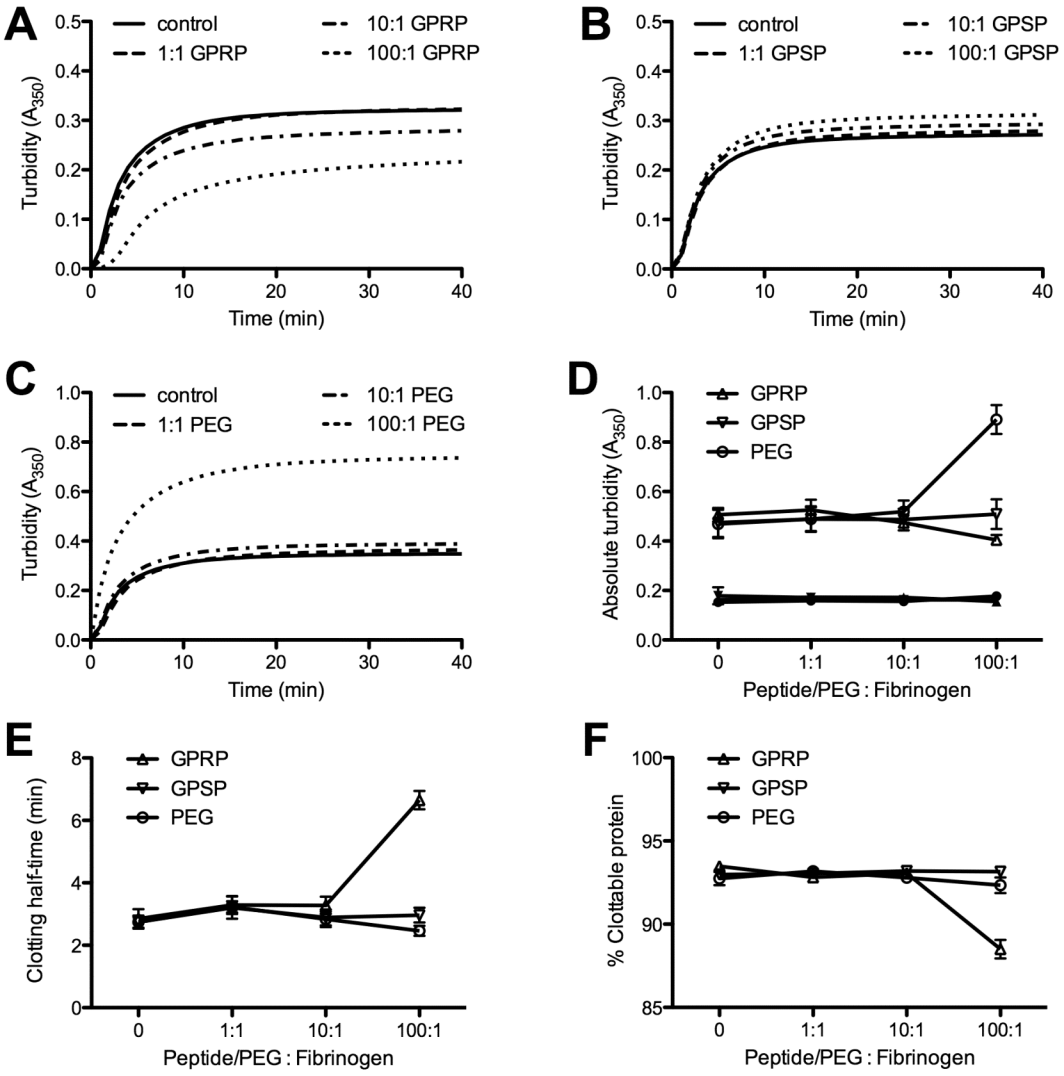

Figure 7. Fibrin polymerization parameters (using 1 mg/mL fibrinogen, 0.25 NIHU/mL thrombin, 5 Loewy units/mL FXIIIa) in the presence of GPRP, GPSP and PEG. Representative turbidity profiles in the presence of GPRP (A), GPSP (B) and PEG (C) at 1:1, 10:1 and 100:1 peptide/PEG-to-fibrinogen molar ratios. (D) Plot of absolute initial (solid symbols) turbidity values and final (empty symbols) turbidity values from the entire experimental data set (n = 6). (E) Clotting half-times, defined as the time required for the clot to reach half the final turbidity value (at 1 h following enzyme addition), calculated from the turbidity curves. (F) The percentage of clottable protein, back-calculated from the amount of soluble protein in the clot liquor extracted from compressed clots, normalized against controls without clotting enzymes.

The fibrin clot was then carefully compressed and the concentration of soluble protein in the liquid fraction (i.e. clot liquor) was assessed. The amount of clotted protein was back-calculated using the respective controls and reported as % clottable protein (Figure 7F). As expected, the results indicate that GPRP, but not the control GPSP, reduced the % clottable protein of the mixtures. Intriguingly, a 100:1 excess of PEG of the mixture had no significant effect on the overall clottability of the mixture despite the increased turbidity of the resulting clot. Further experiments carried out with the knob-PEG conjugates were therefore limited to conjugate-to-fibrinogen molar ratios of 10:1 and below to minimize any confounding effects arising from higher PEG concentrations.

4.4.2. Mixture Clottability and Clotting Half-Time

The effect of $GPRP_n$-PEG and $GPSP_n$-PEG conjugates on fibrin clot formation was assessed at 1:10, 1:1 and 10:1 conjugate-to-fibrinogen molar concentrations. Clots were formed at all three dosages for all the conjugates evaluated in this work. However, the tenuous clots formed at the highest $GPRP_n$-PEG dosages (open symbols/dashed lines) i.e. 10:1, had a comparatively low clottability of 70-80% compared to their respective $GPSP_n$-PEG controls (solid symbols/solid lines) with clottability above 90% (Figure 8A, B). Moreover, the clotting half-times of these mixtures were significantly longer than the controls (Figure 8C, D). At a 1:1 ratio, the clotting half-times for the $GPRP_2$-PEG conjugates were not significantly perturbed and the overall turbidity profiles were similar in shape to that of the controls [144]. A similar phenomenon was observed for the 2 kDa $GPRP_4$-PEG conjugate. In contrast, the profiles for the 10 and 20 kDa $GPRP_4$-PEG conjugates were significantly flatter, nearly doubling the apparent clotting half-time.

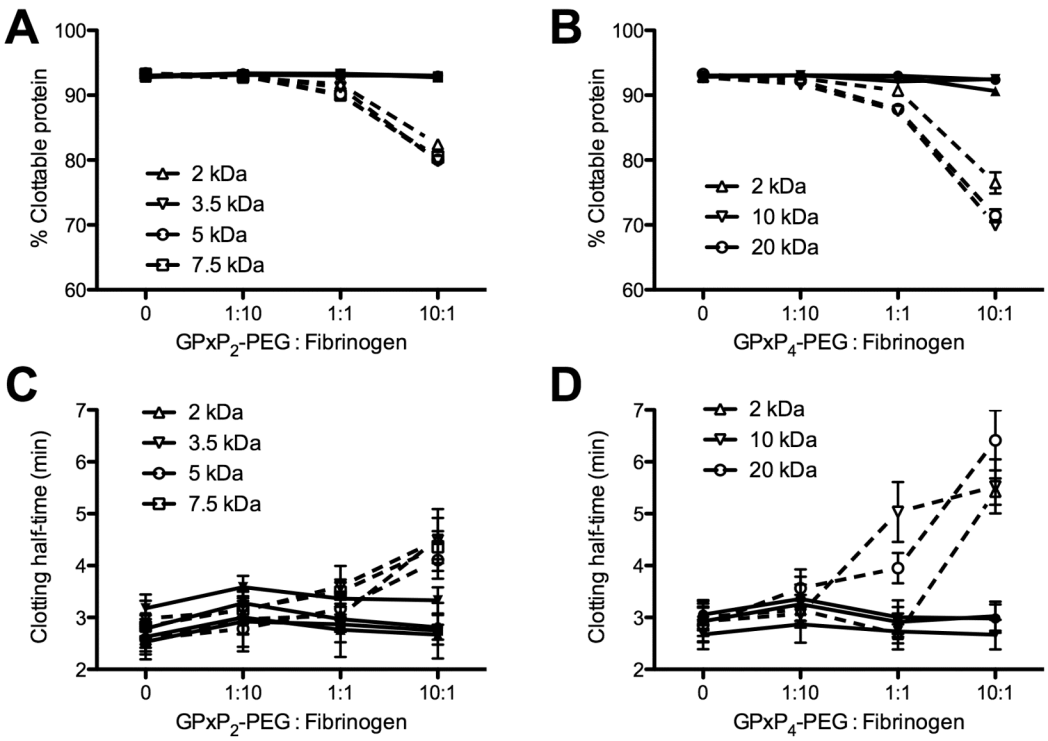

Figure 8. Fibrin polymerization parameters in the presence of knob-PEG conjugates. % Clottable protein of hydrogels formed in the presence of $GPxP_2$-PEG (A) and $GPxP_4$-PEG conjugates (B) at 1:10, 1:1 and 10:1 conjugate-to-fibrinogen molar ratios. Clotting half-times in the presence of $GPxP_2$-PEG (C) and $GPxP_4$-PEG conjugates (D). Solid symbols and lines correspond to data for the $GPSP_n$-PEG control conjugates; empty symbols and dashed lines correspond to data for the $GPRP_n$-PEG conjugates.

4.4.3. Turbidity Measurements

A closer examination of the turbidity profiles indicate that the final absorbances of mixtures at a 10:1 conjugate-to-fibrinogen ratio were consistently lower than the controls, possibly indicative of both reduced overall clottability and structural changes due to the increased clotting half-time. A notable result was observed at a 1:1 ratio, with the 2 kDa $GPRP_2$-PEG conjugate increasing the final turbidity, and the 5 and 7.5 kDa $GPRP_2$-PEG conjugates reducing the overall turbidity (Figure 9A). Similarly, the presence of the 2, 10 and 20 kDa $GPRP_4$-PEG conjugates at a 1:10 ratio slightly

increased the overall absorbance of the mixtures although the opposite phenomenon was observed at the 1:1 and 10:1 conjugate-to-fibrinogen ratios (Figure 9B).

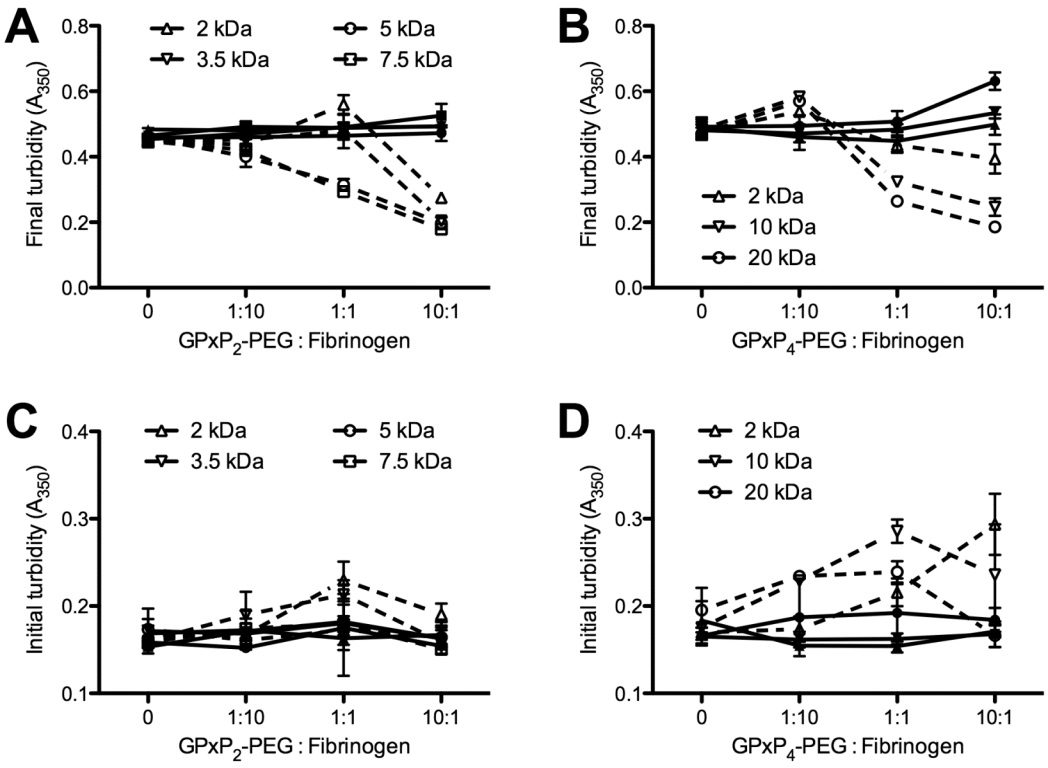

Figure 9. Turbidity of hydrogels formed in the presence of knob-PEG conjugates. Final turbidity values of hydrogels formed in the presence of $GPxP_2$-PEG (A) and $GPxP_4$-PEG conjugates (B) at 1:10, 1:1 and 10:1 conjugate-to-fibrinogen molar ratios. Initial turbidity values of hydrogels formed in the presence of $GPxP_2$-PEG (C) and $GPxP_4$-PEG conjugates (D). Solid symbols and lines correspond to data for the $GPSP_n$-PEG control conjugates; empty symbols and dashed lines correspond to data for the $GPRP_n$-PEG conjugates.

A plot of initial mixture turbidities prior to the addition of clotting enzymes showed that the pre-incubation of the $GPRP_n$-PEG conjugates with fibrinogen generally had the greatest impact on mixture turbidity at a 1:1 ratio (Figure 9C, D). This trend was not observed for the corresponding $GPSP_n$-PEG controls. The increased light scattering at this particular ratio is suggestive of fibrinogen assembly arising from knob:hole

interactions since each fibrinogen has up to 4 available holes for binding to the 2-arm and 4-arm conjugates. Further experiments were therefore pursued using a 1:1 conjugate-to-fibrinogen molar concentration.

4.5. FXIIIa-Mediated Crosslinking

It has been shown that the crosslinking activity of FXIIIa is heavily influenced by fibrin assembly and fiber orientation [41, 42, 54]. Since the clot turbidity results suggest differences in fibril organization in clotting mixtures, the presence of knob-PEG conjugates may consequently alter the crosslinking pattern of the fibrin(ogen) chains within the clot.

4.5.1. Quantitation of α and γ Chain Crosslinking

In general, $GPRP_n$-PEG conjugates appeared to reduce the extent of α chain crosslinking compared to their respective $GPSP_n$-PEG controls, particularly in the case of the 3.5 kDa $GPRP_2$-PEG and 20 kDa $GPRP_4$-PEG (Figure 10A). In contrast, the extent of γ chain crosslinking was not perturbed by the presence of knob-PEG conjugates under the clotting conditions used (Figure 10B). The presence of unconjugated peptide (denoted GPxP) did not perturb the extent of α and γ chain crosslinking.

For further clarification of these results, identical experiments were run in the absence of thrombin and with a large excess of FXIIIa (50 Loewy units/mL) to compensate for its reduced activity in the absence of thrombin. As expected, the results indicate that the presence of the $GPRP_n$-PEG conjugates increased the extent of both α and γ chain crosslinking, notably in the presence of the 10 kDa $GPRP_4$-PEG conjugate (Figure 10C, D). The trend in the % crosslinked chains suggests a size dependency wherein the optimum PEG size for promoting FXIIIa crosslinking in the absence of

thrombin is around 3.5 kDa for $GPRP_2$-PEG and 10 kDa for $GPRP_4$-PEG. These particular conjugates were found to reduce the % α chain crosslinked in the presence of thrombin while smaller conjugates such as the 2 kDa $GPRP_2$-PEG and 2 kDa $GPRP_4$-PEG did not significantly perturb the extent of crosslinking of both α and γ chains.

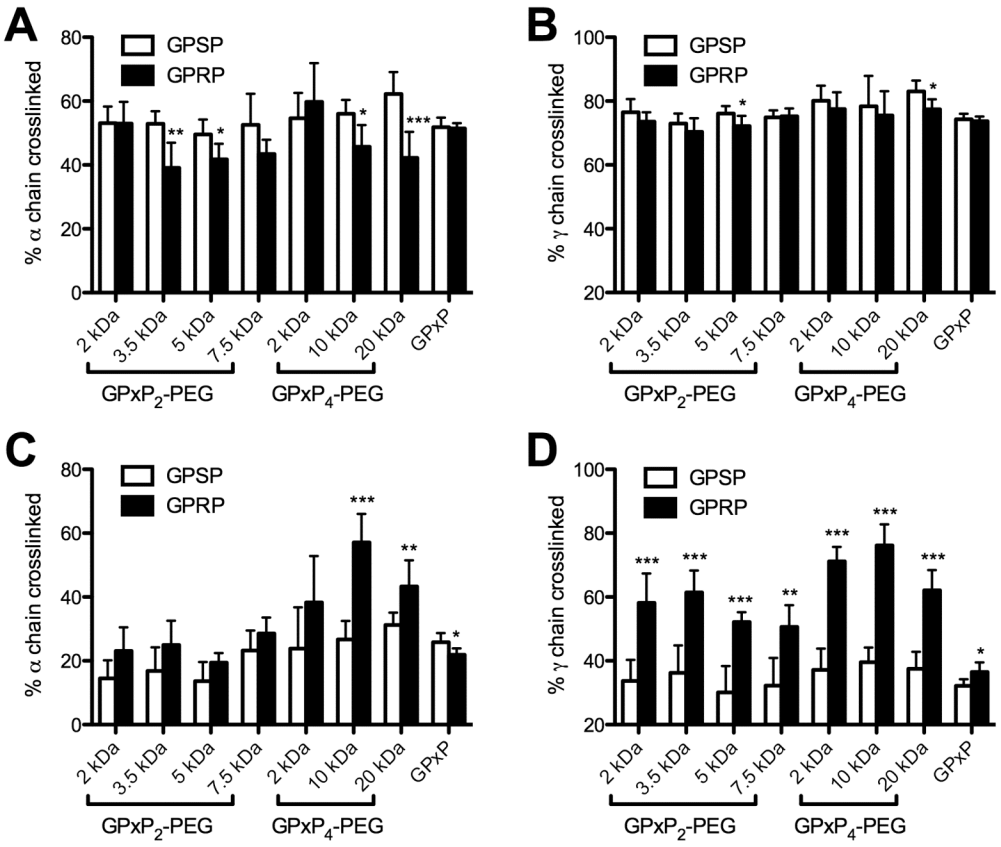

Figure 10. Densitometry analysis of fibrin(ogen) chain species in hydrogels formed in the presence of knob-PEG conjugates at a 1:1 conjugate-to-fibrinogen molar ratio. Bands corresponding to α, β, and γ chains on the Coomassie-stained gels were quantified using ImageJ, normalized against the non-crosslinkable β chain in each sample, then normalized against the uncrosslinked negative controls run on each gel. % crosslinked α chain (A) and γ chain (B) in hydrogels formed in the presence of both thrombin and FXIIIa. % crosslinked α chain (C) and γ chain (D) in hydrogels formed in the presence of 50 Loewy units/mL FXIIIa only. Indicated statistical significance calculated from two-tailed t-tests of $GPRP_n$-PEG conjugates against their respective $GPSP_n$-PEG controls (n ≥ 6).

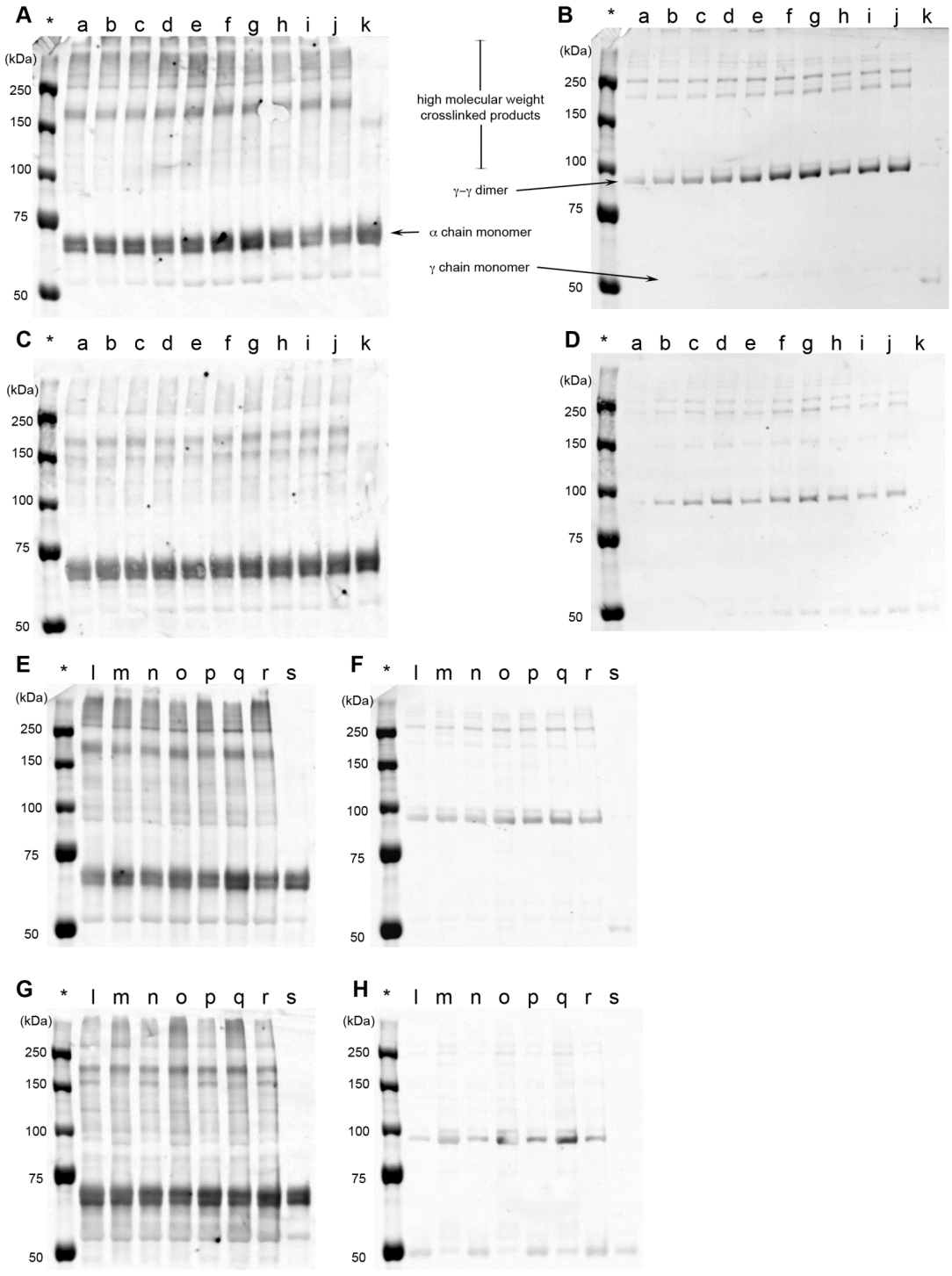

Figure 11. Western blots of solubilized hydrogels formed in the presence of knob-PEG conjugates at a 1:1 conjugate-to-fibrinogen molar ratio. The hydrogels formed under the designated conditions were run on reducing 7.5% SDS-PAGE gels, transferred onto PVDF membranes and blotted sequentially with anti-α and anti-γ chain antibodies. (A,B) Blots illustrating the crosslinking pattern in the presence of GPxP$_2$-PEG conjugates and both clotting enzymes (0.25 NIH U/mL thrombin, 5 Loewy units/mL factor XIIIa). (C,D) Blots illustrating the crosslinking pattern in the presence of GPxP$_2$-PEG conjugates and factor XIIIa (50 Loewy units/mL) only. (E,F) Blots illustrating the

crosslinking pattern in the presence of $GPxP_4$-PEG conjugates and both clotting enzymes. (G,H) Blots illustrating the crosslinking pattern in the presence of $GPxP_4$-PEG conjugates and factor XIIIa only. Lane assignments are: (*) Biorad Precision Plus Protein All Blue Standards, (a) GPRP, (b) GPSP, (c) 2 kDa $GPRP_2$-PEG, (d) 2 kDa $GPSP_2$-PEG, (e) 3.5 kDa $GPRP_2$-PEG, (f) 3.5 kDa $GPSP_2$-PEG, (g) 5 kDa $GPRP_2$-PEG, (h) 5 kDa $GPSP_2$-PEG, (i) 7.5 kDa $GPRP_2$-PEG, (j) 7.5 kDa $GPSP_2$-PEG, (k,s) no enzyme controls, (l) positive (no conjugate) control, (m) 2 kDa $GPRP_4$-PEG, (n) 2 kDa $GPSP_4$-PEG, (o) 10 kDa $GPRP_4$-PEG, (p) 10 kDa $GPSP_4$-PEG, (q) 20 kDa $GPRP_4$-PEG, (r) 20 kDa $GPSP_4$-PEG.

4.5.2. Identification of Crosslinked Species

In attempt to uncover the reason behind the reduced α chain crosslinking in the presence of the $GPRP_n$-PEG conjugates, the electrophoresced samples were transferred to PVDF membranes and probed sequentially with anti-α and anti-γ chain antibodies. The use of both antibodies simultaneously in a multiplexed setup was not considered as we expected to observe the presence of α-γ hybrid crosslinked products. Moreover, the anti-α chain antibody appeared to be weaker and less specific compared to the anti-γ chain antibody, which could also bias the readouts.

Interestingly, Western blots for the α and γ chains did not suggest any striking differences in the crosslinking pattern obtained in the presence of the conjugates as compared to the controls (Figure 11).

4.6. Network Morphology

Fibrin networks have been observed using transmission electron microscopy (TEM) [25] and scanning electron microscopy (SEM) [46, 47]. While these techniques offer excellent resolution down to the nanometer-scale, the sample preparation required for EM in general distorts clot structure due to the high water content of these hydrogels. Instead, we decided to employ confocal microscopy for the visualization of fluorescently-labeled fibrin fibers formed in the presence of the knob-PEG conjugates. While the

resolution of the confocal microscope is only on the micrometer-scale, the advantages of being able to view a hydrated gel on different focal planes (creating a z-stack of images), and the ability to view clot formation and degradation in real time has led to increasing use of this technique in the field [135, 150]. The structure of the fibrin networks formed in the presence the knob-PEG conjugates were also analyzed in relation to their rheological properties.

4.6.1. Confocal Imaging

Using 10% labeled fibrinogen with a final fibrinogen concentration of 1 mg/mL, network formation was clearly visible under control conditions (Figure 12A). In the presence of a 100-molar excess of non-functionalized PEG, where mixture turbidity was significantly increased (Figure 7C), the fibers were thicker and more clearly defined as compared to the control (Figure 12B). Conversely, at a 10:1 peptide-to-fibrinogen molar dosing, a more fine-meshed network was formed in the presence of GPRP (Figure 12C) as compared to GPSP (Figure 12D). The noisy background appears to be an artifact arising from the higher osmolarity of these mixtures due to the added peptide since all the images shown were processed using identical gain settings.

Focusing on the network structure of clots formed in the presence of an equimolar dosing of knob-PEG conjugate, it was noted that clots formed in the presence of the $GPSP_n$-PEG conjugates were similar to the control (compare Figure 12A with 6F, H, J, L, N, P, R), while very clear conjugate size-dependent trends were observed with the $GPRP_n$-PEG conjugates. Notably, the fibers formed in the presence of 2 kDa $GPRP_2$-PEG (Figure 12E) and 2 kDa $GPRP_4$-PEG (Figure 12M) appeared to be thicker and straighter. The networks formed in the presence of 3.5 kDa and 5 kDa $GPRP_2$-PEG (Figure 12G, I)

appeared to resemble their respective $GPSP_2$-PEG controls (Figure 12H, J) the closest, but with the inclusion of tight nodules of proteins dispersed throughout the matrix. In the presence of the larger $GPRP_n$-PEG conjugates – 7.5 kDa $GPRP_2$-PEG, 10 kDa and 20 kDa $GPRP_4$-PEG – the networks appeared to comprise ultrathin and highly-branched fibers nearing the resolution limits of the microscope (Figure 12K, O, Q). These results corroborate the significantly decreased clot turbidities of these mixtures despite their maintained clottability as determined by clottable protein measurements. Tight nodules of protein continued to be visible in these matrices, but not in their respective controls (Figure 12L, P, R), suggesting that these are clusters of $GPRP_n$-PEG-bound fibrinogen/fibrin.

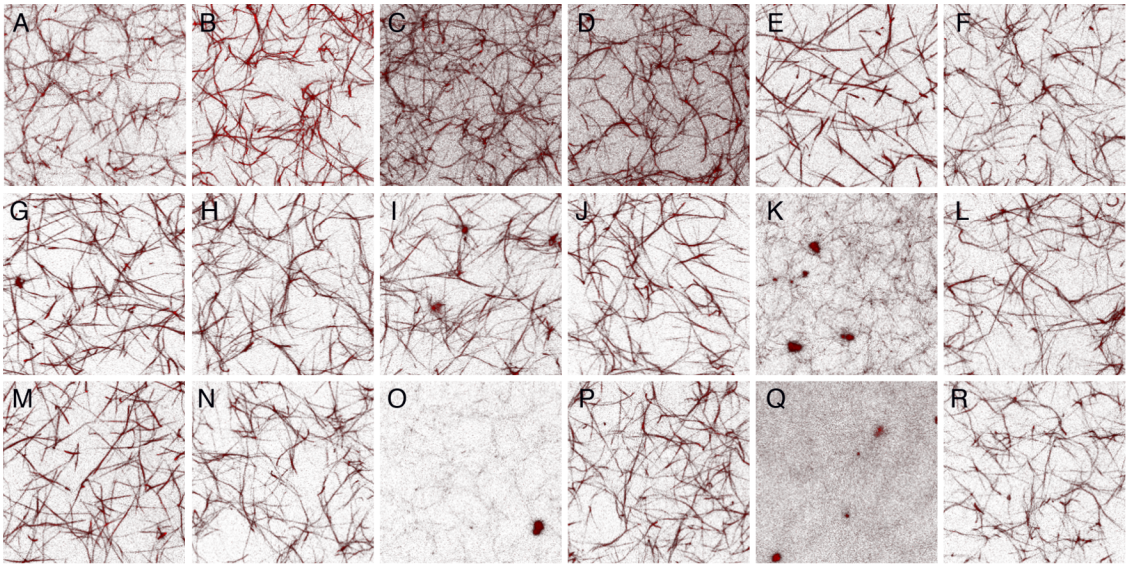

Figure 12. Confocal images of hydrogels. Hydrogels were formed within sealed chambers on glass slides and imaged using laser scanning confocal microscopy. Images were rendered from 45×45×10 µm slices. (A) Control clot (1 mg/mL fibrinogen, 0.25 NIH U/mL thrombin, 5 Loewy units/mL factor XIIIa). (B) Representative network structure formed in the presence of 100:1 molar ratio of PEG-to-fibrinogen. (C) Network structure in the presence of 10:1 molar ratio of GPRP-to-fibrinogen. (D) Network structure in the presence of 10:1 molar ratio of GPSP-to-fibrinogen. Subsequent paired images are of hydrogels formed in the presence of $GPRP_n$-PEG or $GPSP_n$-PEG conjugates at a 1:1 conjugate:fibrinogen molar ratio as follows: 2 kDa $GPxP_2$-PEG (E,F), 3.5 kDa $GPxP_2$-PEG (G,H), 5 kDa $GPxP_2$-PEG (I,J), 7.5 kDa $GPxP_2$-PEG (K,L), 2 kDa $GPxP_4$-PEG (M,N), 10 kDa $GPxP_4$-PEG (O,P), 20 kDa $GPxP_4$-PEG (Q,R).

4.6.2. Rheological Characterization

Utilizing the same clot preparation protocol, the rheological properties of these matrices were assessed using a parallel-plate setup in a constant-stress rheometer. The results suggest that the presence of the $GPRP_n$-PEG conjugates generally reduces the elastic modulus of the clot although the loss tangent, reflecting clot viscosity, was not significantly perturbed (Figure 13). Intriguingly, this trend in elastic moduli appears to recapitulate the trends seen in % α chain crosslinking (Figure 10A), despite the vast differences in network structure observed through confocal imaging (Figure 12), suggesting that clot mechanical properties under our experimental conditions is more dependent upon α chain crosslinking than network structure.

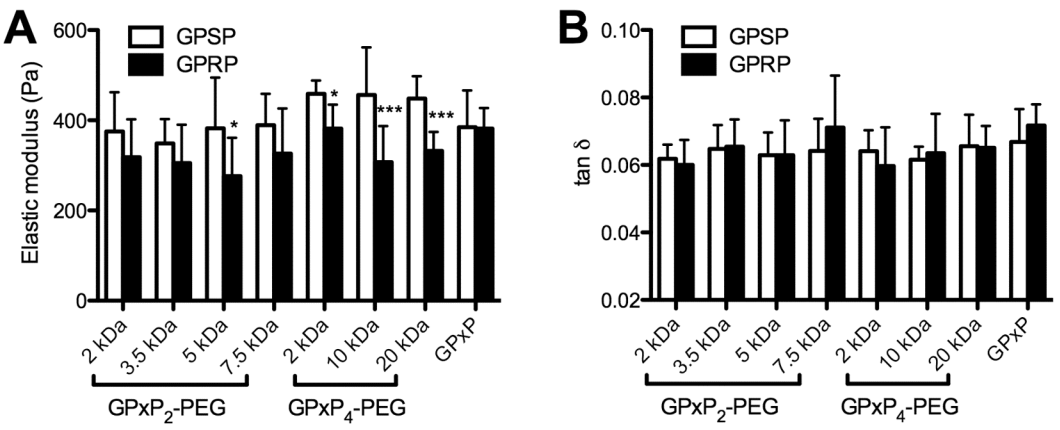

Figure 13. Rheological characterization of hydrogels formed in the presence of knob-PEG conjugates at a 1:1 conjugate:fibrinogen molar ratio. Elastic moduli (A) and loss tangents (B) were obtained from a sample size of at least n = 6 for each condition. Indicated statistical significance calculated from two-tailed t-tests of $GPRP_n$-PEG conjugates against their respective $GPSP_n$-PEG controls.

4.7. Plasmin-Mediated Clot Degradation

Degradation assays were carried out to demonstrate that the clots formed in the presence of the knob-PEG conjugates were still susceptible to normal fibrinolysis and clot degradation.

4.7.1. Clot Degradation

Clots formed in the presence of $GPxP_n$-PEG conjugates were overlaid with plasmin and incubated on a shaker incubator at room temperature. The results suggest that all the clots degraded at a constant rate such that the mixture turned clear in approximately 9 hours, regardless of the starting turbidity of the clot (Figure 14A,B). For a more objective comparison of the degradation rate across the different mixtures, the amount of soluble protein in the overlay was assessed. Interestingly, the results indicate that the degradation rate of the clots did not vary significantly across the different conjugates (Figure 14C,D). Similar results were obtained for clots formed in the presence of varying doses of the conjugates (data not shown).

The rate of exogenous plasmin-induced degradation reflects several parameters, including the diffusion of plasmin into the clot and fiber susceptibility to plasmin degradation. Altering fibrin network structure via fibrinogen and thrombin concentration, early studies have suggested that thin fibers are more resistant to plasmin digestion than thick fibers [59, 151]. While it is now generally accepted that clots comprising thin fibers are digested faster, it is clear that results from clot degradation assays are notoriously difficult to interpret (refer to section 2.1.5 for more detail).

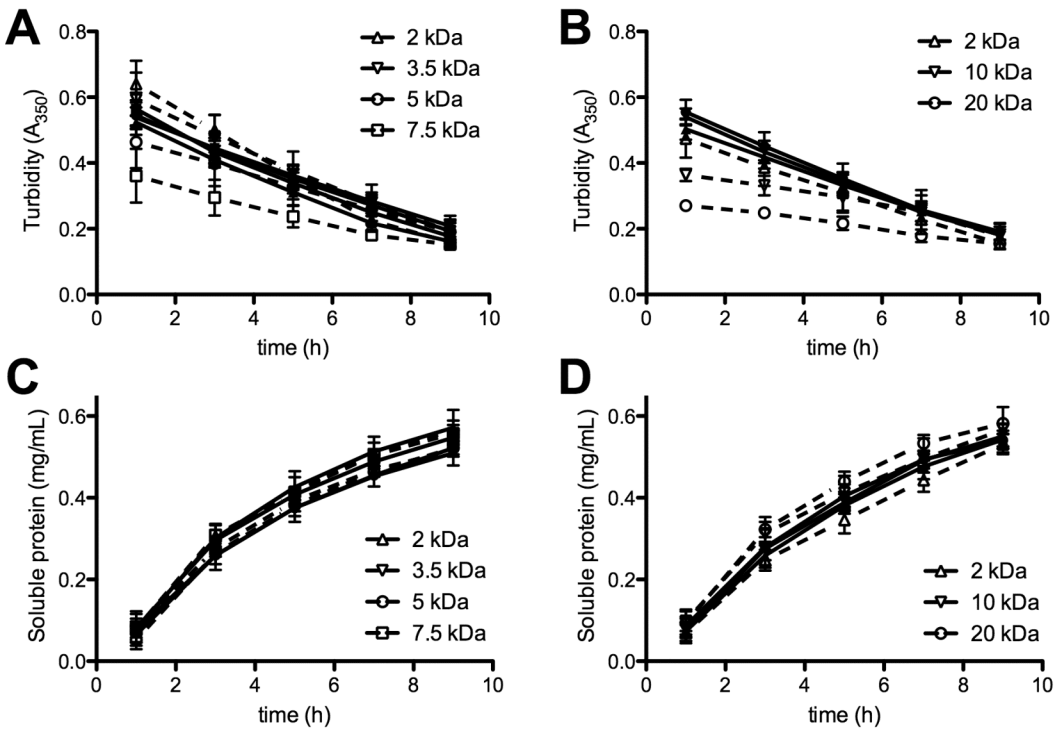

Figure 14. Degradation profiles of hydrogels formed in the presence of knob-PEG conjugates at a 1:1 conjugate-to-fibrinogen molar ratio upon the addition of an equal volume of 0.01 mg/mL (~0.06 μmol/min/mL) plasmin. Change in turbidity of hydrogels formed in the presence of $GPxP_2$-PEG (A) and $GPxP_4$-PEG conjugates (B). Quantitation of soluble protein in the plasmin overlay of hydrogels formed in the presence of $GPxP_2$-PEG (C) and $GPxP_4$-PEG conjugates (D).

4.8. Discussion and Conclusions

Past attempts have been made to alter fibrin matrix properties through the direct conjugation of PEG to fibrinogen, followed by UV-induced crosslinking of the functionalized PEG moieties, or the addition of thrombin to induce gelation [86, 89, 90]. In contrast, the objective of the this work was to explore the possibility of altering fibrin network architecture through the use of multivalent knob-PEG conjugates that actively engage fibrin polymerization holes, potentially facilitating alternative mechanisms of polymerization. In this work, we have identified various techniques of analyzing fibrin

hydrogels and successfully demonstrated the ability to modulate fibrin network structure through the addition of $GPRP_2$-PEG and $GPRP_4$-PEG conjugates.

By varying the size and valency of the knob-PEG conjugate added to fibrinogen, we were able to induce significant changes in fibrin network structure without sacrificing the overall clottability of the mixture. In particular, the results indicate that the larger conjugates used in this study favored the formation of fine highly branched networks, even as fibrinogen, conjugate, thrombin and FXIIIa molar concentrations were kept constant. Moreover, the networks formed were stable and did not appear to change following an overnight incubation (data not shown). This suggests that larger conjugates with long mobile PEG chain linkers between the peptide knobs were interfering with the lateral aggregation of the protofibrils to form thick fibers, possibly by non-directional orienting of fibrinogen molecules mediated by knob:hole interactions prior to thrombin addition. Moreover, the decrease in % α chain crosslinking also suggests that the large knob-PEG conjugates are inhibiting the lateral aggregation and alignment that favors this type of crosslinks.

Intriguingly, these networks are reminiscent of those formed in the presence of high thrombin concentrations, where rapid fibrinopeptide removal and formation of knob:hole interactions results in a fine-meshed but characteristically weaker clot [47, 152]. We speculate that the juxtaposition of the crosslinking sites during the preincubation of the knob-PEG conjugates with fibrinogen prior to the addition of thrombin had an analogous effect. These results would suggest that the design of bisbivalent or double-pincer knob-PEG linkers could favor the formation of coarse

networks with thick fibers by pinning the ends of the fibrinogen molecule together to form protofibril-like structures, even in the absence of clotting enzymes.

CHAPTER 5

TEMPERATURE MODULATION KNOB:HOLE INTERACTIONS

For this chapter, we propose the design of self-assembling mixed protein micelles that exhibit temperature-modulated avidities for fibrinogen though knob peptide display. Polymers that undergo phase transitions in response to changes in temperature and pH have been employed in the creation of a variety of stimuli-responsive conjugates, interfaces and nanocarrier systems [153-155]. Given the extensive background research conducted on ELPs and the development of several inspiring application-directed systems (see section 2.3), we also saw this as an opportunity to employ our expertise in recombinant protein engineering to test out some fundamental principles on ELP assembly and chain collapse.

We designed two ELP diblock proteins that should assemble to form a temperature-responsive peptide-displaying mixed micelle. These ELP diblock proteins share a common C-terminal "core" ELP block (ELP_A) but varying N-terminal "outer" ELP blocks (ELP_B, ELP_C), where $T_{t,A} < T_{t,B} < T_{t,C}$. We hypothesized that the two diblock proteins (ELP_B-ELP_A, ELP_C-ELP_A) would form mixed micelles upon the collapse of ELPA, then exhibit sequential collapse of the outer block, ELP_B, then ELP_C (Figure 15). This sequential collapse should allow the selective display and retraction of the outer end of the ELPB block as the mixed micelles are brought above and below $T_{t,B}$, without triggering coacervation of the entire mixture due to the hydration shell afforded by ELP_C.

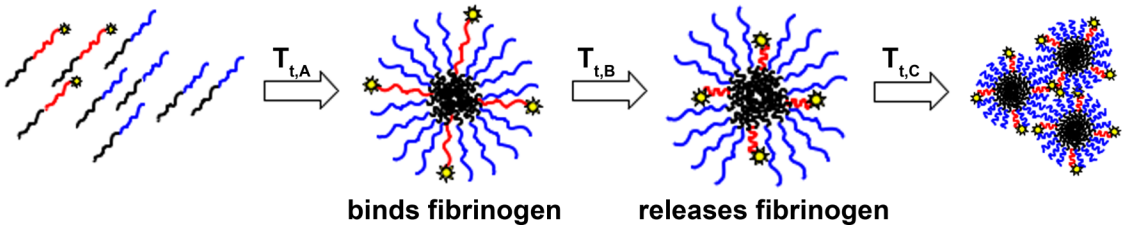

Figure 15. Schematic depicting the idealized assembly and collapse of the engineered ELP diblock proteins in response to increasing temperature (left to right). ELP_A in black, ELP_B in red, ELP_C in blue, where $T_{t,A} < T_{t,B} < T_{t,C}$. Below $T_{t,A}$, both ELP_B-ELP_A and ELP_C-ELP_A exist as free protein chains. Above $T_{t,A}$, the hydrophobic collapse of ELP_A results in the self-assembly of mixed micelles that display fibrinogen-binding peptides (in yellow). Above $T_{t,B}$, the collapse of ELP_B results in the retraction of fibrinogen-binding peptides and concomitant release of fibrinogen. Above $T_{t,C}$, the collapse of ELP_C results in aggregation of the proteins, forming micron-sized aggregates.

We expressed GPRP (or the control GPSP) sequence on the N-terminus of the ELP_B-ELP_A diblock protein to study the interaction of the knob-displaying mixed micelles with fibrinogen at different temperature regimes. We hypothesized that the formulated self-assembling peptide-displaying mixed micelles will display GPRP and bind to fibrinogen at ambient conditions (below $T_{t,B}$), but not at physiological conditions (above $T_{t,B}$) due to selective outer block collapse. Thus, the expectation is that the GPRP-displaying mixed micelles will perturb fibrin network formation at ambient temperatures but not at physiological temperatures, thus triggering normal clot formation *in vivo*.

The results obtained from this project were prepared in a manuscript for submission to Biomacromolecules.

5.1. Experimental Design

An ELP library containing the coding sequences for ELPs of different composition and lengths was created in order to optimize the transition characteristics of the ELP diblock proteins. In particular, these ELP diblock proteins had to form mixed micelles within the desired temperature regime (i.e. ambient temperatures).

ELP transitioning characteristics were evaluated using a protein aggregation assay. The mixed micelles were characterized using light scattering techniques and fluorescence resonance energy transfer (FRET). The avidity of these mixed micelles for fibrinogen was tested at different temperature regimes using several complementary experimental setups. The impact of these mixed micelles on fibrin polymerization dynamics was analyzed using turbidity and confocal imaging.

5.2. Materials and Methods

5.2.1. Development of pET15b Expression System

The entire segment coded between the NcoI and XhoI sites on the Novagen pET15b protein expression plasmid vector (Merck, Darmstadt, Germany) was replaced by a segment coding for the myc tag, the thrombin cleavage site LVPR$^{\downarrow}$GPRP (or control LVPR$^{\downarrow}$GPSP), and the SfiI restriction site (for inserting the ELP open reading frame). Briefly, the following sequences were ordered as 5' phosphorylated PAGE-purified primers from Invitrogen (Carlsbad, CA):

Name	Sequence (5' to 3')
F1	CATGGGCAGCAGCGAACAGAAACTGATCTCTGAAGAGGATCTGAGCAGCGG
F2	CTGGTGCCGCGC**GGCCCCCGTCCG**TTCCCGGCGGCGG*GGCCGGGCTGGCC*GTGAC
F3	CTGGTGCCGCGC**GGCCCCAGCCCG**TTCCCGGCGGCGG*GGCCGGGCTGGCC*GTGAC
F4	TGGCCGGGTGGTTGCTGAC
R1	CCAGGCCGCTGCTCAGATCCTCTTCAGAGATCAGTTTCTGTTCGCTGCTGCC
R2	TCGAGTCAC*GGCCAGCCCGGCC*CCGCCGCCGGGAA**CGGACGGGGGCC**GCGCGGCA
R3	TCGAGTCAC*GGCCAGCCCGGCC*CCGCCGCCGGGAA**CGGGCTGGGGCC**GCGCGGCA
R4	TCGAGTCAGCAACCACCCGGCCAGCC

[1] Underlined sequences are sections for the NcoI and XhoI digest overhangs
[2] Sequences in bold code for the GPRP or GPSP peptides at the thrombin cleavage site
[3] Sequences in italics represent the SfiI recognition site for ELP cloning

Mixtures of 2 μM of each primer (combination #1: F1, F2, R1, R2; combination #2: F1, F3, R1, R3) were made up in 1X ligation buffer and annealed by ramp cooling

from 99°C to 25°C over 60 minutes. The pET15b plasmid was digested with NcoI and XhoI, then dephosphorylated using heat-deactivate-able Antarctic phosphatase. The restriction digest was run on an agarose gel and the band with the digested plasmid was extracted and purified using the QIAquick gel extraction kit (QIAGEN, Valencia, CA). The gel-extracted plasmid and the annealed primers were ligated using T4 DNA Ligase and transformed into electro-competent XL-1 Blue cells. Selection for successfully ligated plasmids containing the insert was made on LB + ampicillin plates. Plasmids were extracted from cultures using the QIAquick Spin Miniprep Kit and verified via sequencing (Eurofins MWG Operon, Huntsville, AL). These modified pET15b plasmids were denoted pET15b-MSfi$_{GPRP}$, pET15b-MSfi$_{GPSP}$.

For plasmid versions coding for a C-terminal cysteine after the SfiI restriction site, the annealed primer pair F4 and R4 was inserted into modified pET15b vectors generated above. Briefly, the pET15b-MSfi$_{GPRP}$, pET15b-MSfi$_{GPSP}$ vectors were digested sequentially with SfiI and XhoI. The digested plasmids were dephosphorylated then gel-purified. The gel-extracted plasmids were ligated with the annealed primer set F4+R4 and transformed into electro-competent XL-1 Blue cells. Selection for successfully ligated plasmids containing the insert was made on LB + ampicillin plates. Plasmids were extracted from cultures using the QIAquick Spin Miniprep Kit and verified via sequencing. These plasmids were denoted pET15b-MSfi$_{GPRP}$-C, pET15b-MSfi$_{GPSP}$-C.

5.2.2. Creation of ELP Coding Sequence Library

3 cloning cassettes were designed to code for 3 different ELPs, namely ELP$_A$ [(VPG<u>I</u>G)$_4$VPGVG]$_{60}$, ELP$_B$ [(VPG<u>A</u>G)$_4$VPGVG]$_{80}$, and ELP$_C$ [(VPG<u>P</u>G)$_4$VPGVGGS]$_{40}$, using the technique of recursive directional ligation in pUC19 as described by Meyer and

Chilkoti [156]. Briefly, the following sequences were ordered as 5' phosphorylated PAGE-purified primers from Invitrogen:

Name	Sequence (5' to 3')
I-F	AATT CTC CAC GGC GTG GGT GTT CCG GGC ATT GGT GTC CCA GGT ATC GGC GTA CCG GGC ATT GGT GTT CCT GGT ATC GGC GTG CCG GGC TGG CA
I-R	AGC TTG CCA GCC CGG CAC GCC GAT ACC AGG AAC ACC AAT GCC CGG TAC GCC GAT ACC TGG GAC ACC AAT GCC CGG AAC ACC CAC GCC GTG GAG
A-F	AATT CTC CAC GGC GTG GGT GTT CCG GGC GCG GGT GTC CCA GGT GCC GGC GTA CCG GGC GCA GGT GTT CCT GGT GCT GGC GTG CCG GGC TGG CA
A-R	AGC TTG CCA GCC CGG CAC GCC AGC ACC AGG AAC ACC TGC GCC CGG TAC GCC GGC ACC TGG GAC ACC CGC GCC CGG AAC ACC CAC GCC GTG GAG
P-F	AATT CTC CAC GGC GTG GGT GGG TCT GTT CCT GGC CCG GGT GTC CCA GGT CCG GGC GTA CCT GGC CCG GGT GTT CCA GGT CCG GGC GTG CCG GGC TGG CA
P-R	AGC TTG CCA GCC CGG CAC GCC CGG ACC TGG AAC ACC CGG GCC AGG TAC GCC CGG ACC TGG GAC ACC CGG GCC AGG AAC AGA CCC ACC CAC GCC GTG GAG

Mixtures of 2 μM for each primer pair were made up in 1X ligation buffer and annealed in a PCR machine by ramp cooling from 99°C to 25°C over 60 minutes. The pUC19 plasmid was digested with EcoRI and HindIII, then dephosphorylated. The gel-extracted plasmids and the annealed primers were ligated and transformed into XL-1 Blue cells. Selection for successfully ligated plasmids containing the insert was made on LB + ampicillin plates. Plasmids were extracted from cultures and verified via sequencing.

In the process of recursive directional ligation, the "host" plasmid was digested with PflMI, then dephosphorylated. The "insert" plasmid was digested with PflMI and BglI, then run on a gel to separate the insert from the plasmid fragments. The band containing the insert was extracted and purified. The gel-extracted host plasmid and insert were ligated and transformed into electro-competent XL-1 Blue cells. Selection for successfully ligated plasmids containing the added insert was made on LB + ampicillin

plates. Plasmids were extracted from cultures and verified via sequencing. This process was repeated until the desired number of repeats in the desired order was attained.

5.2.3. Insertion of ELP Coding Sequences into pET15b-MSfi Vectors

The SfiI site in the multiple cloning site (MCS) was used to insert the ELP open reading frame into the pET15b-MSfi$_{GPRP}$, pET15b-MSfi$_{GPSP}$, pET15b-MSfi$_{GPRP}$-C, pET15b-MSfi$_{GPSP}$-C vectors obtained in section A.1 above using standard molecular cloning techniques. Briefly, the host pET15b-MSfi$_{GPxP}$(-C) plasmid was digested with SfiI, then dephosphorylated. The insert-containing pUC19 plasmid was digested with PflMI and BglI, then run on a gel to separate the desired insert from the host plasmid fragments. The band containing the insert was extracted and purified. The gel-extracted host plasmid and insert were ligated and transformed into electro-competent XL-1 Blue cells. Selection for successfully ligated plasmids containing the insert was made on LB + ampicillin plates. Plasmids were extracted from cultures and verified via sequencing. The plasmids generated were denoted pET15b-MSfi$_{GPRP}$-ELP$_B$-ELP$_A$, pET15b-MSfi$_{GPSP}$-ELP$_B$-ELP$_A$, pET15b-MSfi$_{GPRP}$-ELP$_B$-ELP$_A$-C, pET15b-MSfi$_{GPSP}$-ELP$_B$-ELP$_A$-C, pET15b-MSfi$_{GPRP}$-ELP$_C$-ELP$_A$, pET15b-MSfi$_{GPSP}$-ELP$_C$-ELP$_A$, pET15b-MSfi$_{GPRP}$-ELP$_C$-ELP$_A$-C, pET15b-MSfi$_{GPSP}$-ELP$_C$-ELP$_A$-C.

5.2.4. Protein Production and Purification of ELP Diblock Fusions

pET15-MSfi$_{GPxP}$(-C) plasmids containing the desired ELP inserts were transformed into electro-competent BL21(DE3) E. coli. Protein production of the myc-tagged proteins was induced by the addition of 1 mM IPTG (final) when the culture reached OD_{600} 0.6-0.8. 4 hours following IPTG addition, cells were pelleted by centrifugation at 4^{o}C and resuspended in ice-cold PBS. The lysate was sonicated at

maximum power (without protein foaming) for 10s ON/20s OFF for a total of 90s processing time. The cell debris was removed by centrifugation at 15000×g, 15 min, 4°C. 0.5% polyethyleneimine (final) was added to precipitate out the DNA in the lysate before re-centrifugation.

The cleared lysate was subject to inverse transition cycling (ITC) as described in Meyer et al.[105] Briefly, the lysate was warmed to room temperature before the gradual addition of 5 M NaCl until the ELP begun to precipitate (typically at about 1 M to 2.5 M total NaCl depending on the ELP identity). The mixture was centrifuged at 10000×g, 15 min, 30°C to separate the ELP precipitate from the soluble bacterial proteins remaining in the supernatant, which was discarded. The ELP pellet was resolubilized in cold PBS and centrifuged at 10000×g 15 min, 4°C to separate the soluble ELP from the insoluble bacterial proteins. The ELP-containing solution was transferred to a fresh tube and the pellet was discarded. This process was repeated.

The semi-purified ELP was then incubated overnight with bovine thrombin dosed at 10 U per mg recombinant protein. The process of ITC was then repeated at least another 4 times to purify the cleaved ELP from the thrombin and myc tag, and any remaining bacterial proteins. ELP purity was verified using SDS-PAGE. Western blot using a mouse monoclonal anti-myc antibody (Invitrogen) and IRDye 800 goat anti-mouse IgG (LI-COR) was used to verify complete removal of the myc tag from the ELP fusions. Electrospray ionization mass spectrometry (ESI-MS) performed by the Georgia Institute of Technology Bioanalytical Mass Spectrometry Facility using the Micromass Quattro LC was used to confirm protein size.

The protein solutions were quantified using the Quant-iT protein assay kit (Invitrogen), then aliquoted and stored at -80°C until use. Note: Instances of "GPRP-ELP_B-ELP_A mix" and "GPSP-ELP_B-ELP_A mix" used in this paper refer to 1:4 mixtures of one part of GPRP-ELP_B-ELP_A or GPRP-ELP_B-ELP_A, with four parts of GPSP-ELP_C-ELP_A respectively. In other words, 2 μM of GP(R/S)P-ELP_B-ELP_A and 8 μM of GPSP-ELP_C-ELP_A for a 10 μM ELP solution.

5.2.5. ELP Transition Characterization

Temperature-dependent transitions of the ELP diblock proteins were monitored using a protein-binding fluorescent dye, SYPRO Orange (Invitrogen #S6650). Following a methodology analogous to that reported by Niesen et al. [157], 5× SYPRO Orange (final concentration) was added to 96-well optical PCR plates containing varying concentrations of the ELP in TBS+Ca (25 mM Tris-HCl pH 7.4, 137 mM NaCl, 5 mM $CaCl_2$). The PCR plate was sealed with optical adhesive film and placed into the ABI StepOnePlus real-time PCR system (Life Technologies, Carlsbad, CA). Samples were heated at 0.9°C/min from 10°C to 65°C and the raw data from the ROX channel was used for analysis.

5.2.6. Cloud Point Measurements

The cloud point of 10 μM protein solutions was sampled using the cloud point protocol built into the FP900 thermo system for the FP81HT MBC temperature chamber (Mettler-Toledo, Columbus, OH). Solutions were loaded into the recommended melting point capillaries and inserted into the chamber pre-equilibrated at 25°C. A 1°C/min ramp was used and the solution cloud points were evaluated using the default criteria (i.e. a 4% transmittance drop of the initial value).

5.2.7. Micelle Characterization via Light Scattering

Particle characteristics of solutions containing the ELP diblock proteins were analyzed using dynamic light scattering (DLS) or photon correlation spectroscopy. Briefly, solutions of the ELP diblock were prepared on ice and transferred to a black clear-bottom 384-well plate. The plate was spun down at 3000 g, 10 min, 4°C to eliminate air bubbles before placing in the DynaPro plate reader (Wyatt, Santa Barbara, CA). Following a 15-min thermal equilibration step at 25°C, 20 reads of 20 s acquisitions were recorded for each well. This process was repeated at increments of 1°C or 2°C (where indicated) until particle aggregation led to heterogeneous micron-sized particles generating poor correlation data. Data was collected for at least 4 independently prepared runs. For statistical analysis, data from 9 runs were used. Where indicated, 10 μM of fibrinogen fragment D was added to wells containing 10 μM ELP diblock proteins. The purification of fragment D from a plasmin digest of fibrinogen has been described previously [135].

5.2.8. Mixed Micelle Formation via FRET

ELP diblock proteins with C-terminal cysteines were labeled with either the Alexa Fluor 488 or Alexa Fluor 546 (Invitrogen) via sulfhydryl-maleimide chemistry following the manufacturer's recommended protocol. Combinations of AF488-labeled, AF546-labeled and unlabeled ELP diblock proteins were added to black clear-bottom 384-well plates for a total concentration of 1 μM ELP protein per well (higher concentrations of labeled protein saturated the fluorescence detectors). The 384-well plate was sealed with optical adhesive film and incubated in the H4 Synergy microplate reader (Biotek, Winooski, VT) at 25°C for 15 minutes before excitation at 470 nm and

acquiring the emission spectrum from 500 to 700 nm using a 2 nm step size. The emission spectra were monitored at successive 5°C intervals (30, 35, 40, 45, 50, 55, 60°C) with a 15-minute incubation time allowed for thermal equilibration with each stepwise increase. Changes in the emission peaks were normalized against respective control wells containing only AF488-labeled or AF546-labeled protein and designated as fold change in emission ($F_a = Em_a/Em_{a,control}$; $F_d = Em_d/Em_{d,control}$).

5.2.9. Solid-Phase Fibrinogen Binding Assays

An enzyme-linked immunosorbent assay (ELISA) was used to establish the affinity of fibrinogen for ELP diblock protein covalently immobilized on maleimide-activated plates via their C-terminal cysteines as described previously [135]. Due to the sensitivity of ELP transition characteristics to the Hofmeister effect [158], all assays were conducted in a Tris-based buffer (TBS+Ca) in place of the phosphate buffer recommended in the manufacturer's protocol. Briefly, varying concentrations of sulfhydryl-containing protein/peptides were conjugated to pre-blocked maleimide-activated plates (Pierce, Thermo Scientific, Rockford, IL), which were then quenched with cysteine. ELP-coated wells were incubated with fibrinogen (#FIB3, Enzyme Research Laboratories, South Bend, IN) and the remaining bound fibrinogen after washing was detected using HRP-conjugated goat anti-fibrinogen antibody (MP Biomedicals #55239) and 1-Step Ultra TMB-ELISA (Pierce) with 1 M H_2SO_4 as the stop solution. All intervening wash steps were conducted in TBS+Ca + 0.5% Tween-20. Results were normalized to GPSPFPAC-coated wells (0%) and GPRPFPAC-coated wells (100%).

5.2.10. Solid-Phase Mixed Micelle Binding Assays

A plate-based assay conceptually similar to an ELISA was used to establish the affinity of ELP mixed micelles for immobilized fibrinogen on black 96-well plates. Briefly, fibrinogen was passively adsorbed on 96-well plates at 0.1 mg/mL for 3 h at room temperature. The plates were washed, then blocked with 1% BSA for 1 h at room temperature. The wells were washed with pre-warmed buffer before pre-equilibrated mixed ELP micelles comprising 2 μM unlabeled ELP (the "functional component") and 8 μM labeled GPSP-ELP_C-ELP_A-AF546 (non-fibrinogen binding component) were added to the fibrinogen-coated wells. The plates were incubated at the desired temperatures for 1 h, washed with pre-warmed TBS+Ca to remove the unbound protein, then allowed to equilibrate to room temperature before fluorescence measurements (Ex_{540nm}/Em_{573nm}) were taken. Background fluorescence, evaluated from control BSA-coated wells, was subtracted from the data, with the result reported as relative fluorescence units.

5.2.11. Solution-Phase Turbidity Assays

A plate-based assay was used to establish the affinity of ELP micelles for fibrinogen in solution in clear 384-well plates. ELP mixtures and fibrinogen were equilibrated to the desired temperatures before addition to the wells. The plate was incubated at the desired temperature for 1 h before turbidity measurements (Abs_{350nm}) were taken in the pre-heated plate reader. Background absorbance, evaluated from control wells without fibrinogen was subtracted from the data, with the result reported as relative turbidity.

5.2.12. Turbidity Measurements in the Presence of Thrombin

Enzyme-catalyzed polymerization of mixtures of fibrinogen and mixed micelles was initiated in clear 96-well plates. Briefly, 10 μL of the mixed micelle (20 μM

functional component and 80 μM of GPSP-ELP_C-ELP_A) and 80 μL of 2.5 μM human fibrinogen was pre-incubated at the desired temperature for 1 h. Following, 10 μL of 2.5 NIHU/mL human α-thrombin and 100 Loewy units/mL human FXIIIa (both from Enzyme Research Laboratories) were added to the fibrinogen mixture to initiate polymerization. The turbidity (Abs_{350nm}) of the mixtures was followed using a plate reader. To determine the amount of unclotted protein, the clot was compressed and the isolated clot liquor was analyzed for the soluble protein content through absorbance measurements (Abs_{280nm}) using the Nanodrop 1000 (Thermo Scientific, Wilmington, DE).

5.2.13. Confocal Imaging

Confocal imaging of clots was conducted following the procedure described in section 4.2.5. Briefly, fibrin clots containing 10% Alexa Fluor 555-labeled fibrinogen were prepared as described above (section 5.2.12) on pre-warmed glass slides on a heat block. The slides were sealed and incubated at the desired temperatures for an hour before moving to room temperature for imaging on the confocal microscope.

5.2.14. Statistical Analysis

All data was acquired from at least 3 sets of triplicate experiments, and presented as mean ± SD unless otherwise stated. Two-tailed t-tests were used to evaluate statistical significance ($p < 0.05$) where indicated.

5.3. Knob-ELP Preparation

The coding sequences for the ELP diblock proteins were successfully created and amplified using the pUC19 plasmid. These coding sequences were inserted into the

modified pET15b vectors, and then transformed into E. coli BL21(DE3) for IPTG-induced protein expression under control of the T7 promoter (Figure 16A). The myc-tagged proteins were purified from the bacterial host proteins via ITC, cleaved with thrombin to expose the desired N-terminal peptide sequence, then re-purified via ITC to remove the cleaved myc tag and thrombin (Figure 16B).

Of special note, earlier versions of ELP diblock proteins employing the 6xHis tag instead of the myc tag resulted in issues with thrombin cleavage or problems with the separation of the cleaved 6xHis tag from the ELP using ITC. The dot blots done on these samples indicated the persistent presence of the 6xHis tag even after multiple rounds of ITC (data not shown). Trabbic-Carlson et al. had previously shown successful thrombin-mediated cleavage and removal of ELPs from its fusion partner [106], suggesting that thrombin cleavage efficiency is not affected by the adjoining ELP in such protein fusions. However, the authors also noted that the ELPs had the propensity to associate with hydrophobic proteins even after their cleavage by thrombin [106]. Thus, the decision was made to switch to the highly charged and more hydrophilic myc tag for the production of our knob-ELP diblock proteins.

The following proteins were successfully produced: GPRP-ELP_B-ELP_A, GPSP-ELP_B-ELP_A, GPRP-ELP_C-ELP_A, GPSP-ELP_C-ELP_A. The same set of proteins containing an additional C-terminal cysteine for conjugation of the sulfhydryl to maleimide-containing labels was also successfully generated.

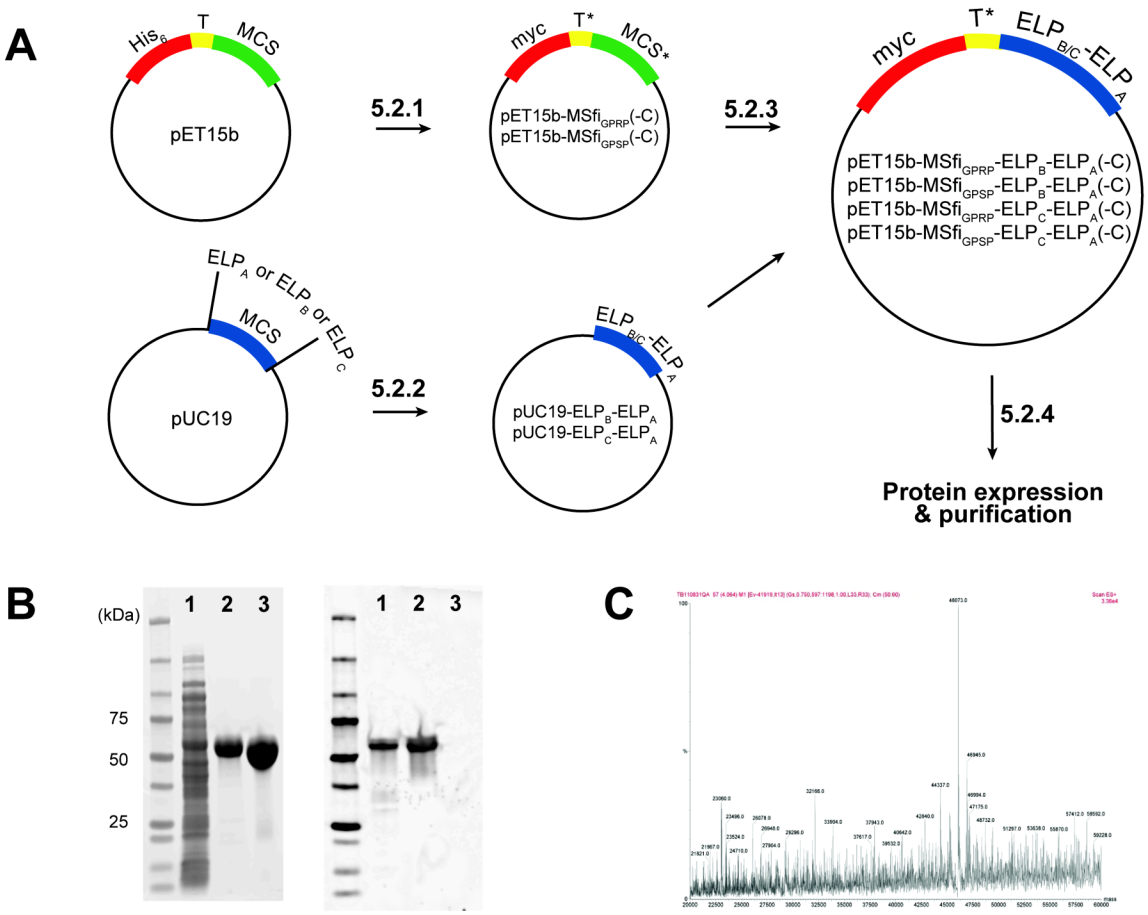

Figure 16. ELP diblock protein design and production. (A) The host pET15b vector was modified to code for the desired N-terminal fibrin binding sequences (GPRP, GPSP) at the thrombin cleavage site and an optional C-terminal cysteine, with an intervening SfiI restriction enzyme site for the insertion of the ELP open reading frame. The open reading frames of the desired ELP blocks (ELP_B-ELP_A, ELP_C-ELP_A) created in the pUC19 plasmid were inserted into the modified pET15b vectors, which were then transformed into E. coli BL21(DE3) for protein expression. Further details may be found in the indicated sections given on the arrows. (B) Representative SDS-PAGE images (left: Coomassie stained gel; right: corresponding Western blot with myc-tag antibody) for GPSP-ELP_C-ELP_A (expected size 43949 Da. ELPs are known to run ~20% larger than expected on SDS-PAGE gels [156]) demonstrating the purity of the purified ELP diblock protein. Lane assignments: 1 – cell lysate; 2 – pre-cleaved ELP diblock protein; 3 – thrombin-cleaved ELP diblock protein. (C) Deconvoluted ESI-MS spectrum for myc-tagged GPSP-ELP_C-ELP_A (expected size 46194 Da; dominant peak on the spectrum shown at 46073 Da) demonstrating the purity and identity of the protein. Attempts to use ESI and MALDI mass spectrometry for the cleaved and purified ELP diblock proteins without the myc tag proved to be unsuccessful, likely due to the lack of charges on the purified protein.

5.4. Transition Temperature Characterization

The transition temperature of ELPs has traditionally been conducted using cloud point measurements upon a temperature ramp of typically 1°C/min [96, 100]. Due to

instrumental limitations, we employed the use of the SYPRO Orange assay to evaluate the phase transitioning behavior of the ELP diblock proteins with temperature ramping in a real-time-PCR machine.

5.4.1. SYPRO Orange

The SYPRO Orange thermal stability assay was used to evaluate the phase transitioning behavior of the ELP diblock proteins with temperature ramping. SYPRO Orange is an environment-sensitive dye that is gaining widespread use in high throughput thermal stability or protein aggregation assays due to its high signal-to-noise ratio [159]. Transition temperatures of ELP protein solutions could be identified by a rapid increase in fluorescence output, corresponding to a peak in the first derivative (Figure 17A,B).

The results indicate the presence of two transitioning points for all the ELPs, including mixtures of different ELP diblocks. The close proximity of the first transition temperature, T_{t1}, for all the solutions at a given ELP concentration (Figure 17C) strongly suggests that this transition is associated with the collapse of the common core ELP_A block, or the self-assembly of ELP diblocks to form micelles. The second transition temperature, T_{t2}, identified was dependent on the identity and relative proportion of the variant outer ELP block, ELP_B or ELP_C, in the protein solution (Figure 17D), suggesting that this temperature is associated with the transition of the outer shell. This may reflect micelle aggregation as the micelle shell collapsed, or overall destabilization of micellar structure to form growing ELP aggregates.

The intermediate T_{t2} identified for mixtures of GP(R/S)P-ELP_B-ELP_A and GPSP-ELP_C-ELP_A, instead of three transition points corresponding to $T_{t,A}$, $T_{t,B}$ and $T_{t,C}$, is highly suggestive of the formation of mixed micelles comprising both species within a

single assembly. In other words, the formation of distinct micelle populations of GP(R/S)P-ELP$_B$-ELP$_A$ and GPSP-ELP$_C$-ELP$_A$ would have resulted in three transition temperatures as the GP(R/S)P-ELP$_B$-ELP$_A$ micelles aggregated ahead of the GPSP-ELP$_C$-ELP$_A$ micelles as the temperature was ramped up. Since this was not observed, the different ELP diblock proteins likely formed mixed assemblies upon the collapse of the common ELP$_A$ block.

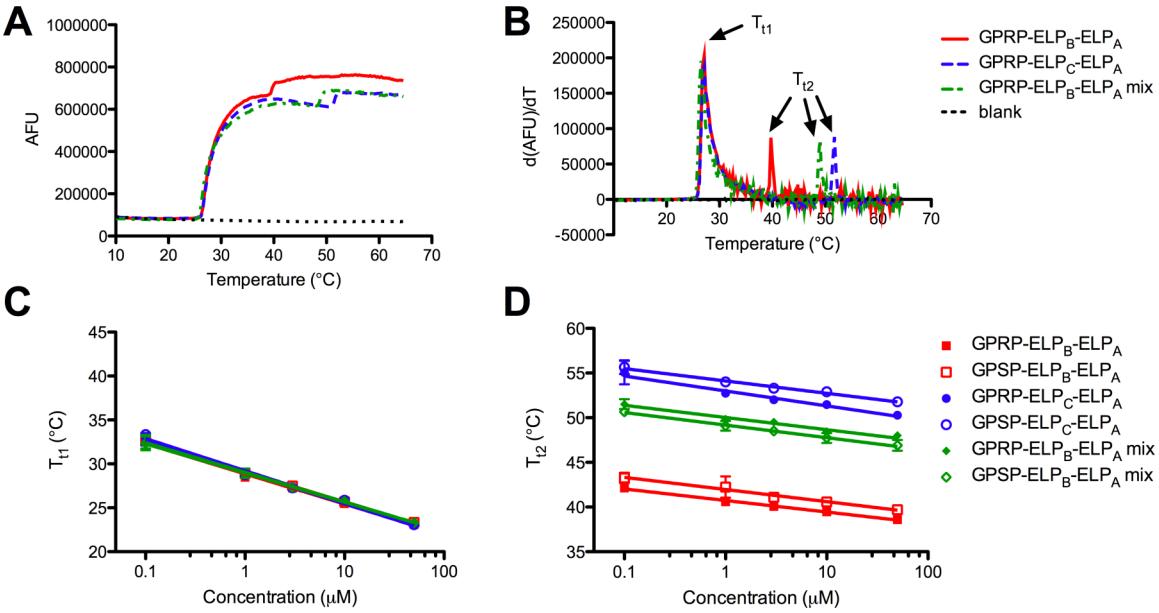

Figure 17. Temperature transition characteristics evaluated using SYPRO Orange. (A) Representative fluorescence readouts from 10 μM solutions of GPRP-ELP$_B$-ELP$_A$, GPSP-ELP$_C$-ELP$_A$ and a 1:4 mixture of GPRP-ELP$_B$-ELP$_A$-to-GPSP-ELP$_C$-ELP$_A$ upon a 0.9°C/min temperature ramp. (B) The calculated derivatives of the fluorescence curves used to obtain the transition temperatures of the solutions. Two distinct transition temperatures (T_{t1}, T_{t2}) were observed for all solutions within the concentration range tested. (C) Plot of T_{t1} as a function of total ELP concentration showing a good overlap of the data points from the different solutions tested. (D) Plot of T_{t2} as a function of total ELP concentration showing dependence of this transition on mixture composition. Data reported as mean ± SD with a semi-log fit.

5.5. Micelle Characterization

Dynamic light scattering (DLS) was used to evaluate the hydrodynamic radius (R_H) of the micelles. Supporting multi-angle laser light scattering (MALLS) was also conducted by Smith for evaluation of the molecular weight (hence micelle coordination number) and radius of gyration (R_G) of the micelles (manuscript in preparation). The formation of mixed micelles was confirmed by the use of FRET.

5.5.1. Micelle DLS Data

Figure 18A,B suggests that the ELP diblock proteins form largely monodisperse (polydispersity < 15%) populations of ~50 nm diameter particles. This is consistent with previously reported data using diblock proteins of comparable molecular weight and composition [121]. Notably, the R_H of GP(R/S)P-ELP_B-ELP_A is approximately 3 nm larger than GP(R/S)P-ELP_C-ELP_A, likely due to the slightly longer length of the GP(R/S)P-ELP_B-ELP_A chain (comprising 140 pentapeptide repeats) compared to the GP(R/S)P-ELP_C-ELP_A chain (100 repeats). The R_H of 1:4 mixtures of GP(R/S)P-ELP_B-ELP_A-to-GPSP-ELP_C-ELP_A appears to approximate that of GP(R/S)P-ELP_B-ELP_A, an expected result if the two diblock proteins came together to form mixed micelles. Moreover, the formation of separate populations of distinctly sized GP(R/S)P-ELP_B-ELP_A and GPSP-ELP_C-ELP_A micelles would be expected to increase particle population polydispersity, a phenomenon we did not observe.

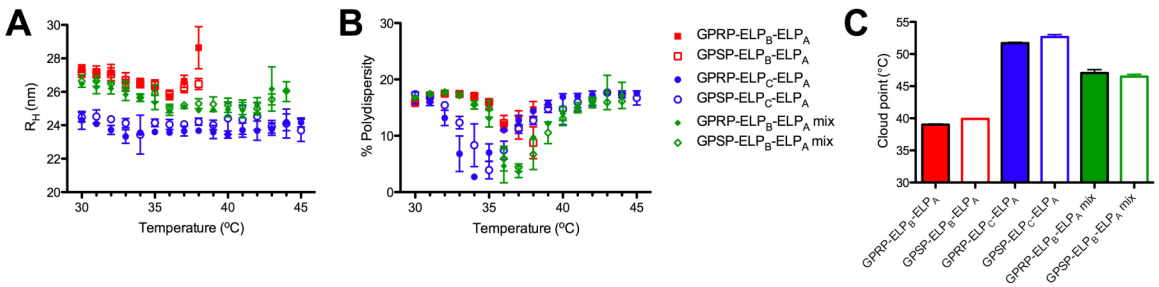

Figure 18. Light scattering data of micelles. (A) Hydrodynamic radius (R_H) of 10 μM protein solutions calculated using the regularization fit provided by the Dynamics software. (B) Corresponding % polydispersity. Data reported as mean ± SD from the averaged data obtained from 4 separate runs. (C) Cloud point of 10 μM protein solutions acquired from the Mettler Toledo cloud point measuring cell.

5.5.2. Cloud Point Measurements

Results from the SYPRO Orange assay suggested a second transition point (T_{t2}) at about 40, 55 and 50°C for 10 μM solutions of GP(R/S)P-ELP$_B$-ELP$_A$, GP(R/S)P-ELP$_C$-ELP$_A$, and GP(R/S)P-ELP$_B$-ELP$_A$ mixes respectively. This approximates the temperatures at which the amplitude of the DLS autocorrelation functions dropped drastically and appears to be associated with the formation of polydisperse micron-sized aggregates. Evaluation of the solutions using a cloud point measuring cell also suggests that T_{t2} is associated with the cloud point of the solutions (Figure 18C).

5.5.3. FRET

The functionality of this self-assembling peptide-displaying micelle system relies on the formation of mixed micelles by ELP diblock proteins sharing a common core ELP$_A$ block. The C-terminal sulfhydryl of cysteine-containing ELP diblock proteins was conjugated to either AF488 or AF546 fluorophores. Given the Förster radius of 6.31 nm for this FRET pair and the ~50 nm diameter of the micelles, a positive FRET signal

would be strongly suggestive of colocalization of the C-terminal ELP_A blocks within the same micelle core.

As expected, FRET, indicated by a reduction in AF488 emission (Em_d) and concomitant increase in AF546 emission (Em_d), was not significant in mixtures at ambient temperatures (Figure 19A), but was observed as temperature increased above T_{t1} (~28.5°C from Figure 17C). The emission spectra of control wells containing either the respective AF488-labeled or AF546-labeled proteins did not change appreciably with temperature (data not shown). Quantifying this change as F_a/F_d, FRET increased from 25°C to 35°C, then stabilized at about 2.4 for all the mixtures tested (Figure 19B). Interestingly, F_a/F_d for the GPRP-ELP_B-ELP_A-AF488 with GPRP-ELP_B-ELP_A-AF546 positive control showed a slight upward trend past 40°C, which may suggest a reorganization of micellar core structure past T_{t2} of the protein solution (~40.5°C from Figure 17D). Nonetheless, the close proximity of the results from all three mixtures suggests that both fluorophores were colocalized within the micelle core, regardless of the identity of the variant outer ELP block, ELP_B or ELP_C.

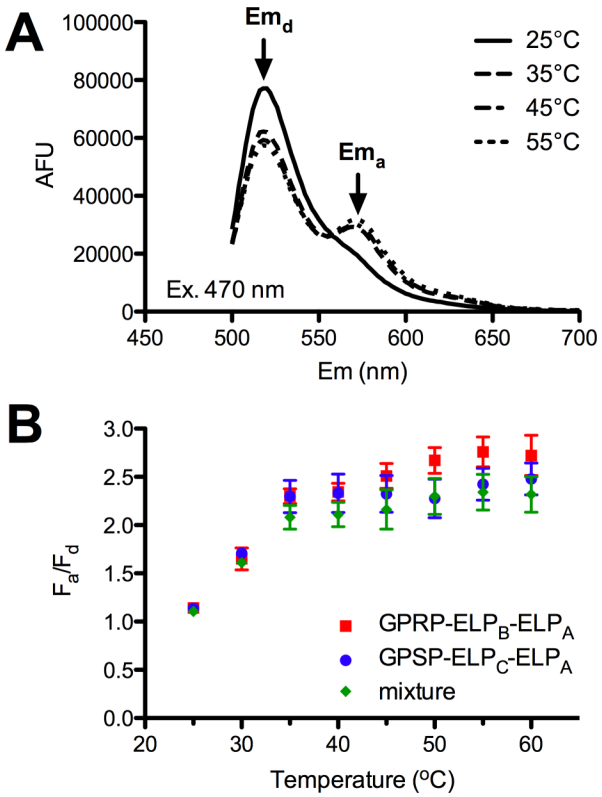

Figure 19. Formation of mixed micelles demonstrated using FRET. (A) Representative emission spectrum obtained from an equimolar mixture of GPRP-ELP$_B$-ELP$_A$-AF488 and GPSP-ELP$_C$-ELP$_A$-AF546 (10% labeled protein of a 10 μM protein solution) excited at 470 nm at various temperatures. Emission peaks of donor AF488 (Em$_d$) and acceptor AF546 (Em$_a$) are indicated by arrows. (B) Results are reported as fold change in Em$_a$ (F$_a$) over fold change in Em$_d$ (F$_d$) for equimolar mixtures of GPRP-ELP$_B$-ELP$_A$-AF488 and GPRP-ELP$_B$-ELP$_A$-AF546 (red), GPSP-ELP$_C$-ELP$_A$-AF488 and GPSP-ELP$_C$-ELP$_A$-AF546 (blue), GPRP-ELP$_B$-ELP$_A$-AF488 and GPSP-ELP$_C$-ELP$_A$-AF546 (green) as a function of temperature.

5.6. Interaction of Mixed Micelles with Fibrinogen

In keeping with the main theme of the document, we are interested in evaluating the affinity between the mixed micelles and fibrinogen. First, we demonstrated that the binding of the ELP diblock proteins to fibrinogen was stable and specific at all the temperature regimes were interested in. We then proceeded to evaluate the interaction of the assembled mixed micelles with fibrinogen using both solid-phase and solution-phase techniques.

5.6.1. Binding Specificity of ELP Diblock Proteins

The binding of fibrinogen to immobilized ELP diblock proteins was evaluated using a standard plate-based ELISA format. As expected, the results indicate that fibrinogen bound specifically to GPRP-ELP_B-ELP_A-C and GPRP-ELP_C-ELP_A-C but not their respective GPSP-displaying controls (Figure 20A). This assay demonstrates the specificity of the GPRP:fibrinogen interaction, validates the use of the GPSP control tetrapeptide sequence, and also indicates the absence of non-specific interactions between the ELP chains and fibrinogen. Interestingly, more fibrinogen bound to saturated GPRP-displaying ELP-coated wells than saturated GPRP-displaying peptide-coated wells (% normalized signal > 100), possibly indicative of steric hindrance when binding to GPRP presented in close proximity to the surfaces of the well.

The binding specificity of the displayed GPRP, versus the control GPSP peptide at elevated temperatures was also verified (Figure 20B-D). The experimental protocol was unchanged, except for the use of pre-warmed buffers following cysteine quenching and incubation of the ELISA plates in a pre-heated incubator. For consistency, TMB incubation was still conducted at room temperature for the same development time before addition of the stop solution. The raw data (not shown) indicated that the amount of soluble fibrinogen bound to control GPRPFPAC-coated wells remained approximately constant at the additional temperatures tested (i.e. 32°C, 37°C, 42°C), suggesting that the integrity of the knob:hole interactions was conserved at these conditions. Control GPSPFPAC-coated wells showed a slight but insignificant increase in background as the temperature increased.

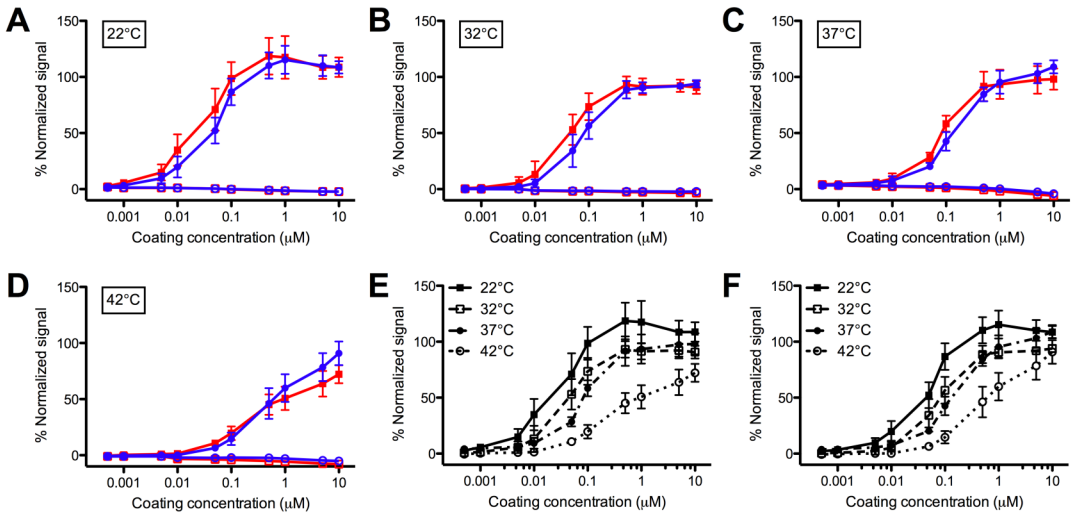

Figure 20. Binding specificity of ELP diblock proteins at elevated temperatures as function of ELP coating concentration. In addition to the results obtained at room temperature (A), ELISA was also conducted at 32°C (B), 37°C (C) and 42°C (D). The data was normalized to control GPSPFPAC-coated wells (0%) and GPRPFPAC-coated wells (100%) at each temperature and presented as % normalized signal. Solid square symbols – GPRP-ELP$_B$-ELP$_A$, open square symbols – GPSP-ELP$_B$-ELP$_A$, solid circle symbols – GPRP-ELP$_C$-ELP$_A$, open circle symbols – GPSP-ELP$_C$-ELP$_A$. The connecting lines are simply to guide the eye. The data is also presented together as % normalized signal at varying temperatures as shown for GPRP-ELP$_B$-ELP$_A$ (E) and GPRP-ELP$_C$-ELP$_A$ (F).

The results suggest that the amount of soluble fibrinogen bound to immobilized GPRP-displaying ELP diblock proteins was highest at 22°C and is not significantly different at 32°C and 37°C (Figure 20E-F). However, binding between the GPRP-displaying ELP diblock proteins and fibrinogen appears to drop at 42°C, suggesting that temperature-induced conformational changes in the ELP blocks may be interfering with binding. Interestingly, the ELISA curves for GPRP-ELP$_B$-ELP$_A$ and GPRP-ELP$_C$-ELP$_A$ were not significantly different at all the temperatures tested, suggesting that changes in the common ELP$_A$ block may be behind binding affinity modulation. Binding to immobilized GPSP-displaying ELP diblock proteins was negligible at all conditions, again affirming the specificity of the interaction between GPRP and fibrinogen.

5.6.2. Binding Specificity of Mixed Micelles

The binding of mixed micelles to immobilized fibrinogen was evaluated using a plate-based format similar to an ELISA. This assay was specifically designed to monitor the binding of mixed micelles, not just (possibly) monomeric ELP diblock proteins, to immobilized fibrinogen. Rather than label all the ELP diblock proteins, only the non-fibrinogen binding GPSP-ELP_C-ELP_A was labeled with AF546. This labeled protein was mixed with the unlabeled "functional component" of the mixed micelle that would be expected to bind to fibrinogen (i.e. GPRP-ELP_B-ELP_A or GPRP-ELP_C-ELP_A). Any GPSP-ELP_C-ELP_A-AF546 associated with the immobilized fibrinogen is interpreted as have been retained in the wells as part of a mixed micelle with the unlabeled functional component (Figure 21A).

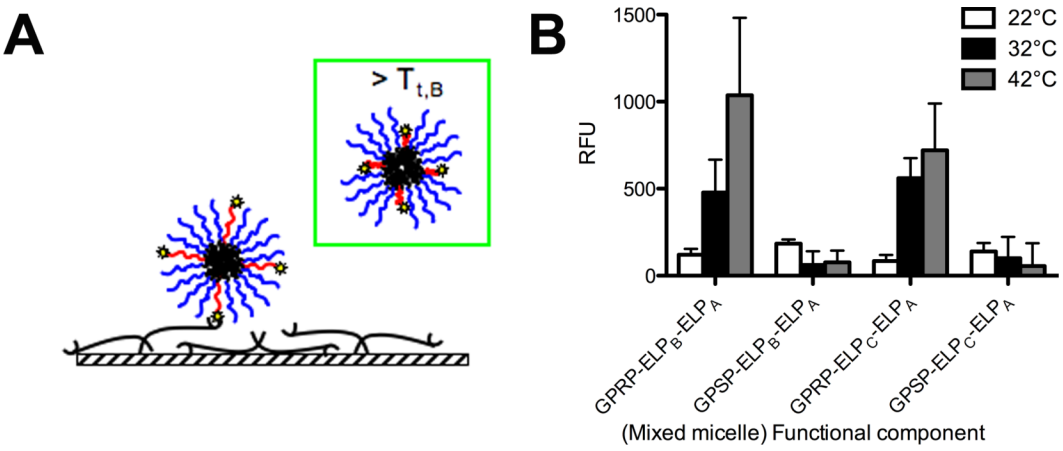

Figure 21. Temperature-responsive binding of mixed micelles to immobilized fibrinogen at 22°C, 32°C, 42°C. (A) Schematic illustrating binding of fluorescently labeled GPSP-ELP_C-ELP_A-AF546 (in blue) to fibrinogen-adsorbed surfaces as part of a mixed micelle with the unlabeled "functional component" GPRP-ELP_B-ELP_A (in red) below $T_{t,B}$. (B) Fluorescence readouts reflecting the amount of GPSP-ELP_C-ELP_A-AF546 recruited to the immobilized fibrinogen by the indicated unlabeled "functional component" at 3 temperatures (22°C, 32°C, 42°C) are reported as relative fluorescent units.

As expected, no significant fluorescence was observed at 22°C, where the ELP diblock proteins were expected to exist as monomers (Figure 21B). At 32°C, where micelle formation was verified, fluorescence was observed in the presence of GPRP-ELP_B-ELP_A and GPRP-ELP_C-ELP_A but not the GPSP controls. This indicates that the unlabeled functional component was successful in retaining the labeled non-fibrinogen-binding GPSP-ELP_C-ELP_A-AF546 within the wells, likely as part of a mixed micelle. Interestingly, at 42°C, an increased fluorescence signal was observed in the presence of both GPRP-ELP_B-ELP_A and GPRP-ELP_C-ELP_A. Due to the collapse of the ELP_B block at this temperature ($T > T_{t,B}$), we expected to observe less binding in the presence of GPRP-ELP_B-ELP_A compared to GPRP-ELP_C-ELP_A. However, it is noted that only ~1% of the originally added labeled protein was retained within the wells, which would have resulted in a drastic change in the effective protein concentration within the wells during the buffer washes. Since T_t is a function of concentration, this unexpected finding may be an experimental artifact. Nonetheless, these results clearly demonstrate the binding specificity of the GPRP-displaying ELP diblock proteins (versus the GPSP controls) at all 3 temperatures of interest, and also the formation of mixed micelles that are capable of interacting with fibrinogen.

5.6.3. Interaction of Mixed Micelles with Soluble Fibrinogen using Turbidity

As both the GPRP-displaying micelles and hole-containing fibrinogen are multivalent entities, we expect to see network formation and an increase in mixture turbidity as these components interact with each other (Figure 22A). This unique phenomenon was presented in the previous chapter where the addition of equimolar

amounts of multivalent GPRP-displaying PEG conjugates to fibrinogen was shown to increase mixture turbidity (refer to section 4.4.3).

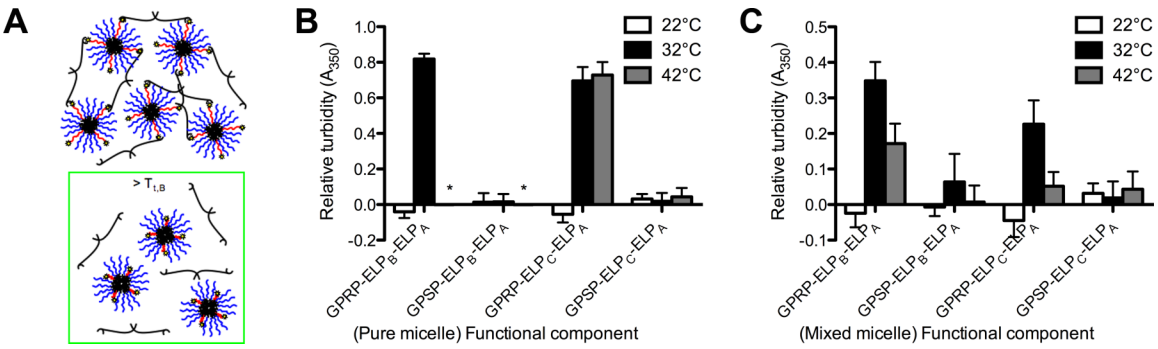

Figure 22. Temperature-responsive binding between micelles and fibrinogen in solution at 22°C, 32°C, 42°C. (A) Schematic illustrating interaction of mixed micelles with fibrinogen below $T_{t,B}$. (B,C) Absorbance readouts reflecting the interaction of the pure micelles (comprising the indicated ELP diblock proteins only) or mixed micelles (1:4 mixtures of the indicated functional component with GPSP-ELP_C-ELP_A) with fibrinogen are reported as relative turbidity. Asterisks indicate wells in which the ELP-only controls precipitated out.

As expected, there were no significant changes in mixture turbidity observed at 22°C, suggesting that the monomeric ELP diblock proteins at this temperature did not form a network with fibrinogen (Figure 22). At 32°C, there was a significant increase in mixture turbidity in the presence of 10 μM GPRP-ELP_B-ELP_A and GPRP-ELP_C-ELP_A (Figure 22B), suggesting that micelle formation at this temperature, coupled with engagement of fibrinogen holes by the displayed GPRP, led to network formation. At 42°C, solutions of GPRP-ELP_B-ELP_A and GPSP-ELP_B-ELP_A were already past their cloud point, invalidating any data obtained from these wells (indicated by asterisks on the graph). However, mixtures of GPRP-ELP_C-ELP_A and fibrinogen exhibited turbidities comparable to those 32°C, suggesting that fibrinogen remained engaged with these micelles at elevated temperatures.

Similar results were obtained in the presence of mixed micelles, wherein no significant changes in mixture turbidity was observed at 22°C, while an increase in turbidity was observed at 32°C due to the micelle formation (Figure 22C). However, mixtures in the presence of mixed micelles exhibit reduced mixture turbidities at elevated temperatures (42°C), which may suggest reduced interaction with fibrinogen at these temperatures. These results are congruent with our initial conceptual design where retraction of GPRP at elevated temperatures ($T > T_{t,B}$) should result in a non-fibrinogen-binding mixed micelle. Interestingly, the relative turbidity in the presence of GPRP-ELP_C-ELP_A mixed micelles was reduced as well. Theoretically, there should not be changes in GPRP presentation for this mixed micelle since the ELP_C-ELP_A section is common to both the functional GPRP-ELP_C-ELP_A component and inactive GPSP-ELP_C-ELP_A component.

5.6.4. Micelle DLS Data in the Presence of Fibrinogen Fragment D

For a more direct evaluation of the interaction between the GPRP-displaying mixed micelles and fibrinogen holes in real time, DLS was used to detect the changes in R_H as fibrinogen binds to the micelle. To avoid network formation and aggregation due to the multivalency of fibrinogen, fibrinogen fragment D comprising a single (instead of paired) set of holes was used.

A statistically significant change in R_H was observed for 10 μM GPRP-ELP_B-ELP_A, compared to the control GPSP-ELP_B-ELP_A, in the presence of 10 μM fragment D until particle aggregation (Figure 23A). A similar trend was observed for GPRP-ELP_C-ELP_A against the control GPSP-ELP_C-ELP_A although the R_H of the micelles exhibited a general decrease in response to temperature (Figure 23B). The moderate increase in R_H

past ~43°C is probably associated with the denaturation of fibrinogen at these temperatures (data not shown).

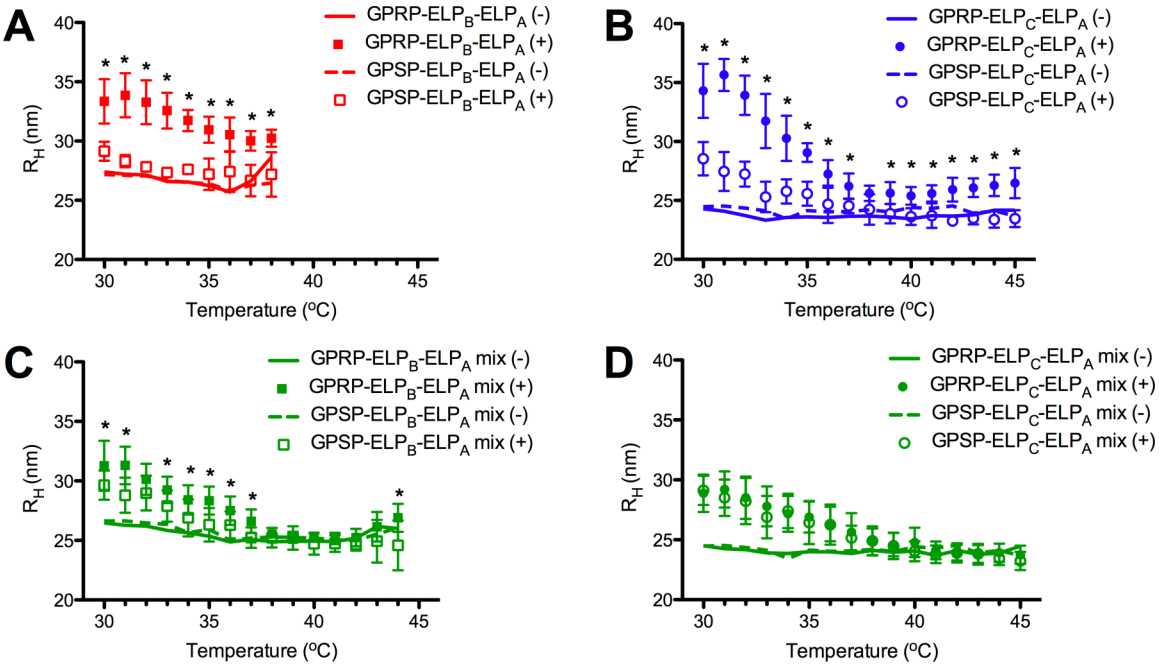

Figure 23. Characterization of interaction of mixed micelles with fibrinogen fragment D in response to a temperature ramp via dynamic light scattering. R_H is reported for pure micelles (A, B) and mixed micelles (C, D) in the presence (symbols) and absence (lines) of fibrinogen fragment D. Standard deviations for data points in the absence of fragment D are not shown for visual clarity. Asterisks indicate statistically significant differences between data sets in the presence of fragment D at each temperature as evaluated using the unpaired Student's t-test.

As the mixed micelles comprised four parts of GPSP-ELP_C-ELP_A for each part of the functional component, it was unsurprising to observe the gradual decrease in R_H for all the mixed micelles in the presence of fragment D (Figure 23C, D). This may be suggestive of an unanticipated temperature-sensitive interaction of the outer ELP_C block with fibrinogen fragment D. Nonetheless, a significant difference in R_H was observed between the GPRP-ELP_B-ELP_A and GPSP-ELP_B-ELP_A mixed micelles, at 37°C and below, but not at higher temperatures, a phenomenon we were anticipating in our initial

conceptual design. Interestingly, no significant difference in R_H was observed for the GPRP-ELP_C-ELP_A and GPSP-ELP_C-ELP_A mixed micelles at all temperatures tested, even though an interaction between the GPRP-ELP_C-ELP_A mixed micelles and fibrinogen was clearly observed for the turbidity assays within this temperature range.

5.7. Impact of Mixed Micelles on Fibrin Polymerization

Early work by Nair et al. suggests that temperature has little effect on the mass-length ratio of fibrin fibers in thrombin-catalyzed clots within the range of 15°C to 37°C [160]. Thus, we do not expect to observe changes in fibrin clot structure within this temperature regime. As described previously for the multivalent knob-PEG conjugates, fibrin clot formation in the presence of mixed micelles was evaluated using mixture turbidity readouts and through confocal imaging of the stabilized network structures.

5.7.1. Turbidity Measurements

The utility of turbidity measurements in the analysis of clot structure has been covered extensively in literature and detailed in previous chapters of this document. Likewise, we employed turbidity measurements for the evaluation of thrombin polymerization dynamics in the presence of the mixed micelles at different temperature regimes. As the mixed micelles have a cloud point of 46°C and above, we expect minimal interference from turbidity increases arising from ELP aggregation at the temperatures tested (22, 32, 42°C).

As discussed in section 5.6.3, only the turbidities of mixtures with GPRP-ELP_B-ELP_A and GPRP-ELP_C-ELP_A mixed micelles were elevated in the absence of thrombin at 32°C and 42°C (Figure 24A; compare with Figure 22C). In the presence of thrombin, the

turbidity of mixtures in the presence of GPRP-ELP_B-ELP_A or GPSP-ELP_B-ELP_A (red overbars) actually stayed constant or increased at 42°C while mixtures in the presence of GPRP-ELP_C-ELP_A or GPRP-ELP_C-ELP_A (blue overbars) actually decreased at these temperatures.

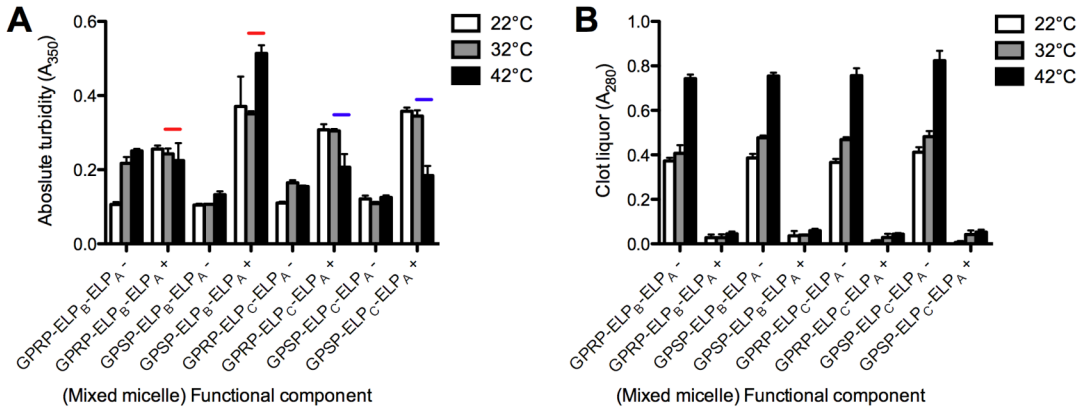

Figure 24. Evaluation of clotting parameters of fibrin gels formed in the presence of mixed micelles. (A) Mixed micelles (2 μM functional component + 8 μM GPSP-ELP_C-ELP_A) were preincubated with fibrinogen (2 μM) at the indicated temperatures for 1 h. The turbidity readouts of fibrin gels formed in the presence (+) or absence (-) of thrombin (0.25 NIHU/mL) following a 1-h incubation at the indicated temperatures were reported. (B) Quantitation of protein in the clot liquor through absorbance measurements (at 280 nm). Due to the presence of a single tryptophan residue in each ELP chain, the absorbance from soluble ELP was expected to be minimal. Thus, the measured absorbance is indicative of the amount of soluble fibrinogen remaining in the clot liquor.

Analysis of the clot liquor suggests that the amount of unclotted protein was similar, regardless of the identity of the mixed micelle present (Figure 24B). This suggests that the clottability of the fibrin gels formed (or not formed in the absence of thrombin) was not affected by the mixed micelles. Taken together, these results are suggestive of a structural reorganization of the fibrin matrix in the presence of the mixed micelles at 32°C and 42°C, not unlike the situation we encountered in the previous chapter (refer to section 4.4).

5.7.2. Confocal Imaging

We proceeded to evaluate clot structure through confocal microscopy as described previously. Regardless of the type of imaging method, we are unable to control the temperature at which the clots are imaged. However, from past experience with confocal imaging (section 4.6), we found that the fibrin clot structures formed following a 1-h room temperature incubation with thrombin were stable for several days. Thus, we assumed that the fibrin clot structures formed following a 1-h incubation with thrombin at the desired temperatures would be similarly stable.

As expected, the fibrin clots formed in the presence of the ELP diblock proteins at 22°C were largely similar (Figure 25). At this temperature ($< T_{t1}$), we expect the ELP diblock proteins to exist as monomers. At an equimolar GPRP:fibrinogen ratio, the impact on fibrin polymerization dynamics should be minimal (refer also to 4.4.1). At 32°C, we observe thinner fibers and large clusters of fibrinogen/fibrin in the presence of GPRP-ELP_B-ELP_A and GPRP-ELP_C-ELP_A mixed micelles. Using labeled ELP diblock proteins, these clusters were shown to comprise both fibrinogen and the ELP diblocks (data not shown). At 42°C, the clusters were smaller and the surrounding fibrin fibers resembled the fibers in the control clot more closely.

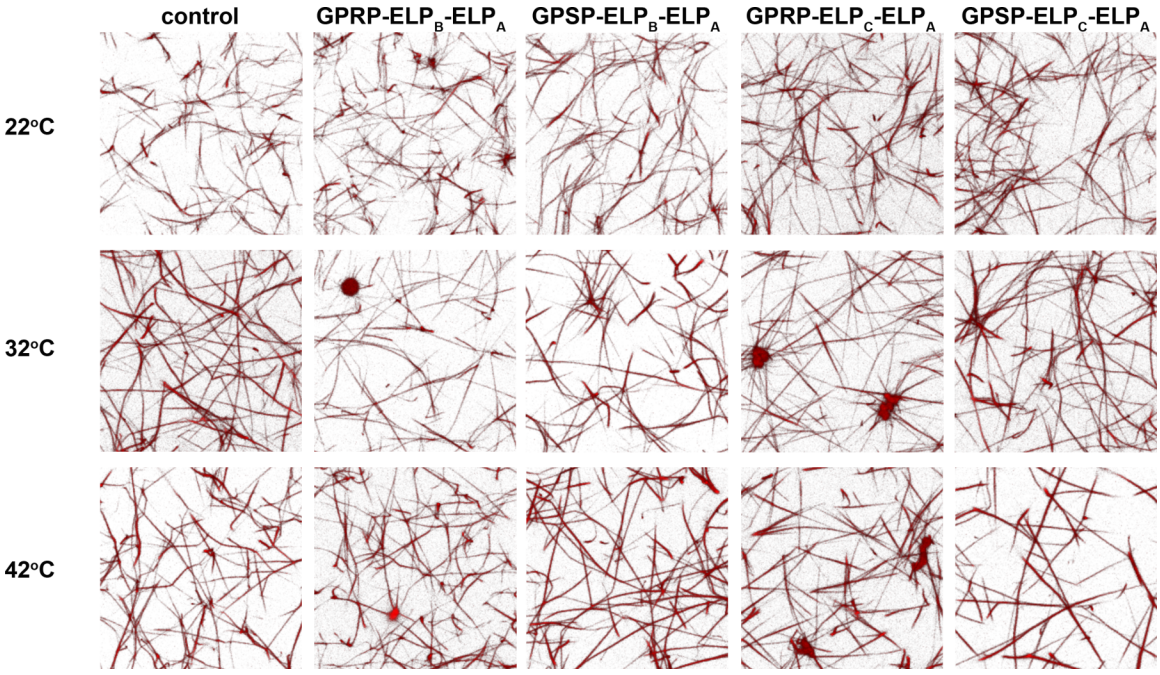

Figure 25. Confocal images of fibrin gels formed in the presence of mixed micelles. Images were rendered from 35 × 35 × 10 μm slices. The hydrogels were formed within sealed chambers on glass slides and imaged using laser scanning confocal microscopy. Control clots (shown in the first column) were formed at the indicated temperatures using 3 μM fibrinogen and 0.25 NIHU/mL thrombin. 15 μM mixed micelles (3 μM functional component + 12 μM GPSP-ELP$_C$-ELP$_A$) were added where indicated.

5.8. Discussions and Conclusions

Many stimuli-responsive systems reported in literature involve temperature- or pH-induced collapse or swelling of selective layers of two- or three-dimensional assemblies. In contrast, this work looks at the selective collapse of a polymer block within a selected layer of a three-dimensional assembly. The differential collapse of polymer blocks amongst non-collapsing polymer blocks poses unique challenges but is of significant value for the future development of multi-responsive 3-D assemblies that maintain structural integrity while displaying different ligands in response to environmental conditions.

Given the extensive literature on ELPs and their transitioning characteristics, the use of ELPs is particularly advantageous to the design of such self-assembling stimuli-responsive display systems. In addition, the ability to synthesize biopolymers with specific sequence compositions and functional handles facilitates the rapid characterization and study of the mixed assemblies formed using high throughput assays such as SYPRO Orange and ELISA. The defined compositions and molecular weights of the ELP diblock proteins used in this work also facilitated the formation of stable nanometer sized micelles with low polydispersities, allowing us to discern subtle changes in R_H due to the binding of fibrinogen fragment D to the peptide-displaying micelle.

The solid- and solution-phase affinity assays together with the DLS data suggest temperature-modulated avidities of the mixed micelles towards fibrinogen at different temperature regimes, likely due to the display of GPRP at lower temperatures, and retraction of GPRP at elevated temperatures, thus validating our starting hypothesis. Evaluation of fibrin clot structures formed within the different temperature regimes also suggest that clot structure was most severely perturbed at 32°C, where we expect GPRP display, and returns to the control morphology at 42°C, where we expect GPRP retraction.

However, it is noted with interest that we did not achieve a clean switch in avidity from a fibrinogen-binding mixed micelle to a non-binding mixed micelle in all the assays presented. This may suggest interference of ELP_B block collapse by the neighboring ELP_C blocks in the mixed micelle. Notably, DLS particle intensity readouts of mixed micelles in the absence of fibrinogen fragment D did not register noticeable changes at

the expected $T_{t,B}$ (data not shown), which would have been a useful indicator of changes in the micellar shell as the ELP_B blocks collapsed.

Alternatively, the 1:4 molar ratio of GPRP-ELP_B-ELP_A-to-GPSP-ELP_C-ELP_A used may not be optimized to dislodge fibrinogen from the collapsed GPRP-ELP_B-ELP_A diblock protein. In particular, it is noted that fibrinogen fragment D was not released from GPRP-ELP_B-ELP_A-only micelles during the temperature ramp (Figure 23A), as expected from ELISA results suggesting that knob:hole interactions are not disrupted at elevated temperatures (Figure 20). The presence of an adequate proportion of GPSP-ELP_C-ELP_A is therefore critical not only for maintaining micelle structural integrity past $T_{t,B}$, but also for allowing successful disengagement of fibrinogen.

CHAPTER 6

RECOMMENDATIONS AND FUTURE OUTLOOK

As the field of regenerative medicine continues to grow, we are seeing a concomitant explosion in the varieties of biomaterials being produced, characterized and tested in laboratories all around the world. This natural association is a result of the need to culture cells outside the body in suitable media to support their growth and development, or even more fundamentally, to understand how cells respond to such materials in order to facilitate the development of the next generation of novel biomaterials. In many instances, cells are known to "reorganize" the surrounding matrix to support their proliferation and/or differentiation. In that sense, biomaterials are not meant to be permanent structures but should simply be engineered to facilitate the process of growth and repair. Fibrin is the ultimate example of such a provisional matrix, being our natural first line of defense against tissue and vascular injury. Thus, fibrin is used in the clinic, as a surgical hemostat and sealant, and also in the laboratory, as a biomaterial.

Nonetheless, the formation of the fibrin matrix from its soluble precursor entails the addition of enzymes, creating handling issues both in the operating theater and on the bench. Thus, our goal was to develop a temperature-triggered polymerizing gel through the use of an adjunct that alters fibrin polymerization dynamics differentially as a function of mixture temperature. As fibrin polymerization is primarily a process of self-assembly mediated by knob:hole interactions, we were interested in evaluating the extent

to which we could perturb this process and to determine if we could exploit it to our advantage.

6.1. Recommendations from Dissertation Work

In Chapter 3, we were primarily interested in evaluating the stability of knob:hole interactions, particularly in the presence of other competing fibrin knobs. From Figure 3, we note that knob 'A' mimic GPRP was much more effective at competing off the bound fibrinogen from immobilized GPRP-FNIII9-10 as compared to the native knob 'A' sequence GPRV. Disappointingly, in the presence of native knobs presented in the context of a fibrin matrix, GPRP-FNIII9-10 was not significantly retained within matrices over longer time periods (Figure 5). Nonetheless, it is noted that under perfusion, GPRP-FNIII9-10 was indeed retained to a much larger extent compared to the non-binding control (work contributed by Brown and Stabenfeldt [135]). This finding seems to suggest that the A:a interactions are indeed more resistant to rupture under shear compared to rupture by thermal dissociation, as proposed by Averett et al. [161]

In Chapter 4, we employed the use of $GPRP_n$-PEG conjugates to evaluate the capacity of such multivalent structures for reorganizing the native fibrin matrix structure. In contrast to the somewhat lackluster performance of monovalent GPRP-FNIII9-10 within fibrin matrices, the $GPRP_n$-PEG conjugates mediated a wide dynamic range of fibrin network morphologies at a 1:1 conjugate:fibrinogen ratio (Figure 12). Notably, this finding concurs with the larger conjugate:fibrinogen ratios required to perturb matrix structure in the case of monovalent GPRP-PEG conjugates of a similar size range [162]. In other words, it appears to be more feasible to manipulate fibrin hydrogel properties through the use of artificial physical crosslinkers, rather than attempting to completely

halt the process of fibril assembly through the addition of monovalent GPRP-displaying peptides or conjugates. Thus we may envision the use of long mobile PEG linkers (such as our 20 kDa $GPRP_4$-PEG) to drive the formation of a loose weak gel, and the use of smaller pincer-type PEG linkers to drive the formation of a tighter stronger gel. In other words, we may be able to create a fibrin hydrogel with temperature-responsive properties through the use of a conjugate that exhibits temperature-responsive structural changes. In view of the likelihood that knob:hole interactions are exceptionally resistant to shear forces, we would expect the conjugate to remain engaged with fibrinogen/fibrin as it undergoes these structural changes.

In Chapter 5, we embarked on the development of a self-assembling system that exhibits temperature-modulated avidities towards fibrinogen. Due to the problems encountered in Chapter 4 regarding the limited characterization techniques available for synthetic conjugates, ELPs were used in this proof-of-principle design. Moreover, ELP diblock proteins may form stable micellar nanostructures [121], offering a convenient means of creating knob-displaying multivalent structures that could perturb fibrin network structure. Thus we found that such self-assembling GPRP-displaying mixed micelles exhibit temperature-modulated avidities for fibrinogen (Figure 22) and exerted variable reorganization capacities on fibrin (Figure 25). However, upon a temperature ramp, it appeared that the disengagement of fibrinogen from the mixed micelles was slower than anticipated (Figure 23). Again, this may be a result of the resistance of the knob:hole interaction towards physical rupture, or it could suggest that we should have used a weaker binder with a higher off-rate, such as GPRV [163]. Indeed, an ideal knob peptide sequence for this application would be one that exhibits a high affinity for

fibrin(ogen) holes at ambient temperatures but a reduced affinity at elevated temperatures. Other process parameters that could be optimized include the ratio of the functional-to-nonfunctional component (currently at 1:4) and the relative lengths of the outer ELP block (now at 80 repeats for ELP_B versus 40 repeats for ELP_C).

Summarizing, this dissertation explored several different methods of modulating fibrin matrix structure via knob:hole interactions. Significantly, we found that fibrin matrix structure can be controlled through the simple addition of multivalent knob-displaying conjugates that act as crosslinkers of fibrinogen. This suggests that stimuli-responsive fibrin mixtures can be engineered through the use of stimuli-responsive crosslinkers without having to modify the fibrin molecule itself.

6.2. Broader Implications

We started this project with the straightforward goal of creating a fibrin-based mixture that is fluid (i.e. predominantly viscous) at ambient temperatures but solid (i.e. predominantly elastic) at physiological temperatures through the use of a temperature-responsive adjunct. Many of the challenges we encountered in the process arose from inherent properties of fibrin molecule itself, as well as our choice of the temperature-responsive component.

6.2.1. Mechanical Aspects of Fibrin as a Scaffold

Unlike the case for most synthetic polymer hydrogels, protein hydrogel networks formed both *in vitro* and *in vivo* typically comprise protein chains that are assembled into fiber bundles. Fibrin monomer assembly involves the formation of double-stranded fibrin protofibrils that assemble laterally to form fibrils that can aggregate to form even larger fibers. In general, lateral aggregation and branching act in opposition to each other such

that coarse/turbid clots comprise thick fibers with few branch points whereas fine/clear clots comprise thin fibers with many branch points. Since fiber thickness and branchpoint density both contribute to clot rigidity, the balance between both factors effects a maximal elastic modulus for clots formed using a fixed amount of fibrinogen [47].

In addition, early permeation experiments suggested that the pore structure in coarse and fine clots were remarkably similar [164], implying some kind of inbuilt mechanism in the fibrin assembly scheme that regulates matrix mechanical properties. The ability to perturb this mechanism through the addition of a non-native crosslinking component, like those studied in this dissertation, is a powerful tool to study the relationship between fibrin assembly and matrix properties. The results from such studies may then be used to shed light on the assembly and formation of protein-based hydrogels using biologically derived proteins such as collagen or gelatin, or recombinantly engineered proteins such as the ELP triblock proteins discussed in section 2.3.3. Significantly, this knowledge would offer a rational means of strengthening such hydrogels without resorting to general covalent crosslinkers like glutaraldehyde or genipin.

Fibrin matrices also exhibit a characteristic strain stiffening behavior common to many protein polymer networks. Using molecular theory, Storm et al. suggested that this nonlinear elastic response is inherent to networks comprising semiflexible filaments with comparable persistence length (l_p) and contour length (L_c) [165]. In the case of fibrin, l_p is about 0.5 μm and L_c ranges from 0.1 to 0.4 μm, depending on the network mesh size [165]. This is in contrast with many synthetic hydrogel networks comprising flexible filaments where $l_p << L_c$. The phenomenon of strain hardening is also related to the

unusual negative normal stresses exhibited by such networks in response to sinusoidal shear strains in the rheometer [166]. This physiologically significant though less well-studied feature allows for the compression and syneresis of fibrin clots under high shear stress, such as in blood vessels [167].

Fibrin matrices demonstrate some of the largest degrees of strain hardening – the shear modulus of fibrin at 50% strain can be as much as 20 times that at low strains (< 10%) [168]. Interestingly, the incorporation and activation of platelets in fibrin networks eliminates this strain hardening behavior and increases the shear modulus at low strains to meet the maximal elastic modulus obtained from the equivalent fibrin-only networks at higher strains [168]. This suggests that we may tune the elastic modulus of fibrin matrices at low strains (typically < 10%) by 20-fold through the facile addition of a contractile component, such as GPRP-ELP_B-ELP_A micelles (from Chapter 5), that interacts with fibrin. It would be interesting to see how cells respond to such "pre-strained" stiff matrices since we would expect the strained fibers to also partially unfold [169, 170], potentially affecting the presentation of protein- and cell-binding sites on the fibers. Since extracellular matrix proteins (such as fibronectin, collagen) are generally under strain in native matrices, such studies can be used to understand cellular responses to strained and unstrained matrices, particularly in a three-dimensional hydrogel.

A final intriguing possibility arises from observing clusters of fibrinogen/fibrin scattered amidst the networks formed in the presence of multivalent conjugates (Figure 12 and 25). Since we were expecting to observe homogeneous fibril networks, the formation of these clusters may reflect topological constraints in fibril organization. However, the ability to create concentrated nodules of proteins may be an advantage by

allowing us to create local increases in crosslink density that increase the bulk modulus while preserving the average mesh size, akin to the system reported by Browning et al. [171]. Under the current experimental conditions, fibrinogen/fibrin cluster formation was associated with the formation of thinner fibrils. This could explain why we did not observe dramatic changes in the mechanical properties of such matrices (Figure 13) even though the clot structures were so different. For this dissertation, we focused on the use of conjugates near an equimolar knob:hole ratio in a dilute fibrinogen solution (~1 mg/mL) at moderate thrombin concentrations (~0.25 NIH U/mL). Changing these parameters could permit the formation of thick fibers with interspersed clusters of fibrinogen/fibrin that could potentially increase the strength of fibrin gels.

6.2.2. ELPs as Structural Actuators

Many comparisons in literature have been made between ELPs and the synthetic polymer equivalent, PNIPAM. In particular, the bulk transition temperature of ELPs exhibits a very strong concentration dependence, which has been attributed to the inherent stiffness of the peptide backbone [102]. However, it would seem that the transition of an ELP as a molecular actuator, inducing some kind of change in response to some kind of stimulus such as the system proposed in Chapter 5, should be dependent on chain transition temperature, rather than the bulk transition temperature.

In the few studies reported that use ELPs as actuators (discussed in section 2.3.5) rather than molecular aggregators, it seems that the transition temperatures were higher than what we would expect, based off the hydrophobicity scale proposed by Urry [96]. This could be because of the dependency of the transition temperature on ELP chain length, or the effect of the adjacent protein sequences on the transition temperature of the

ELP sequence. In the system described in Chapter 5, we used an ELP chain that was much longer than those described in previous studies, thus circumventing the controversies surrounding the behavior of short ELPs (typically < 5 repeats) in comparison to their longer counterparts. However, we also introduced a topological requirement since the transitioning ELP_B blocks had to collapse amidst the more abundant non-transitioning ELP_C block. This subtle change proved difficult to probe under our current experimental settings but is a valuable prelude for the design of single-layer multi-responsive surfaces.

Many of the multi-responsive systems reported in current literature are multi-layer constructs, with each layer responding to a different stimulus. However, such a strategy would not be sustainable for the design of systems that have to respond to more than three different stimuli due to transportation issues across the layers. The ideal system would therefore present all the responsive blocks within the same layer, allowing them equal access to the surroundings. However, this assumes that we are able to achieve independent collapse of individual blocks among the surrounding blocks, a fundamental mechanistic requirement that was out of scope for the present study.

Two major competing models have been proposed to explain the contractility of elastin – the Tamburro and the Urry model [172]. While the Urry model describes the formation of structured β-spirals from consensus VPGXG sequences (described in section 2.3.1), the Tamburro model theorizes the formation of dynamic quasi-folded and semi-extended distorted β structures from consensus XGGYG sequences. While most publications agree that the formation of β-turns plays a fundamental in the protein elasticity, recent molecular simulations and experimental observations seem to suggest

that the ELP structure above the transition temperature is much more dynamic and disordered than previously thought [97, 126]. This could have implications on the use of ELPs in the design of molecular actuators such as that proposed in this dissertation.

6.3. Conclusions

Given the decades of study on protein structure and recombinant protein production, the time is now ripe for the application of this knowledge in the custom engineering of protein-based biomaterials for use in tissue engineering and regenerative medicine. While we have chosen to work with fibrinogen as our scaffold protein in this dissertation, the knowledge gained can be used to outline some basic principles in controlling protein matrix properties since most ECM proteins are similarly fibrillar in nature. The addition of a stimulus-responsive component to our scaffold design also offered a further dimension of control over matrix assembly and morphology in response to an external stimulus, such as temperature.

In conclusion, this dissertation probes some of the fundamental properties of polymerizing or self-assembling proteins for the engineering of matrices with potential applications going far beyond that of basic hemostats or sealants.

APPENDIX A

EVALUATION OF MULTIVALENT GPRP CONJUGATES

GPRP-derived mimics are known to inhibit fibrin assembly while two-headed GPRP linkers have been found to promote FXIIIa activity through fibrinogen assembly [42, 139]. However, if the distance of the linker region were smaller than the minimum distance between abutting holes 'a' of two fibrin(ogen) molecules, the expectation is that the bivalent GPRP conjugate should behave as an inhibitor of fibrin assembly, albeit with increased avidity. Everse et al. found that the distance between the terminal glycines of two bound knobs in abutting holes 'a' was 32 Å [18], corresponding closely to the solution length of the 900 Da PEG linker used by Lorand et al. [42]. Thus, we hypothesize that the conjugation of GPRPAAC to bis(maleimido)ethane, with a spacer arm length of only 8 Å, would result in the formation of a two-headed ligand that does not span the required 32 Å. This bivalent conjugate, denoted as $GPRP_2$-M, should therefore inhibit fibrin polymerization, possibly to a greater extent as compared to the GPRP peptide alone. As a control, we also created a monovalent conjugate using N-ethylmaleimide, denoted as GPRP-M, to show that the conjugation process had no adverse effect on peptide efficacy.

A.1. Materials and Methods

$GPxP_2$-M and GPxP-M were prepared in the same manner as the PEG conjugates used in chapter 4 (see section 4.2.1 for details). GPRPAAC and GPSPAAC peptides were sourced from Genscript, bis(maleimido)ethane from Thermo Scientific, N-ethylmaleimide from Alfa Aesar. However, due to the small sizes of both the peptides

and the maleimide-containing moieties that precludes dialysis as a separation method, we employed equimolar sulhydryl-to-maleimide reaction ratios during the conjugation and did not attempt to purify the product.

Turbidity measurements and analyses of the % clottable protein were conducted as described in section 4.2.2.

A.2. Results and Discussion

As expected, the non-binding peptide GPSP has no significant impact on fibrin polymerization (Figure 26A), while GPRP reduced mixture turbidity in a dose-dependent manner (Figure 26B). The turbidity profiles in the presence of a 100:1 knob:fibrinogen molar ratio for GPSP-M and $GPSP_2$-M suggests a perturbation of fibrin clot structure at these concentrations (Figure 26C, E). This is likely to be a result of the trace amounts of dimethyl sulfoxide (DMSO) required to dissolve the reagents used in the conjugation reaction. Disregarding the spurious results at the 100:1 knob:fibrinogen dosage for GPRP-M and $GPRP_2$-M, we note that GPRP-M seems to behave similarly to GPRP, suggesting that the conjugation process itself has no significant impact on peptide function (Figure 26B, D). As expected, $GPRP_2$-M appears to have a greater impact on the turbidity profiles compared to GPRP-M or GPRP at a 10:1 knob:fibrinogen ratio (Figure 26F).

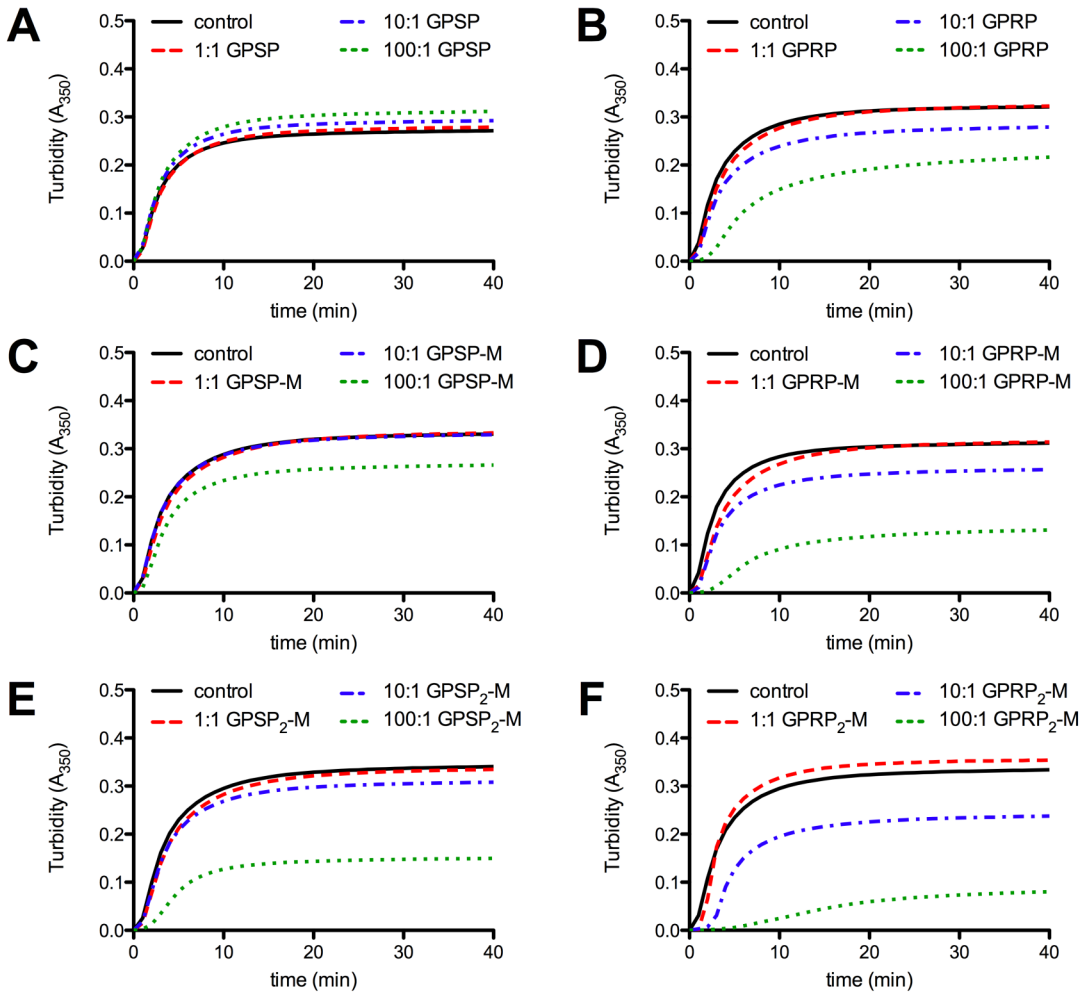

Figure 26. Representative turbidity profiles in the presence of peptides and peptide conjugates at the indicated knob:fibrinogen molar ratios. Data presented for GPSP (A), GPRP (B), GPSP-M (C), GPRP-M (D), $GPSP_2$-M (E), $GPRP_2$-M (F).

Next, we evaluated the amount of unclotted protein remaining in the clot liquor retrieved from these clots. The results suggest that the bivalent $GPRP_2$-M conjugates were indeed more efficient at inhibiting fibrin polymerization compared to the monovalent GPRP-M conjugates or the control GPRP peptide (Figure 27), thus supporting our hypothesis.

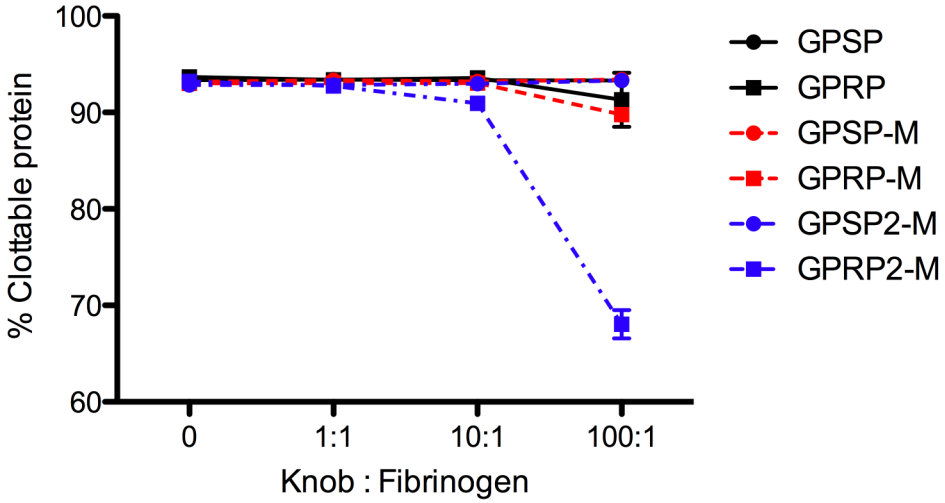

Figure 27. % Clottable protein of hydrogels formed in the presence of peptides and peptide conjugates.

APPENDIX B

EFFECT OF FIBRINOGEN ON ELP TRANSITION TEMPERATURES

The transition characteristics of ELPs are affected by changes in the surface hydrophobicity of their fusion partner [101, 131]. Thus, one of the concerns in our design of the knob-displaying mixed micelle system is the effect of fibrinogen binding on the transition characteristics of the ELP diblock proteins. Due to the large size of fibrinogen (~340 kDa) in comparison to the ELP diblock protein (~50 kDa), it is possible that the binding of soluble fibrinogen to the GPRP-displaying protein would increase its transition temperatures (T_{t1} and T_{t2}). Here, we were interested in evaluating the transition temperatures of the ELP diblock proteins in the presence of fibrinogen and fibrinogen fragment D. The choice of fragment D as a second control was based upon its smaller size (~88 kDa) and the fact that it comprises only a single set of holes (see Figure 1A), thus eliminating potential confounding effects arising from network formation (see also section 5.6.3).

B.1. Materials and Methods

The SYPRO Orange assay was carried out as described in section 5.2.5. The experiments were conducted using a standard concentration of 10 μM ELP mixtures (comprising 2 μM of the indicated "functional component" and 8 μM of GPSP-ELP_C-ELP_A) and 2 μM of fibrinogen or fragment D.

B.2. Results and Discussion

SYPRO Orange is one of several different protein-binding fluorescent dyes used for the evaluation of protein stability and/or protein aggregation [159]. Thus, we expected to observe an increase in the SYPRO Orange fluorescent signal beginning at about 45°C in the presence of fibrinogen and fragment D, corresponding to protein denaturation (Figure 28A). In Figure 28B, we note that T_{t1} was not affected by the presence of fibrinogen nor fragment D, suggesting that micelle formation was not adversely affected (see also sections 5.4.1 and 5.5.1.). However, the presence of fibrinogen led to an increase in the error associated with the evaluation of T_{t2} due to the background signal arising from the denaturing protein. Nonetheless, it would appear from these results that the presence of fibrinogen and fragment D did not substantially change the transition temperatures of the ELP mixtures.

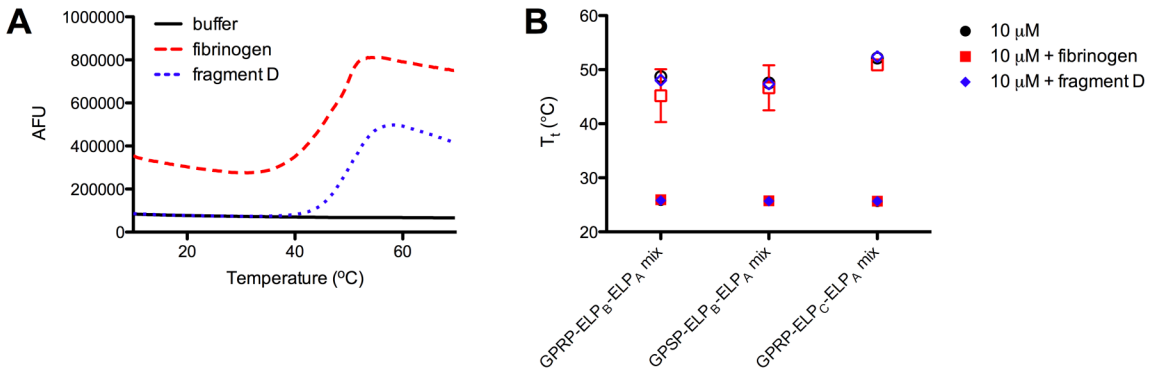

Figure 28. Temperature transition characteristics of ELP diblock proteins in the presence of fibrinogen evaluated using SYPRO Orange. (A) Representative fluorescent readouts from 2 μM fibrinogen and 2 μM fibrinogen fragment D, compared against the buffer blank. (B) Transition temperatures of 10 μM 1:4 functional:GPSP-ELP$_C$-ELP$_A$ mixtures in the presence of fibrinogen and fragment D. Closed symbols correspond to T_{t1} and open symbols correspond to T_{t2}. Data reported as mean ± SD.

APPENDIX C

QUANTIFICATION OF FIBRIN NETWORK STRUCTURE USING IMAGEJ

Parameters that can be used to quantify network morphology include fiber diameter, fiber density and branchpoint density. Such quantifications of fibrin network structures have been made using scanning electron micrographs and reflection laser scanning micrographs [47, 150]. For this project, the fibrin networks were visualized using fluorescently-labeled fibrinogen under confocal laser scanning microscopy, making it challenging to discern between true branchpoints and fibers that have simply crossed over at different depths. Nonetheless, we should be able to obtain a measure of the relative fiber diameters across the different networks observed (Figures 12 and 25). With this goal in mind, Peter J. Yang contributed a macro script that could be run using the NIH image processing software, ImageJ. Briefly, the script converted the 3D networks rendered using the Carl Zeiss ZEN 2008 LE software, into binary images, which were then skeletonized. The ratio of the pixels from the binary images to the pixels from the skeletonized images (thresholded-over-skeletonized) should then provide a relative estimate of fiber diameter.

C.1. Materials and Methods

As proof of principle, the confocal images obtained from the multivalent PEG conjugate project (refer to section 4.2.5 for the image acquisition technique) were used in the analysis. The main processing script is shown in Figure 29.

```
function processFile(infilePath,infileName,infileDirectory) {
	// Open image.
	showStatus("Image "+progress+" of "+progressEnd+": Opening image...");
	open(infilePath);

	outfileDirectory = newDirectory(infileDirectory);
	outfileName = newName(infileDirectory,infileName,"");
	getDimensions(imageWidth, imageHeight, imageChannels, imageSlices, imageFrames);

	if (isStack())
		return;

	// Define the new path.
	outfilePath = outfileDirectory + outfileName;

	// Convert to grayscale.
	run("8-bit");

	// Smooth the stack if desired.
	if(optionSmooth)
		run("Smooth","stack");

	run("Set Scale...", "distance="+optionPixels+" known="+optionMicrons+" pixel=1 unit=µm");
	areaRatio = (optionMicrons/optionPixels)^2;

	// Set threshold for image and skeletonize.
	setThreshold(optionThresholdLow, optionThresholdHigh);
	run("Convert to Mask");
	width = getWidth();
	height = getHeight();
	totalPixels = width * height;
	numberActive = 0;
	for (i=0;i<height;i++) {
		for (j=0;j<width;j++) {
			if (getPixel(j,i) != 0)
				numberActive++;
		}
	}
	numberActive = numberActive * areaRatio;
	threshold = outfilePath + "-thresholded.jpg";

	run("Skeletonize");
	numberSkeleton = 0;
	for (i=0;i<height;i++) {
		for (j=0;j<width;j++) {
			if (getPixel(j,i) != 0)
				numberSkeleton++;
		}
	}
	numberSkeleton = numberSkeleton * areaRatio;

	ratio = numberActive/numberSkeleton;
	text = outfileName+"\tThresholded:\t"+numberActive+"\tSkeletonized:\t"+numberSkeleton+"\tRatio:\t"+ratio;
	print(outputLog, text);
```

Figure 29. Main processing function for calculating relative fiber diameters on confocal images of fluorescently-labeled fibrin networks.

C.2. Results and Discussion

From a representative image of a fibrin clot formed in the presence of an equimolar concentration of the 5 kDa $GPRP_2$-PEG conjugate, clusters of fibrinogen/fibrin can be observed (Figure 30A; compare with Figure 12). These aggregates were found to cause problems during the skeletonization of the binary image since an irregular cluster is clearly not a fiber (Figures 30B, C). To overcome this problem, sections of the micrograph with such aggregates were cropped out (Figure 30D), converted into binary (Figure 30E), then skeletonized (Figure 30F). The resulting skeletonized network appeared to be more representative of the actual fiber network structure.

The results obtained from the analysis of "unprocessed" micrographs without the aggregates removed are shown in Figure 30G. It can be seen that the presence of these aggregates had artificially increased the thresholded-over-skeletonized ratio for $GPRP_2$-PEG conjugates larger than 2 kDa in size. However, it can also be seen that the thresholded-over-skeletonized ratio is comparable across all the $GPSP_2$-PEG controls, as well as the no conjugate control (data not shown), indicating that the script does work as a matter of principle, as long as a homogeneous fiber network is present.

The results from the analysis performed on "processed" micrographs with existing aggregates manually cropped out are shown in Figure 30H. These results suggest that that the thresholded-over-skeletonized ratios in the presence of the $GPRP_2$-PEG conjugates were reduced, which is what we would expect from our observation of thinner fibers in these clots.

However, several drawbacks to this method are noted. First, the thresholded-over-skeletonized ratios of the control clots were already quite low to begin with (~2.8) and

since this methodology has a lower boundary of 1.0 (i.e. a fiber with 1 unit diameter), it would be difficult for us to observe any stark differences using these values. In addition, the tenuous fibrin networks formed in the presence of the larger conjugates such as the 7.5 kDa $GPRP_2$-PEG, 10 kDa and 20 kDa $GPRP_4$-PEG conjugates were near the lower threshold limit of the images and did not render well following the masking and skeletonizing procedure. In other words, the script did not yield any results from several of these images since there was no visible network seen after thresholding. Nonetheless, this script provides a useful starting point for acquiring numerical data from a large number of raw images, allowing us to make quantitative and statistical comparisons across multiple data sets.

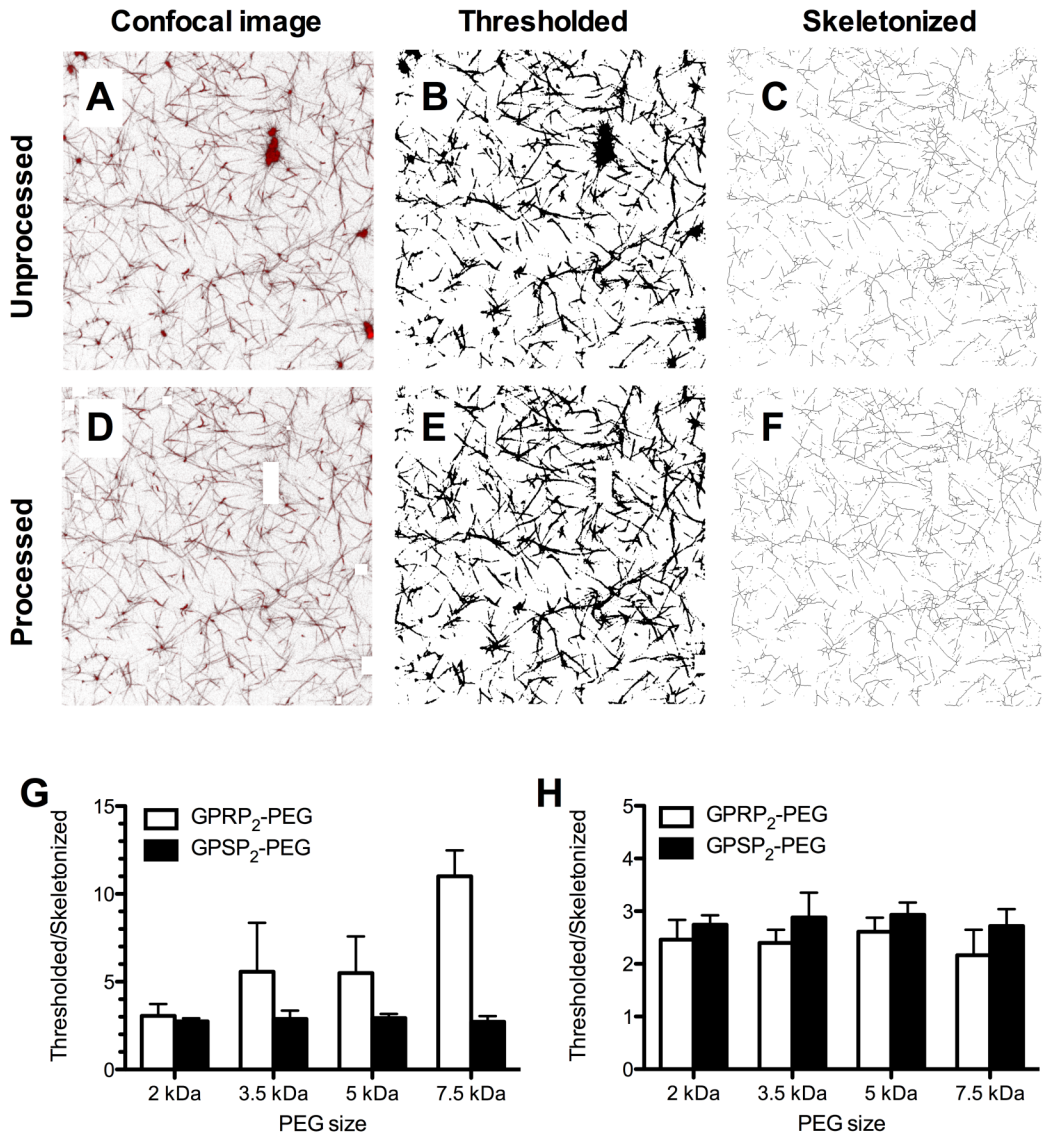

Figure 30. Quantification of fibrin networks formed in the presence of $GPRP_2$-PEG and $GPSP_2$-PEG conjugates. (A) Representative confocal image of a clot (1 mg/mL fibrinogen, 0.25 NIH U/mL thrombin, 5 Loewy units/mL factor XIIIa) formed in the presence of an equimolar concentration of 5 kDa $GPRP_2$-PEG. Image was rendered from a 89×89×10 µm slice (i.e. Z-stack of the complete field of view under the 100× objective). (B) Appearance of the thresholded image after conversion to 8-bit grayscale, smoothing, then conversion to binary. (C) Appearance of the skeletonized image after skeletonizing. (D-F) Same procedure carried out on the processed image with the aggregates manually cropped out. (G) Thresholded-to-skeletonized ratio from the analysis of unprocessed images containing aggregates. (H) Thresholded-to-skeletonized ratio from the analysis of processed images without aggregates.

REFERENCES

[1] Champion HR, Bellamy RF, Roberts CP, Leppaniemi A. A profile of combat injury. The Journal of trauma 2003;54:S13.

[2] Sauaia A, Moore FA, Moore EE, Moser KS, Brennan R, Read RA, Pons PT. Epidemiology of trauma deaths: a reassessment. The Journal of trauma 1995;38:185.

[3] Mannucci PM, Levi M. Prevention and treatment of major blood loss. The New England journal of medicine 2007;356:2301.

[4] Johansson PI, Ostrowski SR, Secher NH. Management of major blood loss: an update. Acta anaesthesiologica Scandinavica 2010;54:1039.

[5] Tomizawa Y. Clinical benefits and risk analysis of topical hemostats: a review. J Artif Organs 2005;8:137.

[6] Spotnitz WD, Burks S. Hemostats, sealants, and adhesives: components of the surgical toolbox. Transfusion 2008;48:1502.

[7] Spotnitz WD. Fibrin sealant: past, present, and future: a brief review. World journal of surgery 2010;34:632.

[8] Jackson MR. Fibrin sealants in surgical practice: An overview. American journal of surgery 2001;182:1S.

[9] Radosevich M, Goubran HI, Burnouf T. Fibrin sealant: scientific rationale, production methods, properties, and current clinical use. Vox sanguinis 1997;72:133.

[10] Laudano AP, Doolittle RF. Studies on synthetic peptides that bind to fibrinogen and prevent fibrin polymerization. Structural requirements, number of binding sites, and species differences. Biochemistry 1980;19:1013.

[11] Slaughter BV, Khurshid SS, Fisher OZ, Khademhosseini A, Peppas NA. Hydrogels in regenerative medicine. Advanced materials (Deerfield Beach, Fla 2009;21:3307.

[12] Lutolf MP, Hubbell JA. Synthetic biomaterials as instructive extracellular microenvironments for morphogenesis in tissue engineering. Nature biotechnology 2005;23:47.

[13] Malafaya PB, Silva GA, Reis RL. Natural-origin polymers as carriers and scaffolds for biomolecules and cell delivery in tissue engineering applications. Advanced drug delivery reviews 2007;59:207.

[14] Laurens N, Koolwijk P, de Maat MP. Fibrin structure and wound healing. J Thromb Haemost 2006;4:932.

[15] Mosesson MW. Fibrinogen and fibrin structure and functions. J Thromb Haemost 2005;3:1894.

[16] Ahmed TA, Dare EV, Hincke M. Fibrin: a versatile scaffold for tissue engineering applications. Tissue engineering 2008;14:199.

[17] Lee MG, Jones D. Applications of fibrin sealant in surgery. Surgical innovation 2005;12:203.

[18] Everse SJ, Spraggon G, Veerapandian L, Riley M, Doolittle RF. Crystal structure of fragment double-D from human fibrin with two different bound ligands. Biochemistry 1998;37:8637.

[19] Litvinov RI, Gorkun OV, Owen SF, Shuman H, Weisel JW. Polymerization of fibrin: specificity, strength, and stability of knob-hole interactions studied at the single-molecule level. Blood 2005;106:2944.

[20] Litvinov RI, Gorkun OV, Galanakis DK, Yakovlev S, Medved L, Shuman H, Weisel JW. Polymerization of fibrin: Direct observation and quantification of individual B:b knob-hole interactions. Blood 2007;109:130.

[21] Geer CB, Tripathy A, Schoenfisch MH, Lord ST, Gorkun OV. Role of 'B-b' knob-hole interactions in fibrin binding to adsorbed fibrinogen. J Thromb Haemost 2007;5:2344.

[22] Blomback B, Hessel B, Hogg D, Therkildsen L. A two-step fibrinogen--fibrin transition in blood coagulation. Nature 1978;275:501.

[23] Lewis SD, Shields PP, Shafer JA. Characterization of the kinetic pathway for liberation of fibrinopeptides during assembly of fibrin. The Journal of biological chemistry 1985;260:10192.

[24] Pechik I, Yakovlev S, Mosesson MW, Gilliland GL, Medved L. Structural basis for sequential cleavage of fibrinopeptides upon fibrin assembly. Biochemistry 2006;45:3588.

[25] Weisel JW. Fibrin assembly. Lateral aggregation and the role of the two pairs of fibrinopeptides. Biophysical journal 1986;50:1079.

[26] Shainoff JR, Dardik BN. Fibrinopeptide B and aggregation of fibrinogen. Science (New York, N.Y 1979;204:200.

[27] Hanss M, Biot F. A database for human fibrinogen variants. Annals of the New York Academy of Sciences 2001;936:89.

[28] Kuyas C, Haeberli A, Walder P, Straub PW. Isolation of human fibrinogen and its derivatives by affinity chromatography on Gly-Pro-Arg-Pro-Lys-Fractogel. Thrombosis and haemostasis 1990;63:439.

[29] Laudano AP, Cottrell BA, Doolittle RF. Synthetic peptides modeled on fibrin polymerization sites. Annals of the New York Academy of Sciences 1983;408:315.

[30] Kawasaki K, Miyano M, Hirase K, Iwamoto M. Amino acids and peptides. XVIII. Synthetic peptides related to N-terminal portion of fibrin alpha-chain and their inhibitory effect on fibrinogen/thrombin clotting. Chemical & pharmaceutical bulletin 1993;41:975.

[31] Muszbek L, Yee VC, Hevessy Z. Blood coagulation factor XIII: structure and function. Thrombosis research 1999;94:271.

[32] Ariens RA, Lai TS, Weisel JW, Greenberg CS, Grant PJ. Role of factor XIII in fibrin clot formation and effects of genetic polymorphisms. Blood 2002;100:743.

[33] Greenberg CS, Shuman MA. The zymogen forms of blood coagulation factor XIII bind specifically to fibrinogen. The Journal of biological chemistry 1982;257:6096.

[34] Dickneite G, Metzner HJ, Kroez M, Hein B, Nicolay U. The importance of factor XIII as a component of fibrin sealants. The Journal of surgical research 2002;107:186.

[35] Lorand L, Chenoweth D, Gray A. Titration of the acceptor cross-linking sites in fibrin. Annals of the New York Academy of Sciences 1972;202:155.

[36] Lewis KB, Teller DC, Fry J, Lasser GW, Bishop PD. Crosslinking kinetics of the human transglutaminase, factor XIII[A2], acting on fibrin gels and gamma-chain peptides. Biochemistry 1997;36:995.

[37] Tamaki T, Aoki N. Cross-linking of alpha 2-plasmin inhibitor and fibronectin to fibrin by fibrin-stabilizing factor. Biochimica et biophysica acta 1981;661:280.

[38] Kanaide H, Shainoff JR. Cross-linking of fibrinogen and fibrin by fibrin-stablizing factor (factor XIIIa). The Journal of laboratory and clinical medicine 1975;85:574.

[39] Siebenlist KR, Meh DA, Mosesson MW. Protransglutaminase (factor XIII) mediated crosslinking of fibrinogen and fibrin. Thrombosis and haemostasis 2001;86:1221.

[40] Mosesson MW, Siebenlist KR, Hainfeld JF, Wall JS. The covalent structure of factor XIIIa crosslinked fibrinogen fibrils. Journal of structural biology 1995;115:88.

[41] Samokhin GP, Lorand L. Contact with the N termini in the central E domain enhances the reactivities of the distal D domains of fibrin to factor XIIIa. The Journal of biological chemistry 1995;270:21827.

[42] Lorand L, Parameswaran KN, Murthy SN. A double-headed Gly-Pro-Arg-Pro ligand mimics the functions of the E domain of fibrin for promoting the end-to-end crosslinking of gamma chains by factor XIIIa. Proceedings of the National Academy of Sciences of the United States of America 1998;95:537.

[43] Wolberg AS. Thrombin generation and fibrin clot structure. Blood reviews 2007;21:131.

[44] Di Stasio E, Nagaswami C, Weisel JW, Di Cera E. Cl- regulates the structure of the fibrin clot. Biophysical journal 1998;75:1973.

[45] Blomback B, Bark N. Fibrinopeptides and fibrin gel structure. Biophysical chemistry 2004;112:147.

[46] Weisel JW, Nagaswami C. Computer modeling of fibrin polymerization kinetics correlated with electron microscope and turbidity observations: clot structure and assembly are kinetically controlled. Biophysical journal 1992;63:111.

[47] Ryan EA, Mockros LF, Weisel JW, Lorand L. Structural origins of fibrin clot rheology. Biophysical journal 1999;77:2813.

[48] Bale MD, Muller MF, Ferry JD. Rheological studies of creep and creep recovery of unligated fibrin clots: comparison of clots prepared with thrombin and ancrod. Biopolymers 1985;24:461.

[49] Bale MD, Muller MF, Ferry JD. Effects of fibrinogen-binding tetrapeptides on mechanical properties of fine fibrin clots. Proceedings of the National Academy of Sciences of the United States of America 1985;82:1410.

[50] Shimizu A, Ferry JD. Ligation of fibrinogen by factor XIIIa with dithiothreitol: mechanical properties of ligated fibrinogen gels. Biopolymers 1988;27:703.

[51] Nelb GW, Gerth C, Ferry JD. Rheology of fibrin clots. III. Shear creep and creep recovery of fine ligated and coarse unligated closts. Biophysical chemistry 1976;5:377.

[52] Shen LL, Hermans J, McDonagh J, McDonagh RP, Carr M. Effects of calcium ion and covalent crosslinking on formation and elasticity of fibrin cells. Thrombosis research 1975;6:255.

[53] Glover CJ, McIntire LV, Brown CH, 3rd, Natelson EA. Rheological properties of fibrin clots. Effects of fibrinogen concentration, Factor XIII deficiency, and Factor XIII inhibition. The Journal of laboratory and clinical medicine 1975;86:644.

[54] Ryan EA, Mockros LF, Stern AM, Lorand L. Influence of a natural and a synthetic inhibitor of factor XIIIa on fibrin clot rheology. Biophysical journal 1999;77:2827.

[55] Collet JP, Moen JL, Veklich YI, Gorkun OV, Lord ST, Montalescot G, Weisel JW. The alphaC domains of fibrinogen affect the structure of the fibrin clot, its physical properties, and its susceptibility to fibrinolysis. Blood 2005;106:3824.

[56] Standeven KF, Carter AM, Grant PJ, Weisel JW, Chernysh I, Masova L, Lord ST, Ariens RA. Functional analysis of fibrin {gamma}-chain cross-linking by activated factor XIII:

determination of a cross-linking pattern that maximizes clot stiffness. Blood 2007;110:902.

[57] Weisel JW, Litvinov RI. The biochemical and physical process of fibrinolysis and effects of clot structure and stability on the lysis rate. Cardiovascular & hematological agents in medicinal chemistry 2008;6:161.

[58] Carr ME, Jr., Alving BM. Effect of fibrin structure on plasmin-mediated dissolution of plasma clots. Blood Coagul Fibrinolysis 1995;6:567.

[59] Kolev K, Tenekedjiev K, Komorowicz E, Machovich R. Functional evaluation of the structural features of proteases and their substrate in fibrin surface degradation. The Journal of biological chemistry 1997;272:13666.

[60] Collet JP, Lesty C, Montalescot G, Weisel JW. Dynamic changes of fibrin architecture during fibrin formation and intrinsic fibrinolysis of fibrin-rich clots. The Journal of biological chemistry 2003;278:21331.

[61] Doolittle RF, Pandi L. Binding of synthetic B knobs to fibrinogen changes the character of fibrin and inhibits its ability to activate tissue plasminogen activator and its destruction by plasmin. Biochemistry 2006;45:2657.

[62] Siebenlist KR, Mosesson MW. Progressive cross-linking of fibrin gamma chains increases resistance to fibrinolysis. The Journal of biological chemistry 1994;269:28414.

[63] Leckband D, Sheth S, Halperin A. Grafted poly(ethylene oxide) brushes as nonfouling surface coatings. Journal of biomaterials science 1999;10:1125.

[64] Amiji M, Park K. Surface modification of polymeric biomaterials with poly(ethylene oxide), albumin, and heparin for reduced thrombogenicity. Journal of biomaterials science 1993;4:217.

[65] Knop K, Hoogenboom R, Fischer D, Schubert US. Poly(ethylene glycol) in drug delivery: pros and cons as well as potential alternatives. Angewandte Chemie (International ed 2010;49:6288.

[66] Greenwald RB, Conover CD, Choe YH. Poly(ethylene glycol) conjugated drugs and prodrugs: a comprehensive review. Critical reviews in therapeutic drug carrier systems 2000;17:101.

[67] Lin CC, Anseth KS. PEG hydrogels for the controlled release of biomolecules in regenerative medicine. Pharmaceutical research 2009;26:631.

[68] Fishburn CS. The pharmacology of PEGylation: balancing PD with PK to generate novel therapeutics. Journal of pharmaceutical sciences 2008;97:4167.

[69] Veronese FM, Pasut G. PEGylation, successful approach to drug delivery. Drug discovery today 2005;10:1451.

[70] Chapman AP. PEGylated antibodies and antibody fragments for improved therapy: a review. Advanced drug delivery reviews 2002;54:531.

[71] Bell SJ, Fam CM, Chlipala EA, Carlson SJ, Lee JI, Rosendahl MS, Doherty DH, Cox GN. Enhanced circulating half-life and antitumor activity of a site-specific pegylated interferon-alpha protein therapeutic. Bioconjugate chemistry 2008;19:299.

[72] Yu P, Zheng C, Chen J, Zhang G, Liu Y, Suo X, Zhang G, Su Z. Investigation on PEGylation strategy of recombinant human interleukin-1 receptor antagonist. Bioorganic & medicinal chemistry 2007;15:5396.

[73] Chi Y, Zhang H, Huang W, Zhou J, Zhou Y, Qian H, Ni S. Microwave-assisted solid phase synthesis, PEGylation, and biological activity studies of glucagon-like peptide-1(7-36) amide. Bioorganic & medicinal chemistry 2008;16:7607.

[74] Natarajan A, Xiong CY, Albrecht H, DeNardo GL, DeNardo SJ. Characterization of site-specific ScFv PEGylation for tumor-targeting pharmaceuticals. Bioconjugate chemistry 2005;16:113.

[75] Hermanson GT. Bioconjugate Techniques. Oxford, UK: Academic Press, 1996.

[76] Kramer RH, Karpen JW. Spanning binding sites on allosteric proteins with polymer-linked ligand dimers. Nature 1998;395:710.

[77] Baird EJ, Holowka D, Coates GW, Baird B. Highly effective poly(ethylene glycol) architectures for specific inhibition of immune receptor activation. Biochemistry 2003;42:12739.

[78] Das R, Baird E, Allen S, Baird B, Holowka D, Goldstein B. Binding mechanisms of PEGylated ligands reveal multiple effects of the PEG scaffold. Biochemistry 2008;47:1017.

[79] Temenoff JS, Athanasiou KA, LeBaron RG, Mikos AG. Effect of poly(ethylene glycol) molecular weight on tensile and swelling properties of oligo(poly(ethylene glycol) fumarate) hydrogels for cartilage tissue engineering. Journal of biomedical materials research 2002;59:429.

[80] Bryant SJ, Chowdhury TT, Lee DA, Bader DL, Anseth KS. Crosslinking density influences chondrocyte metabolism in dynamically loaded photocrosslinked poly(ethylene glycol) hydrogels. Annals of biomedical engineering 2004;32:407.

[81] Peyton SR, Raub CB, Keschrumrus VP, Putnam AJ. The use of poly(ethylene glycol) hydrogels to investigate the impact of ECM chemistry and mechanics on smooth muscle cells. Biomaterials 2006;27:4881.

[82] Raeber GP, Lutolf MP, Hubbell JA. Molecularly engineered PEG hydrogels: a novel model system for proteolytically mediated cell migration. Biophysical journal 2005;89:1374.

[83] Drury JL, Mooney DJ. Hydrogels for tissue engineering: scaffold design variables and applications. Biomaterials 2003;24:4337.

[84] Zhang JZ, Redman C. Fibrinogen assembly and secretion. Role of intrachain disulfide loops. The Journal of biological chemistry 1996;271:30083.

[85] Seliktar D. Extracellular stimulation in tissue engineering. Annals of the New York Academy of Sciences 2005;1047:386.

[86] Almany L, Seliktar D. Biosynthetic hydrogel scaffolds made from fibrinogen and polyethylene glycol for 3D cell cultures. Biomaterials 2005;26:2467.

[87] Dikovsky D, Bianco-Peled H, Seliktar D. The effect of structural alterations of PEG-fibrinogen hydrogel scaffolds on 3-D cellular morphology and cellular migration. Biomaterials 2006;27:1496.

[88] Drinnan CT, Zhang G, Alexander MA, Pulido AS, Suggs LJ. Multimodal release of transforming growth factor-beta1 and the BB isoform of platelet derived growth factor from PEGylated fibrin gels. J Control Release 2010;147:180.

[89] Zhang G, Wang X, Wang Z, Zhang J, Suggs L. A PEGylated fibrin patch for mesenchymal stem cell delivery. Tissue engineering 2006;12:9.

[90] Barker TH, Fuller GM, Klinger MM, Feldman DS, Hagood JS. Modification of fibrinogen with poly(ethylene glycol) and its effects on fibrin clot characteristics. Journal of biomedical materials research 2001;56:529.

[91] Frisman I, Orbach R, Seliktar D, Bianco-Peled H. Structural investigation of PEG-fibrinogen conjugates. Journal of materials science 2009;21:73.

[92] Urry DW, Luan CH, Peng SQ. Molecular biophysics of elastin structure, function and pathology. Ciba Foundation symposium 1995;192:4.

[93] Chilkoti A, Christensen T, MacKay JA. Stimulus responsive elastin biopolymers: applications in medicine and biotechnology. Current Opinion in Chemical Biology 2006;10:652.

[94] Rodriguez-Cabello JC, Reguera J, Girotti A, Arias FJ, Alonso M. Genetic engineering of protein-based polymers: The example of elastinlike polymers. Adv Polym Sci 2006;200:119.

[95] Urry DW, Trapane TL, Prasad KU. Phase-structure transitions of the elastin polypentapeptide-water system within the framework of composition-temperature studies. Biopolymers 1985;24:2345.

[96] Urry DW, Gowda DC, Parker TM, Luan CH, Reid MC, Harris CM, Pattanaik A, Harris RD. Hydrophobicity scale for proteins based on inverse temperature transitions. Biopolymers 1992;32:1243.

[97] Reguera J, Lagarón JM, Alonso M, Reboto V, Calvo B, Rodriguez Cabello JC. Thermal Behavior and Kinetic Analysis of the Chain Unfolding and Refolding and of the Concomitant Nonpolar Solvation and Desolvation of Two Elastin-like Polymers. Macromolecules 2003;36:8470.

[98] Arkin H, Bilsel M. How conformational transition depends on hydrophobicity of elastin-like polypeptides. The European physical journal 2010.

[99] Urry DW. Physical chemistry of biological free energy transduction as demonstrated by elastic protein-based polymers. J Phys Chem B 1997;101:11007.

[100] Meyer DE, Chilkoti A. Quantification of the effects of chain length and concentration on the thermal behavior of elastin-like polypeptides. Biomacromolecules 2004;5:846.

[101] Trabbic-Carlson K, Meyer DE, Liu L, Piervincenzi R, Nath N, LaBean T, Chilkoti A. Effect of protein fusion on the transition temperature of an environmentally responsive elastin-like polypeptide: a role for surface hydrophobicity? Protein Eng Des Sel 2004;17:57.

[102] Yamaoka T, Tamura T, Seto Y, Tada T, Kunugi S, Tirrell DA. Mechanism for the phase transition of a genetically engineered elastin model peptide (VPGIG)40 in aqueous solution. Biomacromolecules 2003;4:1680.

[103] Reguera J, Urry DW, Parker TM, McPherson DT, Rodriguez-Cabello JC. Effect of NaCl on the exothermic and endothermic components of the inverse temperature transition of a model elastin-like polymer. Biomacromolecules 2007;8:354.

[104] McPherson DT, Xu J, Urry DW. Product purification by reversible phase transition following Escherichia coli expression of genes encoding up to 251 repeats of the elastomeric pentapeptide GVGVP. Protein expression and purification 1996;7:51.

[105] Meyer DE, Chilkoti A. Purification of recombinant proteins by fusion with thermally-responsive polypeptides. Nature biotechnology 1999;17:1112.

[106] Trabbic-Carlson K, Liu L, Kim B, Chilkoti A. Expression and purification of recombinant proteins from Escherichia coli: Comparison of an elastin-like polypeptide fusion with an oligohistidine fusion. Protein Sci 2004;13:3274.

[107] Christensen T, Trabbic-Carlson K, Liu W, Chilkoti A. Purification of recombinant proteins from Escherichia coli at low expression levels by inverse transition cycling. Analytical biochemistry 2007;360:166.

[108] Hyun J, Lee WK, Nath N, Chilkoti A, Zauscher S. Capture and release of proteins on the nanoscale by stimuli-responsive elastin-like polypeptide "switches". Journal of the American Chemical Society 2004;126:7330.

[109] Sun XL, Haller CA, Wu X, Conticello VP, Chaikof EL. One-pot glyco-affinity precipitation purification for enhanced proteomics: the flexible alignment of solution-phase capture/release and solid-phase separation. Journal of proteome research 2005;4:2355.

[110] Urry DW, Pattanaik A, Xu J, Woods TC, McPherson DT, Parker TM. Elastic protein-based polymers in soft tissue augmentation and generation. Journal of biomaterials science 1998;9:1015.

[111] Betre H, Setton LA, Meyer DE, Chilkoti A. Characterization of a genetically engineered elastin-like polypeptide for cartilaginous tissue repair. Biomacromolecules 2002;3:910.

[112] Lee J, Macosko CW, Urry DW. Phase transition and elasticity of protein-based hydrogels. Journal of biomaterials science 2001;12:229.

[113] Welsh ER, Tirrell DA. Engineering the extracellular matrix: a novel approach to polymeric biomaterials. I. Control of the physical properties of artificial protein matrices designed to support adhesion of vascular endothelial cells. Biomacromolecules 2000;1:23.

[114] Trabbic-Carlson K, Setton LA, Chilkoti A. Swelling and mechanical behaviors of chemically cross-linked hydrogels of elastin-like polypeptides. Biomacromolecules 2003;4:572.

[115] Lim DW, Nettles DL, Setton LA, Chilkoti A. In situ cross-linking of elastin-like polypeptide block copolymers for tissue repair. Biomacromolecules 2008;9:222.

[116] McHale MK, Setton LA, Chilkoti A. Synthesis and in vitro evaluation of enzymatically cross-linked elastin-like polypeptide gels for cartilaginous tissue repair. Tissue engineering 2005;11:1768.

[117] Wright ER, Conticello VP. Self-assembly of block copolymers derived from elastin-mimetic polypeptide sequences. Advanced drug delivery reviews 2002;54:1057.

[118] Nagapudi K, Brinkman WT, Leisen J, Thomas BS, Wright E, Haller C, Wu X, Apkarian RP, Conticello VP, Chaikof EL. Protein-Based Thermoplastic Elastomers. Macromolecules 2005;38:345.

[119] Rabotyagova OS, Cebe P, Kaplan DL. Protein-based block copolymers. Biomacromolecules 2011;12:269.

[120] Herrero-Vanrell R, Rincon AC, Alonso M, Reboto V, Molina-Martinez IT, Rodriguez-Cabello JC. Self-assembled particles of an elastin-like polymer as vehicles for controlled drug release. J Control Release 2005;102:113.

[121] Dreher MR, Simnick AJ, Fischer K, Smith RJ, Patel A, Schmidt M, Chilkoti A. Temperature triggered self-assembly of polypeptides into multivalent spherical micelles. Journal of the American Chemical Society 2008;130:687.

[122] Simnick AJ, Valencia CA, Liu R, Chilkoti A. Morphing Low-Affinity Ligands into High-Avidity Nanoparticles by Thermally Triggered Self-Assembly of a Genetically Encoded Polymer. ACS nano 2010.

[123] Fujita Y, Mie M, Kobatake E. Construction of nanoscale protein particle using temperature-sensitive elastin-like peptide and polyaspartic acid chain. Biomaterials 2009;30:3450.

[124] Urry DW, Haynes B, Zhang H, Harris RD, Prasad KU. Mechanochemical coupling in synthetic polypeptides by modulation of an inverse temperature transition. Proceedings of the National Academy of Sciences of the United States of America 1988;85:3407.

[125] Urry DW, Urry KD, Szaflarski W, Nowicki M. Elastic-contractile model proteins: Physical chemistry, protein function and drug design and delivery. Advanced drug delivery reviews 2010;62:1404.

[126] Li B, Alonso DO, Daggett V. The molecular basis for the inverse temperature transition of elastin. Journal of molecular biology 2001;305:581.

[127] Krukau A, Brovchenko I, Geiger A. Temperature-induced conformational transition of a model elastin-like peptide GVG(VPGVG)(3) in water. Biomacromolecules 2007;8:2196.

[128] Reiersen H, Clarke AR, Rees AR. Short elastin-like peptides exhibit the same temperature-induced structural transitions as elastin polymers: implications for protein engineering. Journal of molecular biology 1998;283:255.

[129] Reiersen H, Rees AR. An engineered minidomain containing an elastin turn exhibits a reversible temperature-induced IgG binding. Biochemistry 1999;38:14897.

[130] Megeed Z, Winters RM, Yarmush ML. Modulation of single-chain antibody affinity with temperature-responsive elastin-like polypeptide linkers. Biomacromolecules 2006;7:999.

[131] Kim B, Chilkoti A. Allosteric actuation of inverse phase transition of a stimulus-responsive fusion polypeptide by ligand binding. Journal of the American Chemical Society 2008;130:17867.

[132] Kuyas C, Doolittle RF. Gly-Pro-Arg-Pro derivatives that bind to human plasma albumin and prevent fibrin formation. Thrombosis research 1986;43:485.

[133] Homandberg GA, Wai T. Insertion of fibrin peptides into urokinase enhances fibrin affinity. Thrombosis research 1990;58:403.

[134] Hua ZC, Chen XC, Dong C, Zhu DX. Characterization of a recombinant chimeric plasminogen activator composed of Gly-Pro-Arg-Pro tetrapeptide and truncated urokinase-type plasminogen activator expressed in Escherichia coli. Biochemical and biophysical research communications 1996;222:576.

[135] Soon AS, Stabenfeldt SE, Brown WE, Barker TH. Engineering fibrin matrices: the engagement of polymerization pockets through fibrin knob technology for the delivery and retention of therapeutic proteins. Biomaterials 2010;31:1944.

[136] Martino MM, Mochizuki M, Rothenfluh DA, Rempel SA, Hubbell JA, Barker TH. Controlling integrin specificity and stem cell differentiation in 2D and 3D environments through regulation of fibronectin domain stability. Biomaterials 2009;30:1089.

[137] Petrie TA, Capadona JR, Reyes CD, Garcia AJ. Integrin specificity and enhanced cellular activities associated with surfaces presenting a recombinant fibronectin fragment compared to RGD supports. Biomaterials 2006;27:5459.

[138] Leahy DJ, Aukhil I, Erickson HP. 2.0 A crystal structure of a four-domain segment of human fibronectin encompassing the RGD loop and synergy region. Cell 1996;84:155.

[139] Laudano AP, Doolittle RF. Synthetic peptide derivatives that bind to fibrinogen and prevent the polymerization of fibrin monomers. Proceedings of the National Academy of Sciences of the United States of America 1978;75:3085.

[140] Laudano AP, Doolittle RF. Influence of calcium ion on the binding of fibrin amino terminal peptides to fibrinogen. Science (New York, N.Y 1981;212:457.

[141] Taylor SJ, McDonald JW, 3rd, Sakiyama-Elbert SE. Controlled release of neurotrophin-3 from fibrin gels for spinal cord injury. J Control Release 2004;98:281.

[142] Kawasaki K, Hirase K, Miyano M, Tsuji T, Iwamoto M. Amino acids and peptides. XVI. Synthesis of N-terminal tetrapeptide analogs of fibrin alpha-chain and their inhibitory effects on fibrinogen/thrombin clotting. Chemical & pharmaceutical bulletin 1992;40:3253.

[143] Pandi L, Kollman JM, Lopez-Lira F, Burrows JM, Riley M, Doolittle RF. Two families of synthetic peptides that enhance fibrin turbidity and delay fibrinolysis by different mechanisms. Biochemistry 2009;48:7201.

[144] Soon AS, Lee CS, Barker TH. Modulation of fibrin matrix properties via knob:hole affinity interactions using peptide-PEG conjugates. Biomaterials 2011;32:4406.

[145] Gong XW, Wei DZ, He ML, Xiong YC. Discarded free PEG-based assay for obtaining the modification extent of pegylated proteins. Talanta 2007;71:381.

[146] Nag A, Mitra G, Ghosh PC. A colorimetric assay for estimation of polyethylene glycol and polyethylene glycolated protein using ammonium ferrothiocyanate. Analytical biochemistry 1996;237:224.

[147] Carr ME, Gabriel DA. The effect of dextran 70 on the structure of plasma-derived fibrin gels. The Journal of laboratory and clinical medicine 1980;96:985.

[148] Carr ME, Jr., Powers PL, Jones MR. Effects of poloxamer 188 on the assembly, structure and dissolution of fibrin clots. Thrombosis and haemostasis 1991;66:565.

[149] Carr ME, Jr., Carr SL, High AA. Effects of poloxamer 407 on the assembly, structure and dissolution of fibrin clots. Blood Coagul Fibrinolysis 1996;7:109.

[150] Collet JP, Park D, Lesty C, Soria J, Soria C, Montalescot G, Weisel JW. Influence of fibrin network conformation and fibrin fiber diameter on fibrinolysis speed: dynamic and structural approaches by confocal microscopy. Arteriosclerosis, thrombosis, and vascular biology 2000;20:1354.

[151] Gabriel DA, Muga K, Boothroyd EM. The effect of fibrin structure on fibrinolysis. The Journal of biological chemistry 1992;267:24259.

[152] Weisel JW. The mechanical properties of fibrin for basic scientists and clinicians. Biophysical chemistry 2004;112:267.

[153] Hoffman AS, Stayton PS. Conjugates of stimuli-responsive polymers and proteins. Progress in Polymer Science 2007;32:922.

[154] Cole MA, Voelcker NH, Thissen H, Griesser HJ. Stimuli-responsive interfaces and systems for the control of protein-surface and cell-surface interactions. Biomaterials 2009;30:1827.

[155] Ganta S, Devalapally H, Shahiwala A, Amiji M. A review of stimuli-responsive nanocarriers for drug and gene delivery. J Control Release 2008;126:187.

[156] Meyer DE, Chilkoti A. Genetically encoded synthesis of protein-based polymers with precisely specified molecular weight and sequence by recursive directional ligation: examples from the elastin-like polypeptide system. Biomacromolecules 2002;3:357.

[157] Niesen FH, Berglund H, Vedadi M. The use of differential scanning fluorimetry to detect ligand interactions that promote protein stability. Nature protocols 2007;2:2212.

[158] Cho Y, Zhang Y, Christensen T, Sagle LB, Chilkoti A, Cremer PS. Effects of Hofmeister anions on the phase transition temperature of elastin-like polypeptides. J Phys Chem B 2008;112:13765.

[159] Senisterra GA, Finerty PJ, Jr. High throughput methods of assessing protein stability and aggregation. Molecular bioSystems 2009;5:217.

[160] Nair CH, Shah GA, Dhall DP. Effect of temperature, pH and ionic strength and composition on fibrin network structure and its development. Thrombosis research 1986;42:809.

[161] Averett LE, Schoenfisch MH, Akhremitchev BB, Gorkun OV. Kinetics of the multistep rupture of fibrin 'A-a' polymerization interactions measured using atomic force microscopy. Biophysical journal 2009;97:2820.

[162] Stabenfeldt SE, Aboujamous NM, Soon AS, Barker TH. A new direction for anticoagulants: Inhibiting fibrin assembly with PEGylated fibrin knob mimics. Biotechnology and bioengineering 2011.

[163] Stabenfeldt SE, Gossett JJ, Barker TH. Building better fibrin knob mimics: an investigation of synthetic fibrin knob peptide structures in solution and their dynamic binding with fibrinogen/fibrin holes. Blood 2011;116:1352.

[164] Okada M, Blomback B. Factors influencing fibrin gel structure studied by flow measurement. Annals of the New York Academy of Sciences 1983;408:233.

[165] Storm C, Pastore JJ, MacKintosh FC, Lubensky TC, Janmey PA. Nonlinear elasticity in biological gels. Nature 2005;435:191.

[166] Kang H, Wen Q, Janmey PA, Tang JX, Conti E, MacKintosh FC. Nonlinear elasticity of stiff filament networks: strain stiffening, negative normal stress, and filament alignment in fibrin gels. J Phys Chem B 2009;113:3799.

[167] Janmey PA, McCormick ME, Rammensee S, Leight JL, Georges PC, MacKintosh FC. Negative normal stress in semiflexible biopolymer gels. Nature materials 2007;6:48.

[168] Shah JV, Janmey PA. Strain hardening of fibrin gels and plasma clots. Rheologica Acta 1997;36:262.

[169] Houser JR, Hudson NE, Ping L, O'Brien ET, 3rd, Superfine R, Lord ST, Falvo MR. Evidence that alphaC region is origin of low modulus, high extensibility, and strain stiffening in fibrin fibers. Biophysical journal 2010;99:3038.

[170] Brown AE, Litvinov RI, Discher DE, Purohit PK, Weisel JW. Multiscale mechanics of fibrin polymer: gel stretching with protein unfolding and loss of water. Science (New York, N.Y 2009;325:741.

[171] Browning MB, Wilems T, Hahn M, Cosgriff-Hernandez E. Compositional control of poly(ethylene glycol) hydrogel modulus independent of mesh size. J Biomed Mater Res A 2011;98:268.

[172] Martino M, Perri T, Tamburro AM. Biopolymers and biomaterials based on elastomeric proteins. Macromolecular Bioscience 2002;2:319.

VITA

ALLYSON S. C. SOON

Allyson was born in Johor, Malaysia. She attended public schools in Malaysia and Singapore, received a B. Eng. in Chemical Engineering from the National University of Singapore in 2004, before embarking on a career path in research, beginning with a position at the Bioprocessing Technology Institute that same year. She came to Georgia Tech in 2006 to pursue a doctorate in Biomedical Engineering.